Fabrication of PSQ-L polymer photonic devices

Jie Teng

UNIVERSITEIT
GENT

Promoters:

Prof. dr. ir. G.Morthier   Universiteit Gent, INTEC

Prof. dr. Mingshan Zhao   Dalian University of Technology, School of Physics and Optoelectronic Engineering

Examiners

Prof. dr. ir. R. Baets	Universiteit Gent, INTEC
Prof. dr. ir .D. Van Throurhout	Universiteit Gent, INTEC
Prof. dr. ir. G.Morthier (Promoter)	Universiteit Gent, INTEC
Prof. dr. Mingshan Zhao (Promoter)	Dalian University of Technology, School of Physics and Optoelectronic Engineering
Prof. dr. ir. D. De Zutter	Gent University, INTEC
Prof. dr. ir. J. Vanfleteren	Gent University, ELIS
Prof. dr. ir. H. Ottevaere	Vrije Universiteit Brussel, Dept.TOMA

Universiteit Gent
Faculty of Engineering
Department of Information Technology (INTEC)
Sint Pietersnieuwstraat 41
B-9000 Gent
Belgium
Tel: +32-9-264 89 34
Fax: +32-9-264 35 93

Acknowledgement

Actually, this is almost the last part of my writing of the thesis. I feel a little bit sad, not only because I have to say goodbye to the long and hard writing process, but also because I have to say goodbye to a part of my life and some people I used to work with. I was quite busy with writing in the last few months and till now I don't know where the next stop of my life is. But I'm quite sure that one day I will miss the days as a PhD student and have the same thankful feeling as now to the people who helped me, encouraged me and worked with me during that period.

First of all, I'd like to thank my professor Mingshan Zhao in China who first guided me to the subject in my PhD study and provided me a chance to work with another group of people. I'd also like to thank my professor Geert Morthier who then guided me and helped me a lot in Gent. Every time I saw his careful correction in my thesis, I feel really grateful. My thanks also go to Prof. Roel Baets and Prof. Dries Van Thourhout, who helped me and gave me some advices on my work.

I'm so lucky to work with so many nice colleagues. As this is a joint-PhD program, I need to thank both my colleagues in China I used to work with and also my colleagues I'm now working with in Belgium.

As this is an interdisciplinary subject, I first worked with my colleagues from the department of polymer science and materials at Dalian University of Technology. I still remember it was a really a working time. Because we did something new and we had to face a lot of problems. Thanks Yuan Song, Hongbo Zhang, Linke LI, Yuhui Liu, Man li, who used to work with me and shared knowledge with me. I'd also like to express my thanks to the colleagues who worked with me in Gent: Stijn guided me to do the imprint at first and he also shed some light on me; Steven helped me to do some fabrication; Lisebet did a lot of SEM for me; Yu did a lot of RIE etching for me; and a lot of other people helped me. Thanks to all these people and I have learned a lot from you.

I would like to thank O.B.S.G., who provides the nice housing for foreign students.

I also want to thank many Chinese friends in Gent who helped me a lot, especially when I just arrived. Yes, I will also help the other new comers because I know what it means to them.

I would also like to thank the CSC (China Scholarship Council) and Ghent University BOF-cofunding for the financial support of my living in Gent.

Last but not the least, I thank my parents. I know they are really proud of me, all the time, no matter who I am, where I am, what I have got. I think we don't have many chances to express our gratitude to our parents in our life and most of the time we even forgot to be grateful to them. Thanks for the last 28 years of love and support! Your love really means a lot to me!

Jie Teng
Dec.,1st, 2009

Samenvatting

Fabricatie van polymeer gebaseerde optische componenten

Polymeren komen op als een belangrijk materiaal in het gebied van geïntegreerde fotonica. Polymeermaterialen zijn compatibel met verschillende eenvoudige fabricageprocessen, en zullen de kosten van de fotonische componenten naar verwachting doen afnemen. Bovendien kan de moleculaire structuur van de materialen worden ontworpen al naargelang de vereisten gesteld door specifieke toepassingen. Zodra de passieve optische polymeertechnologie voldoende ontwikkeld is, kunnen versterking en elektro-optische effecten eenvoudig worden bereikt door selectieve doping.

Er zijn reeds enkele soorten optische polymeren op de markt beschikbaar. Toch is de thermische stabiliteit nog steeds een belemmering voor een ruime toepassing van polymeer-gebaseerde componenten. Sommige aspecten van de optische polymeren moeten nog worden verbeterd voor sommige toepassingen. Het doel van dit werk is om bepaalde soorten van optische polymeren met geschikte eigenschappen te ontwikkelen en toe te passen in bepaalde optische componenten.
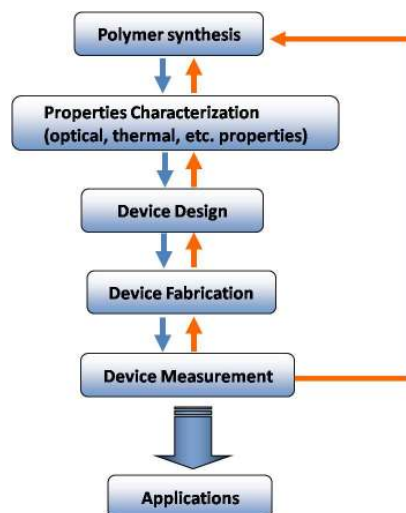
Figuur 1 Het kader van deze werkzaamheden

Dit werk omvat verschillende onderdelen: polymeersynthese, karakterisatie van de eigenschappen, optisch component ontwerp, de fabricatie van optische

componenten en componentmetingen (zoals weergegeven in Figuur 1). Eerst worden de polymeren gesynthetiseerd door onze collega's van de chemische afdeling van de Technische Universiteit van Dalian in China. Dan worden polymeerfilmen voorbereid m.b.v. het spin-coating proces voor het testen van de eigenschappen en voor verdere fabricatie. De syntheseprocessen worden nadien aangepast om betere eigenschappen van de materialen te bereiken op basis van de feedback verkregen bij de metingen. De polymeer-gebaseerde componenten worden ontworpen en vervaardigd op basis van de gemeten parameters en polymeereigenschappen. Wanneer het syntheseproces volwassen genoeg is en de polymeereigenschappen een aanvaardbaar niveau bereiken voor de toepassing, worden de fabricatietechnologieën ontwikkeld voor het polymeermateriaal. Elk deel van het werk geeft feedback over de eigenschappen van de polymeren en deze worden indien mogelijk aangepast en verbeterd bij de synthesefase.

We hebben twee belangrijke soorten van polymeermaterialen ontwikkeld: PPESK en PSQ-L. De optische en andere eigenschappen van deze materialen werden onderzocht. Aangezien de synthesetechnologie voor de polymeer PSQ-L voldoende ontwikkeld is en de eigenschappen van dit soort polymeer kunnen voldoen aan de fundamentele eisen voor optische toepassingen, zijn de fabricatietechnologieën van deze polymeer eerst onderzocht. Naast de traditionele fabricatieprocessen voor optische golfgeleiders van lithografie en RIE-etsen, zijn ook nieuwe technologieën zoals de nanoimprint fabricatietechnologie hier onderzocht. Een eenvoudige UV-gebaseerde soft-lithografie-technologie is ontwikkeld voor de productie van PSQ-L golfgeleiders (Figuur 2). In tegenstelling tot conventionele afdrukprocessen, wordt de afdrukstap voor het structureren hier het eerst gedaan op de mantellaag eerder dan op de kernlaag van de golfgeleider en wordt deze gevolgd door het opvullen van de aangebrachte structuren d.m.v. een spin-coating stap. Dit ontwerp van de golfgeleiderdoorsnede vermijdt dat de dikte van de residuele kernlaag (h1 in Figuur 2) nauwkeurig moet gecontroleerd worden. Eenvoudige PSQ-L ringresonatoren werden vervaardigd op deze manier. De polymeer microringresonatoren werden gekarakteriseerd na fabricatie. Figuur 3 toont het transmissiespectrum van de PSQ-L ringresonatoren. Het mooie resonantiespectrum geeft een aanduiding van het lage absorptieverlies van het materiaal en van de geschiktheid van de fabricatietechniek voor dit materiaal.
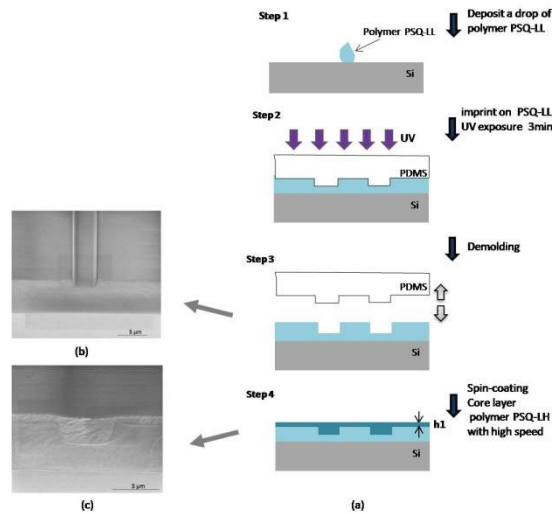
Figuur 2 Fabricatie van PSQ-L golfgeleiders door een UV-gebaseerd soft-lithografie-proces
(a) de fabricatieprocedure (b) SEM beeld van de bedrukte lage index PSQ-LL laag (d) SEM
beeld van de golfgeleider dwarsdoorsnede (na spin-coating van de hoge index PSQ-LH laag)

(a)   (b)
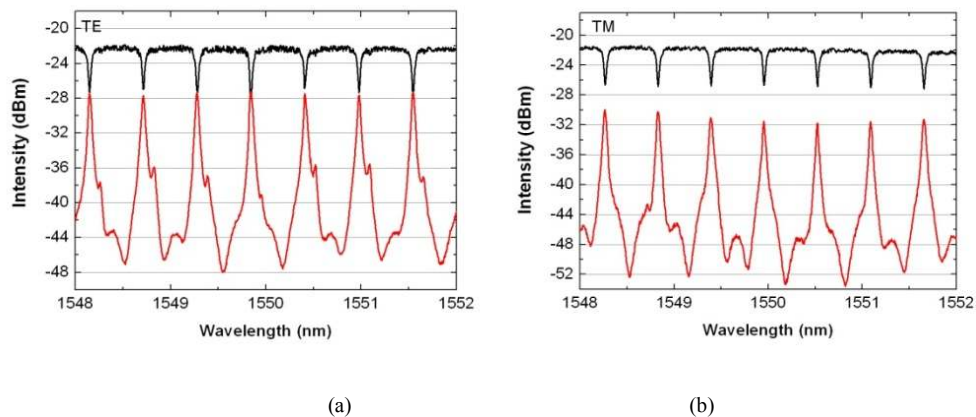
Figuur 3 transmissiespectrum van een PSQ-L ringresonator gefabriceerd door
soft-lithografie (a) TE modus (b) TM-modus

Tijdens het doctoraat werd de synthese van PPESK polymeer niet ontwikkeld genoeg geacht voor toepassingen. Daarom is de fabricatietechnologie het meest toegespitst op de PSQ-L serie polymeer. Op korte termijn was het ons doel om de 'huisbereidde' polymeer toe te passen bij de fabricatie van basis optische golfgeleider componenten. Polymeer PSQ-L ringresonatoren werden succesvol gefabriceerd en gekarakteriseerd, hetgeen het potentieel aantoont van die polymeer

voor de fabricatie van optische componenten. Op lange termijn, na het succesvol demonstreren van fundamentele componenten, zullen een aantal toepassingen worden nagestreefd van op polymeer gebaseerde componenten of van hybrieden van polymeer en andere materialen. Verdere optimalisering van de fabricatietechnologie en van de toepassingen van deze componenten zijn voorzien in de nabije toekomst.

Athermische SOI componenten

Silicium-gebaseerde fotonische componenten trokken veel aandacht in de afgelopen jaren. Het gebruik van de volwassen CMOS (Complementary Metal Oxide Semiconductor) fabricatietechnologie laat toe om in het siliciumplatform zeer compacte circuits te fabriceren tegen lage kosten en om betere prestaties te bekomen. Echter, silicium heeft een grote thermo-optische coëfficiënt (TO_Si:1.8×10^{-4}/°C). De grote temperatuursafhankelijkheid van silicium degradeert de prestaties van silicium-gebaseerde componenten. Externe verwarming of koeling, die extra plaats inneemt en extra vermogen verbruikt, moet worden aangewend in de circuits teneinde de temperatuur van de chip te stabiliseren.

Een eenvoudige manier om athermische optische componenten te bereiken is ze te voorzien van een polymeer overlay (bekleding) en gebruik te maken van de negatieve thermo-optische's (TO) coëfficiënt van de polymeer om de positieve TO coëfficiënt van de golfgeleiderkern te compenseren. Het grootste obstakel daarbij voor silicium golfgeleiders is dat de thermo-optische coëfficiënt van silicium van dezelfde orde van grootte is als die van het polymeer materiaal (10^{-4}/°C). Voor het bereiken van athermisch gedrag is dan vereist dat bijna de helft van het licht uit het silicium doordringt in de polymeerbekleding.

Om meer licht te hebben in de polymeerbekleding, moet de dimensie van de silicium golfgeleiders sterk worden gereduceerd. We gebruiken versmalde SOI golfgeleiders met een polymeer PSQ-L bekleding om athermische SOI componenten te bereiken.Standaard SOI wafers (met een hoogte van het silicium van 220nm) worden gebruikt. De ideale breedte vereist voor het bekomen van athermische SOI golfgeleiders is theoretisch berekend. De SOI golfgeleiders worden vervaardigd door middel van diepe UV-lithografie en een droog etsproces.

Athermische SOI ring resonatoren en MZ interferometers zijn met succes gerealiseerd op deze manier. De temperatuursafhankelijkheid van de resonantiegolflengte van ringresonatoren wordt gereduceerd van 54.2±1.0pm/°C tot -4.7±1.0pm/°C voor 350nm brede ringresonatoren na het bekleden met een polymeer bekleding (Figuur 4).

Andere, meer ingewikkelde componenten zoals AWGs, zijn toegevoegd in de tweede run. Echter, het gedrag van deze componenten met ingevoegde smalle golfgeleiders beantwoordde niet aan de verwachtingen. Athermische silicium componenten met betere performantie zullen in de toekomst mogelijk zijn met een verbeterde fabricage technologie.

(a)

(b)

(c)

(d)
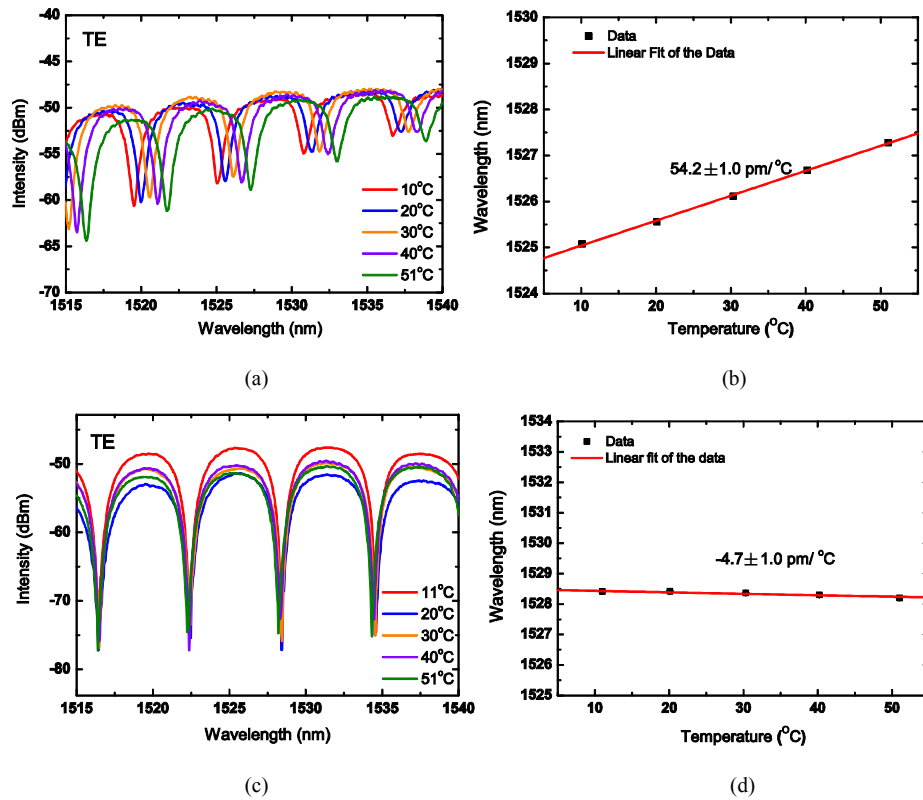
Figuur 4 (a) Transmissiespectrum van een ringresonator met een breedte van 350 nm bij verschillende temperaturen zonder een polymeerbekleding (b) lineaire fit van de golflengte versus temperatuur (c) Transmissie spectrum van een ringresonator met een breedte van 350 nm bij verschillende temperaturen met een polymeerbekleding (d) Lineaire fit van de golflengten versus temperatuur
(Breedte = 350 nm, Gap = 180nm, L = 2μm, R = 15μm)

Summary

Fabrication of polymer based optical devices

Polymers are emerging as an important material in the field of integrated optics. As the polymer materials are compatible with several simple fabrication processes, the cost of the optical devices is expected to be lowered down to meet economic criteria. Moreover, the molecular structure of the materials can be designed to fit some application requirements. Once the passive optical polymer technology is established, amplification and electro-optic effects can be easily achieved by selective doping.

There are some kinds of optical polymers available in the market. However, the thermal stability is still hindering a wide application of polymer-based devices. Some aspects of the optical polymers still need to be improved for some applications. The objective of this work is to develop some kinds of optical polymers with appropriate properties and apply them in the optical applications.
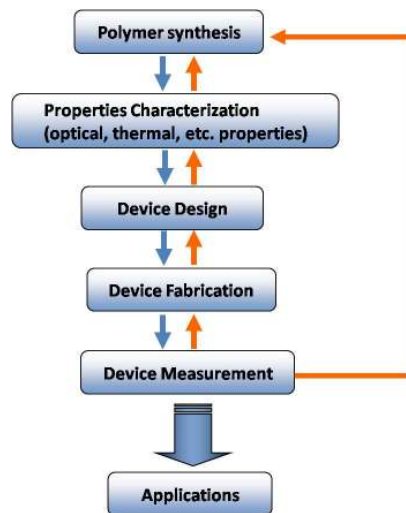
Figure 1 The frame of this work

This work involves several parts of work, from polymer synthesis to device fabrication (as shown in Figure 1). First, the polymers are synthesized by our colleagues from the chemical department at Dalian University of Technology. Then the polymer films are prepared by the spin-coating process for property tests and further fabrications. The synthesis processes are adjusted to achieve better properties of the materials from the feedback of the property measurements. The polymer-based

devices are designed and fabricated based on the parameters measured from the polymer properties. When the synthesis process is mature enough and the properties of the polymer reach an acceptable level for application, the fabrication technologies are developed for the polymer materials. After fabrication, the polymer-based devices are measured. Each part of the work gives feedback to the properties of the polymers and the properties of the polymer are expected to be adjusted and improved from the synthesis phase.

We have developed two main kinds of polymer materials: PPESK and PSQ-L. The optical properties and other properties of these materials are investigated. As the synthesis technology for polymer PSQ-L is mature and the properties of this kind of polymer can meet the basic demands for optical applications, the fabrication technologies of this polymer are first investigated. Apart from the traditional fabrication process of photo-lithography and etching for optical waveguides, new fabrication technologies like nanoimprint technology are explored here. A simple UV-based soft-lithography technology has been developed for fabrication of PSQ-L waveguides (Figure 2). Unlike in conventional imprint processes, the imprint step for structuring is done first on the cladding layer rather than on the core layer and is followed by a spin-coating step to fill the imprinted features with core layer material. This waveguide cross-section design smartly avoids controlling the thickness of the residual core layer (h1 in Figure 2). Simple PSQ-L ring resonators are fabricated in this way. The all-polymer microring resonators have been characterized after fabrication. Figure 3 shows the transmission spectrum of the PSQ-L ring resonators. The nice resonance spectrum indicates the low absorption loss of the material and appropriate fabrication technique for this material. These devices have potential applications in the optical communications and sensing applications.
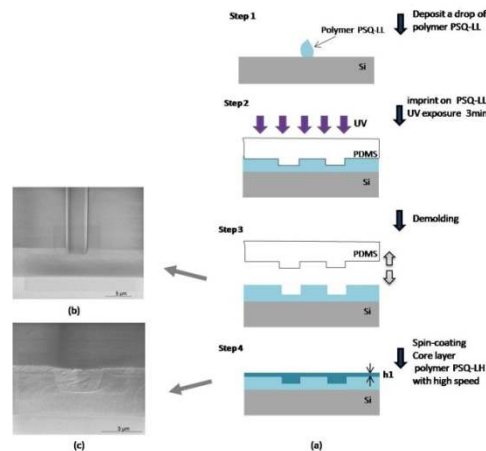
Figure 2 Fabrication of PSQ-L waveguides by a UV-based soft-lithography process (a) fabrication procedure (b) SEM picture of the imprinted low index PSQ-LL layer (d) SEM picture of the waveguide cross-section (after spin-coating the high index PSQ-LH layer)
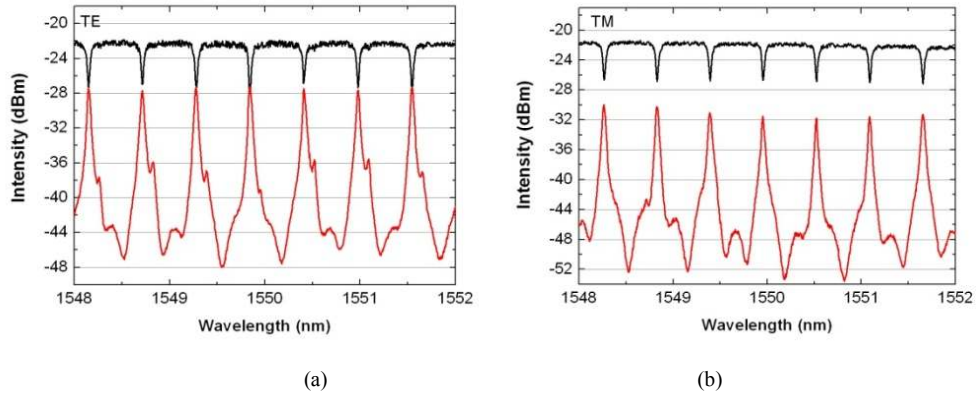
Figure 3 Transmission spectrum of PSQ-L ring resonator fabricated by soft-lithography (a) TE mode (b) TM mode

During the PhD study, the synthesis of PPESK series polymer was not mature enough to put into applications. Therefore the fabrication technology is most dedicated to PSQ-L series polymer. In the first run, our aim is to apply the home-made polymer to fabricate basic optical waveguide devices. Polymer PSQ-L ring resonators were successfully fabricated and characterized, which proves the possibility and promise of using this polymer to fabricate optical devices. In the long run, after successfully achieving basic devices, some applications of polymer-based devices and hybrids of polymer and other materials circuits are expected to be pursued. Further optimization of the fabrication technology and application of these devices are foreseen in the near future.

Athermal SOI devices

The other part of this work is about application of these polymer materials to SOI (Silicon-on-insulator) circuits.

Silicon-based devices have attracted a lot of attention in recent years. With mature CMOS (Complementary Metal Oxide Semiconductor) fabrication technology, the silicon platform can provide highly compact circuits with low cost, multi-functionality and enhanced performance. However, silicon has a large thermo-optic coefficient (TO_Si: 1.8×10^{-4}/°C). The large temperature dependence of silicon degrades the performance of silicon-based devices. External heaters or coolers have to be employed in the circuits to stabilize the chip's temperature, which takes extra space and consumes extra power.

A simple way to achieve athermal optical devices is to overlay a polymer cladding on the circuit using the polymer's negative thermo-optical (TO) coefficient to counterbalance the waveguide core's positive TO coefficient. The biggest obstacle for silicon waveguides to use this method is that the thermo-optic coefficient of silicon is the same order of magnitude as that of the polymer material (10^{-4}/°C). This

requires almost half of the light to penetrate out of the silicon core into the polymer cladding to achieve the athermal condition.

In order to have more light into the polymer cladding, the dimension of the silicon waveguides should be highly reduced. We use narrowed SOI waveguides with a polymer PSQ-L cladding on top to achieve athermal SOI devices. Standard SOI wafers (with a silicon height of 220nm) are used. The ideal width to achieve athermal SOI waveguides is theoretically calculated. The SOI waveguides are fabricated by deep UV lithography and dry etching process.

Athermal SOI ring resonators and MZ interferometers have been successfully achieved in this way. The temperature dependence of the resonance wavelength of ring resonators is reduced from 54.2±1.0pm/°C to -4.7±1.0pm/°C for 350nm-width ring resonators after overlaying a polymer cladding (Figure 4).

Other more complicated devices, like AWGs are also added into the second run. However, this device performs poorly with inserted narrowed waveguides. Athermal silicon devices with better performance are foreseen in the future with improved fabrication technology.

Figure 4 (a) Transmission spectrum of a ring resonator with width of 350nm at different temperatures before overlaying a polymer cladding (b) Linear fit of the wavelength versus temperatures (c) Transmission spectrum of a ring resonator with width of 350nm at different temperatures after overlaying a polymer cladding (d) Linear fit of the wavelengths versus temperatures (Width=350nm, Gap=180nm, L=2μm, R=15μm)

Content

List of Acronyms

AWG	Arrayed waveguide grating
BCB	Benzocyclobutene
CMOS	Complementary Metal Oxide Semiconductor
CTE	Coefficients of temperature expansion
CTE	Coefficient of thermal expansion
DCS	4,4'-Bis(4-chlorophenyl) sulfone
DFK	4,4'-difluorobenzophenone
DHPZ	4-(4-Hydroxyphenyl)-2,3-phthalazin-1-one
DI water	Deionized water
DOS	Digital optical switches
DUV	Deep Ultra-Violet
FIB	Focused Ion Beam
FSR	Free Spectral Range
FTIR	Fourier transform infrared spectroscopy
FWHM	Full Bandwidth at Half-Maximum
HF	Hydrofluoric acid
ICP	Inductively Coupled Plasmas
IPA	Isopropyl Alcohol
MCM	Multi-chip modules
MOCVD	Metalorganic vapour phase epitaxy
MZI	Mach-Zehnder interferometers
NMP	N,N'-dimethylacetamide, N-methyl-2-pyrrolidinone
OLED	Organic light-emitting diodes
PC	Polycarbonate
PCB	Printed Circuits Board
PDMS	Polydimehysiloxane
PMMA	Poly(methylmethacrylate)
PON	Passive optic networks
PPES	Poly(phthalazinone ether sulfone)
PPESK	Poly(phthalazinone ether sulfone ketone)
PS	Polystyrene
PSQ-L	Polysilisiquioxane
PU	Polyurethane
RIE	Reactive Iron Etching
SLED	Super-luminescent light-emitting diode
SOI	Silicon on insulator
T_d	Decomposition temperature
TE	Transverse Electric
T_g	Glass transition temperature
TGA	Thermo-Gravimetric Analysis
TM	Transverse Megetic

List of Symbols

A	Power Attenuation Coefficient per round trip
α_{sub}	Thermo expansion coefficient of the substrate
β	Phase propagation constant
dn/dT	Thermo-optic Coefficient
h	Height
h1	Residual layer thickness
κ	Coupling coefficient of the electric field amplitude
K	Coupling coefficient of Power
n	Refractive Index
n_c	Refractive index of cladding
n_{eff}	Effective Index
n_g	Group Index
Q	Quality factor
R	Radius of the ring
S	Sensitivity
T	Temperature, Transmission coefficient of Power
t	Transmission coefficient of the electric field amplitude
T_d	Decomposition Temperature
T_g	Glass Transition Temperature
w	Width
Γ	Confinement factor
$\Delta\lambda_{FWHM}$	Full Bandwidth at Half-Maximum
λ	Wavelength

Chapter 1 Introduction

1.1 Original motivation

The photonics industry demands standardized component platforms that can be manufactured in high volume at low cost. These platforms will have uncompromised performance and a significant reduction in the cost of optical components. In the past decades, several material systems have been pursued as integrated optic platforms. The properties of these materials are listed in Table 1.1. Silica is most widely used material systems for passive devices, like AWGs and splitters while indium phosphide is most widely used material systems for active devices, like lasers and detectors. Other platforms for integrated optics are also being pursued, including silicon on insulator, silicon oxynitride, lithium niobate, gallium arsenide, sol-gels, and polymers.

As can be seen from Table 1. 1, the polymer materials offer more advantages than silica once the polymer material was synthesized properly, such as larger index contrast and lower birefringence. They are also compatible with a lot of fabrication processes to reduce the device costs. The polymer material can meet the cost need for both hybrid circuits and monolithic circuits. Polymer-based devices have been fabricated and tested for both passive and active functions. The future trend is to replace silica-based devices by polymer-based devices. During the next decade, the polymer material will continue to be a critical material in commercial, hybrid photonic circuits.

Table 1. 1 Properties of key integrated optic materials at 1550 nm wavelength (T/O = thermo-optic, E/O = electro-optic) [1]

	Propagation Loss (dB/cm)	Pigtail loss (dB/cm)	Refractive Index (n)	Index Contrast Range in Waveguide (Δn)	Birefringence (n_{TE}-n_{TM})	T/O coef. dn/dT (/K)	Maximum Modulation Frequency	Passive /Active
Silica [SiO$_2$]	0.1	0.5	1.5	0-1.5% (Channel)	10^{-4}-10^{-2}	10^{-5}	1kHz (T/O)	Y/Y
Silicon [Si]	0.1	1.0	3.5	70% (Silicon on insulator Rib)	10^{-4}-10^{-2}	1.8×10^{-4}	1kHz (T/O)	Y/N
Silicon Oxynitride [SiO$_x$N$_y$]	0.1	1.0	SiO$_2$:1.5 Si$_3$N$_4$:2.0	0-30% [30%: Si$_3$N$_4$ core] (Channel, SiO$_2$ clad)	10^{-3}-5×10^{-6}	10^{-5}	1kHz (T/O)	Y/N
Sol-Gels	0.1	0.5	1.2-1.5	0-1.5% (Channel)	10^{-4}-10^{-2}	10^{-5}	1kHz (T/O)	Y/Y
Polymers	0.1	0.5	1.3-1.7	0-35% (Channel)	10^{-5}-10^{-2}	$-1\sim-3\times10^{-4}$	>100GHz(E/O) 1kHz(T/O)	Y/Y
Lithium Niobate [LiNbO$_3$]	0.5	2.0	2.2	0-0.5% (Channel)	10^{-2}-10^{-1}	10^{-5}	40GHz (E/O)	Y/Y
Indium Phosphide [InP]	3	10	3.1	0-3% (Channel)	10^{-3}	0.8×10^{-4}	40GHz (E/O)	Y/Y

Gallium Arsenide [GaAs]	0.5	2.0	3.4	0-14% [14%, AlAs clad, Rib]	10^{-3}	2.5×10^{-4}	20GHz (E/O)	Y/Y

However, polymer photonics cannot achieve every function needed in photonics integrated circuits. The platform needs to deliver performance without compromise. A realistic roadmap is multi-material-system chip-level integration, which enables full functionality and high performance. DuPont Company has been dedicated for years to develop polymer platforms (Figure 1. 1) and also a hybrid system with co-integration of other materials. No matter which material platform is used, the future evolution roadmap is to integrate electronic functions and photonics functions on a single chip.
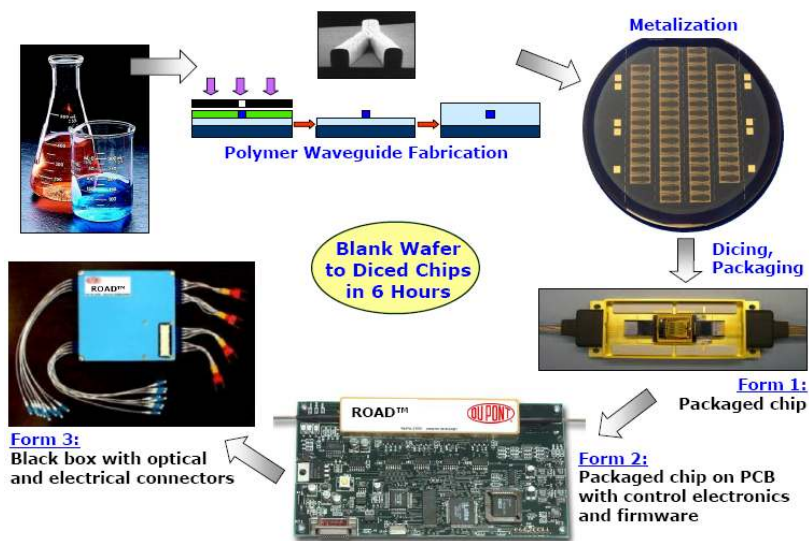
Figure 1. 1 Polymer-on-silicon photonics IC component manufacturing [2]

The original motivation of this work with polymer waveguides comes from the concept of fiber-to-the-home (FTTH), which demands low cost passive optical components such as splitters. As polymer materials are compatible with molding and stamping process, the fabrication cost of polymer devices are expected to be highly reduced. Low cost optical polymers with high performance are highly required for this optical application. As most commercial optical polymers still have long term thermal stability problems (or other problems in realistic application), exploring a kind of optical polymer with low cost and high performance is a major task of this work.

Apart from optical components in WDM system, other applications of polymer-based waveguides are also pursued in recent years [3, 4] since the FTTH age does not come so soon as expected.

1.2 This work

With the motivation mentioned in the last section, fundamental research work on the fabrication of polymer waveguides is presented here. Our aim is to develop some kinds of polymer with appropriate properties and apply them in the optical applications.

As this is a joint Ph.D program, some part of the work is done in Dalian University of Technology while some part of the work is done in Ghent University. The polymers are developed at Dalian University of Technology with the collaboration of the chemical department. The fabrication technologies developed for this kind of polymer materials are mostly investigated at Ghent University.

This work covers several parts of work as shown in Figure 1. 2. First, the polymers are synthesized by our colleagues from the chemical department. Then the polymer films are prepared for property tests and further fabrications. The synthesis processes are adjusted from the feedback from the results of the property measurements. The polymer-based devices are designed and fabricated based on the parameters measured from the polymer properties. When the synthesis process is mature enough and the properties of the polymer reach an acceptable level for application, the fabrication technologies are developed for the polymer materials. After fabrication, the polymer-based devices are measured. Each part of the work gives feedback about the properties of the polymers and the properties of the polymer are expected to be adjusted from the synthesis phase.

In the first run, our aim is to apply home-made polymer to fabricate basic optical waveguide devices. In the long run, after successfully achieving basic devices, some applications of polymer-based devices and hybrid of polymer and other materials circuits are pursued.
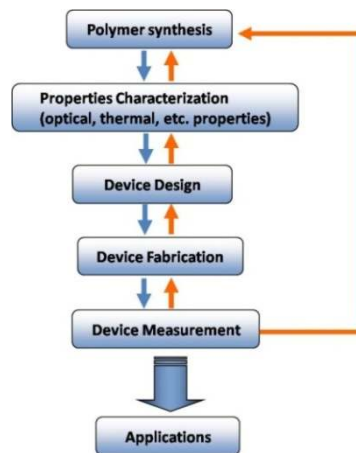
Figure 1. 2 The frame of this work

We have developed two main kinds of polymer materials: PPESK and PSQ-L. The optical properties and other properties are investigated. As the synthesis technology of polymer PSQ-L is mature and the properties of this kind of polymer can meet the basic demands for optical applications, the fabrication technologies are

investigated. Apart from the traditional fabrication process of lithography and RIE etching process for optical waveguides, new fabrication technologies like nanoimprint technology are explored here. We have developed a simple fabrication process for PSQ-L waveguides. Simple PSQ-L ring resonators are fabricated in this way.

During the PhD study, the synthesis of PPESK series polymer was not mature enough to put into applications. Therefore the fabrication technology is most dedicated to PSQ-L series polymer. Basic devices based on polymer PSQ-L like ring resonators are fabricated and tested. Further optimization of the fabrication technology and application of these devices are foreseen in the near future.

On the other hands, applications of polymer PSQ-L are also being explored. Athermal SOI (silicon-on-insulator) devices have been successfully achieved by overlaying a polymer PSQ-L cladding on top of narrowed waveguides. The wavelength temperature dependence of silicon ring resonators is reduced to less than 5 pm/°C, almost eleven times less than air-clad counterparts.

1.3 Literature review

Polymer-based devices have attracted a lot of attention in recent years [2, 5, 6]. Many labs and companies are dedicated to developing high performance optical polymers and applying them in integrated optics fields. The background of this work is reviewed in this section. The related research that has been done by other groups is also introduced here. This section starts from the application requirements for optical polymer materials. Then some commercial optical polymers are introduced. Several fabrication technologies for polymer waveguides are discussed in the following. Finally, some polymer-based functional devices and new applications are introduced.

1.3.1 Requirements for optical polymer materials

The optical polymers are playing an important role in the field of integrated optics since they can offer rapid processibility, cost effectiveness, high yields and high performance. Compared to the silica counterparts, some optical polymers can achieve lower birefringence and lower optical loss. In addition, the polymer materials can also achieve higher power efficiency due to a larger thermo-optic coefficient and higher compactness of circuits due to larger index contrast.

Another advantage of using a polymer material based platform is that the properties of the materials can be adjusted during synthesis. The molecular structures can be designed to fit the application requirements. Furthermore, this platform can incorporate more complex material functionalities. Once the passive optical polymer technology is established, amplification and electro-optic effects can be easily achieved by selective doping.

In this section, the polymer properties requirements for optical waveguides applications are discussed. The basic requirements include four aspects: refractive index, optical loss, environmental performance, processibility and mechanical properties (as shown in Table 1. 2). The polymer material properties related to the performance are explained in more detail in the following part.

Table 1. 2 Requirements for polymers in optical waveguides applications

Main aspects	Properties requirements
Refractive Index	Variable refractive index difference (Δn)
	Low birefringence
	Large thermo-optic coefficient (dn/dT)
	Low refractive index dispersion (dn/dλ)
Optical loss	Low absorption loss
	Low polarization dependent loss (PDL)
	Low pigtail loss
Environmental performance	Thermal stability
	Stability with humidity
	Stability with optical power
Processibility and Mechanical Properties	Adhesion (to substrate, self, electrodes)
	Full curability
	Machinability (cleaving, dicing, polishing)
	Patternability with low scattering loss
	Manufacturability with repeatable properties

➢ **Refractive index**
The polymer materials normally have a refractive index value of 1.3-1.7 at the wavelength of 1550nm. An important feature of polymer materials is that the index contrast can be controlled by the synthesis process (e.g. with different monomers). The index contrast can be achieved up to 35% for polymer materials, which enables high-density compact waveguide structures with small radii of curvature.

➢ **Birefringence**
The birefringence ($\Delta n = n_{TE} - n_{TM}$) indicates the optical anisotropy of a material. In an isotropic material, the birefringence is also related to the stress build-up within the material due to processing or thermal treatment. Unlike inorganic materials, polymers can be molecularly designed to be more isotropic and homogeneous to achieve low birefringence. Some aromatic polymers, such as polyimide, exhibit a very large birefringence (up to 0.24) that is attributed to the strong preference of aromatic chains to align with their planes oriented along the film surface [7]. However, the birefringence can be very low (10^{-5} to 10^{-6}, the limit of the measurement limit) for some three-dimensionally cross-linked polymers [1].

➢ **Thermo-optic coefficient**
The polymer materials have a large negative thermo-optic coefficient (TO coefficient of $-1 \sim -3 \times 10^{-4}$), which is one order of magnitude larger than silica. The combination of a high thermo-optic coefficient and a low thermal conductivity makes polymers ideal materials for thermo-optic devices such as optical switches, attenuators and tunable filters[2]. Furthermore, as the TO coefficients of the polymer materials are negative while those of inorganic materials are positive, temperature insensitive inorganic-materials based devices can be achieved by using a polymer cladding.

➢ **Optical absorption loss**
The material absorption loss is an important property for polymers in optical waveguide applications. For polymer materials, both electronic and vibrational

absorptions are likely to contribute to optical loss. In the 1300nm-1600nm range, the overtones of fundamental molecular vibrations are dominant in absorption loss. Both C-H and -OH overtones give high absorption in the telecommunication windows. Partially replacing C-H bonds with C-F or C-Cl bonds can reduce the absorption loss at the interest wavelength range.

In general, it is difficult to directly determine the absorption loss of the polymer material. There are several ways to measure the loss of the materials. Some groups extracted the absorption loss of the materials from the IR absorption spectrum. Some also use photothermal deflection spectroscopy (PDS [8]) to measure the absorption loss. It has to be mentioned that the measurement methods used to extract the absorption loss has an influence on the measured value since sometimes it is hard to distinguish the scattering loss from the total absorption. The optical loss of the waveguides can be estimated by the cut-back method which also includes the scattering loss caused by sidewall roughness. At present, some polymer can achieve below 0.1dB/cm absorption loss at all the key communication wavelengths.

➢ **Polarization-dependent loss**

The polarization dependent loss (PDL=loss_{TE}-loss_{TM}) varies with process conditions. The TE mode loss measured in planar waveguides can be higher than the TM mode loss when the vertical sidewalls have a higher degree of roughness than the horizontal sidewalls, and it can be lower when the vertical evanescent tails overlap absorptive substrates. By optimizing the edge roughness and the waveguide structure, a small polarization dependent loss of the waveguides can be achieved.

➢ **Fiber pigtail loss**

The fiber pigtail loss can be minimized by tuning the index contrast, the index profile and the core dimensions to match the mode of the planar waveguide and the fiber. By optimizing the alignment of the waveguides and the fiber, and using appropriate index-matched adhesives at the interfaces to minimize the Fresnel reflections, the fiber pigtail loss can also be reduced.

➢ **Environmental performance**

The environmental stability of optical polymers (i.e. the stability of their optical properties with humidity and temperature) is an important issue since most polymers do not have properties for operation in communication environments. A key characteristic for practical applications is the thermal stability of the optical properties because polymeric materials are subject to yellowing upon thermal aging. This yellowing is strongly influenced by the chemical structures of the original polymers. The choice of the linkages and monomers or oligomers ultimately determines the characters of the resulting polymer. In fully halogenated materials, yellowing becomes almost negligible at any wavelength because of the absence of hydrogen. Some polymers have passed the Bellcore 1209 and 1221 environmental tests.

➢ **Processibility and Mechanical Properties**

The polymer materials provide the flexible properties for fabrication of optical waveguides. The films can be made by spin-coating processes. A wide range of rigid or flexible substrates can be used, including glass, quartz, oxidized silicon, printed circuit board and flexible polymer films. There are several techniques for

the fabrication of polymer waveguides, such as direct lithographic patterning, soft lithography, embossing, molding and casting in addition to the conventional photoresist patterning. This permits the rapid, low cost shaping for both waveguide formation and material removal for grafting other elements.

Unlike other optical material systems, the polymers can be designed and synthesized by chemical modification of constitute molecules to have desired properties, such as by tuning the molecular weight and molecular structure to control the viscosity, or by adding certain monomer or prepolymer to achieve photo- or thermo-cross-linking, or to enhance mechanical properties. Some commercial polymers are developed to have appropriate processibility and mechanical properties to facilitate fabrication process.

1.3.2 Commercial optical polymers

Some conventional optical polymers are commonly used for fabrication of optical waveguides, such as poly(methylmethacrylate) (PMMA), polystyrene (PS), polycarbonate (PC), polyurethane (PU) and epoxy resin. However, these polymers exhibit low thermal stability (e.g. T_g of PMMA is 105°C) and high optical absorption loss. Therefore these polymers cannot fully satisfy the optical application requirements. Some companies and laboratories have developed novel optical polymers with high performance in recent years. Some properties of the commercial novel optical polymers are listed in Table 1.3.

Table 1. 3 Key properties of novel optical polymers developed globally by companies [9]

Company	Polymer type	Patterning techniques	Propagation loss, Single-mode waveguide [dB/cm] (wavelength, [nm])	Other properties
Optical Crosslinks (formerly Dupont and Polymer Photonics)	Acrylate (Polyguide)	Diffusion	0.18 (800) 0.2 (1300) 0.6 (1500)	Laminated sheets Excimer-laser machinable
Coring (formerly Allied Signal)	Acrylate	Photoexposure/wet etch, RIE, laser ablation	0.02 (840) 0.3 (1300) 0.8 (1550)	Birefringence: 0.0002 (1550) Crosslinked, Tg: 25°C, Environmentally stable
	Halogenated acrylate	Photoexposure/wet etch, RIE, laser ablation	0.02 (840) 0.06 (1300) 0.2 (1550)	Birefringence: 0.0001 (1550) Crosslinked, Tg: -50°C, Environmentally stable
NTT	Halogenated acrylate	RIE	0.02 (830) 0.07 (1310) 1.7 (1550)	Birefringence: 0.000006 (1310) Tg: 110°C,
	Deuterated polysiloxane	RIE	0.17 (1310) 0.45 (1550)	Environmentally stable
	Fluorinated polyimide	RIE	TE: 0.3, TM: 0.7 (1310)	PDL: 0.4dB/cm (1310) Environmentally stable

Amoco	Fluorinated polyimide (Ultradel)	Photoexposure/ wet etch	0.4 (1310) 1.0 (1550)	Birefringence: 0.025, crosslinked, thermally stable
General Electric	Polyetherimide (Ultem)	RIE, laser ablation	0.24 (830)	Thermally stable
Hitachi	Fluorinated polyimide	Photoexposure/ wet etch	TE: 0.5, TM: 0.6 (1300)	Birefringence: 0.009 (1300) PDL:0.1dB/cm, Tg: 310°C, thermally stable
Dow Chemical	Perfluorocyclobutane (XU 35121)	Photoexposure/ wet etch	0.25 (1300) 0.25 (1550)	Tg: 400°C
	Benzocyclobutene (Cyclotene)	RIE	0.8 (1300) 1.5 (1550)	Tg> 350°C
Asahi Glass	Perfluorovinyl ether Cyclopolymer (CYTOP)			N=1.34, Tg: 108°C
Dupond	Tetrafluoroethylene and perfluorovinyl ether copolymer (Teflon AF)			n=1.31 (AF1600) n=1.29 (AF2400)
JDS Uniphase (formerly Akzo Nobel)	Polycarbonate (BeamBox)	RIE	0.6 (1550)	Thermally stable
Telephotonics	(OASIC)	Photoexposure/wet etch, RIE, laser ablation	<0.01 (840) 0.03 (1300) 0.1 (1550)	Environmentally stable
Gemfire	(Gemfire)	Photoexposure/ wet etch	1.0 (1550)	Birefringence: 0.0002 (1550) Crosslinked,
K-JIST	Fluorinated Poly(arylene ether sulfide) (FPAESI)	RIE	TE: 0.42, TM: 0.4 (1550)	Birefringence: 0.0003 (1550), PDL: 0.02dB/cm (1550), crosslinked, thermally stable
Redfern	Inorganic polymer glass (IPG)	RIE		Environmentally stable
Hoechst Celanse	PMMA copolymer (P2ANS)	Photobleaching	1.0 (1300)	NOL polymer
PacificWave	Polycarbonate with CLD-1 chromophore (PC-LCD-1)	RIE	1.8 (1550)	NOL polymer Γ_{33}=70pm/V (1310), pigtail loss=1.5dB/facet
Lumera	Polyurethane with FTC chromophore (PU-FTC)	RIE	2.0 (1330)	NOL polymer Γ_{33}=25pm/V (1310), pigtail loss=5dB/facet
Ipitek	Poly(methymethacrylate) With CLD-1 chromophore (PMMA-CLD-1)	RIE	5.0 (1300)	NOL polymer Γ_{33}=60pm/V (1300), pigtail loss=3.5dB/facet

Deuterated or halogenated polyacrylates are a category of commonly developed optical polymers. Allied-Signal developed a wide variety of photo-crosslinkable, optically transparent polymers based on the combination of multifunctional halogenated acrylate monomers and oligomers. These polymers are particularly suitable for practical low-loss optical devices.

Although acrylate-derived polymers have demonstrated many attractive

properties, they do not possess the needed thermal stability (as high as 300°C) for some applications. In this regard, polyimide is a class of polymer with high thermal stability (above 300°C). The conventional polyimide used in semiconductor industry has poor properties and is unsuitable for use as optical material. In the past decades, several types of fluorinated polyimide have been developed by Amoco, General Electric, NTT and Hitachi.

Some poly(aryl ether) perfluorocyclobutyl(PFCB) are developed by Dow Chemical. They possess high performance and processibility. Other fluorinated dendrimers polymers and miscellaneous highly fluorinated polymers are developed by some groups. However, these polymers are still in the laboratory stage and some are not accessible.

Electo-optic (E-O) polymers have been intensively investigated and developed during the past decades. Due to the ever-increasing demand of faster switching speed and higher bandwidth in telecommunications, several companies including PacificWave, Lumera, and Lockheed Martin have tried to commercialize E-O modulators and switches based on E-O polymers. However, it is still difficult to obtain robust E-O polymers with both thermal stability and low optical loss.

1.3.3 Fabrication methods for polymer waveguides

Many fabrication methods and techniques have been developed for polymer waveguides. The flexible properties of the polymer material make it compatible with a variety of fabrication methods to achieve low-cost devices. Polymer films can be simply prepared by spin-coating process. Apart from conventional photoresist-based patterning, polymer waveguides can be fabricated by some replication techniques. These methods are more promising to simplify fabrication processes and reduce the cost of the devices. Soft-lithography and nanoimprint lithography (NIL) are two prototype processes to replicate polymer waveguides. Various replication methods originate from these two processes.

Another group of methods for fabrication of polymer waveguides are based on direct laser writing technology. These processes avoid the costly mask-making. Normally these methods, such as laser beam writing, proton beam writing, laser ablation, are used to fabricate straight and simple waveguide structures with large waveguide dimensions. In this section, several basic fabrication methods for polymer waveguides will be described.

1.3.3.1 Photoresist-based patterning
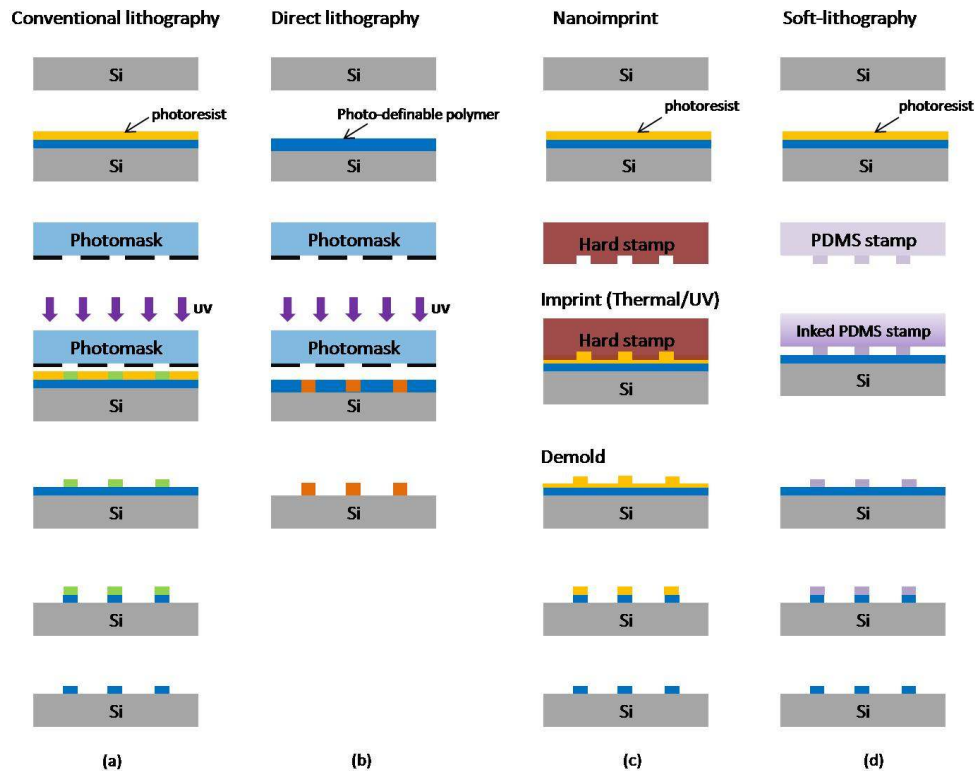
Figure 1. 3 Different methods to transfer patterns to the substrates

Standard semiconductor processing technology can be applied to fabricate polymer waveguides. The patterns are first transferred to the photoresist layer and then go through the RIE or ICP etching process (Figure 1. 3 (a)). However, these processes cope with the same problems as semiconductor lithography processes. Significant effort has to be made to optimize the waveguide fabrication process, especially for reducing the roughness of the vertical sidewall. ICP (inductively coupled plasma) etching has proven to produce better sidewall roughness than conventional RIE (reactive ion etching) etching for fabrication of polymer waveguides. As polymer material can also be synthesized as photo sensitive resist, the fabrication process can be simplified by direct lithography patterning and develop process as the process of photoresist (Figure 1. 3 (b)). For polymers in this application, the sidewall roughness depends on the exposure conditions as well as the properties of the polymer itself. Commercial photo-definable polymers like SU-8 and BCB (Benzocyclobutene) are commonly used to directly define polymer waveguides.

1.3.3.2 Direct laser writing

Other technologies based on direct laser writing or laser ablation are also explored to fabricate polymer waveguides. These fabrication technologies avoid costly mask fabrication. Large core polymer waveguides (e.g. 50μm×50μm) can be fabricated by excimer laser ablation [10, 11] . These methods are mostly dedicated to fabricate optical interconnections on printed circuit boards (PCB) [10, 11]. Optimization of the ablation parameters is required in order to achieve smooth side walls.

Polymer waveguides can also be directly written on photosensitive polymer films by UV-laser beam writing [12], proton beam writing [13, 14], or electronic beam writing [15]. The resolution of the UV-laser writing is limited by the focused beam size and normally on the order of micrometer. E-beam writing provides high resolution (sub-micrometer or even nanometer) but less efficient for high throughput.

1.3.3.3 Nanoimprint lithography

Apart from conventional lithography to transfer the pattern to the substrates, nanoimprint lithography (NIL) provides a low-cost and high-throughput technique for patterning polymer nanostructures. This technique was initially proposed and developed by the Chou group [16]. Since the NIL has the ability of patterning sub-10nm features [17], it has become one of the most promising technologies for nano-scale patterning.

The principle of nanoimprint lithography is quite simple. As shown in Figure 1.4(a), NIL uses a hard mold that contains nanoscale features on its surface to emboss into polymer material on the wafer substrates under certain temperatures and pressures. In the early days, thermo-plastic polymers, such as PMMA, PS and PC were used to do the imprint. The imprint temperatures are normally chosen at 70°C-80°C above the material's glass transition temperature (T_g) to allow the material to become viscous. Thus this imprint process is often carried out at high temperature and high pressure.

S-FIL (step-and-flash imprint lithography) is another imprint process using a transparent mold and low viscous polymer [18]. As the polymer is UV curable and has low viscosity, this imprint process is normally carried at low temperature and low pressure. Therefore this process is more preferable than NIL.
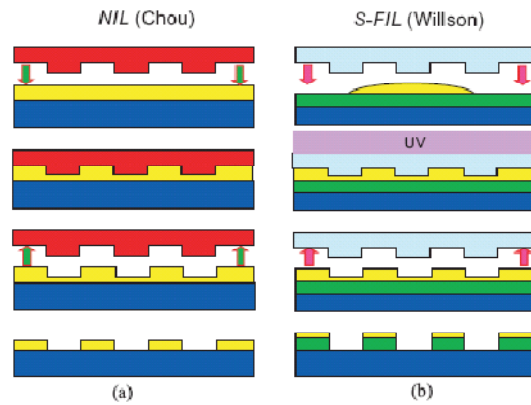
Figure 1. 4 (a) Nanoimprint lithography (NIL) (b)Step-and-flash imprint lithography (S-FIL)[19]

The hard mold is normally made in silicon, glass or metal by conventional lithography or e-beam writing. The imprint polymers can be thermal plastic or low viscous precursors that can be curable either thermally or by UV light. Novel imprint polymers, like fast thermally cured liquid resists or UV-curable resists are developed to facilitate fast room temperature nanoimprint [20]. However, this hard mold imprint also has its own problems and limitations. The molds and the substrates should be very clean. Otherwise, dust or particles between the molds can cause defects and non-uniformity of the imprinted pattern.

As nanoimprint technology offers high resolution and high throughput patterning, it is ideally suited for photonic device applications. J. L. Guo et al first use nanoimprint technologies to replicate PMMA polymer ring resonators (as shown in Figure 1. 5) [21] . Later, other groups also use S-FIL to imprint polymer waveguides[22] .
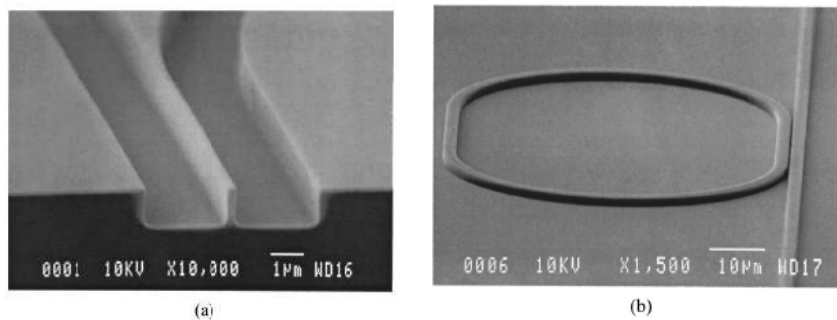
Figure 1. 5 (a) SEM picture of a SiO₂ mold with trench depth of 1.5 μm, which will replicate the polymer waveguides; the 200 nm thick narrow wall defines the gap distance between the two coupled waveguides. (b) Microring resonator in the shape of a racetrack fabricated by direct imprint technique [21].

The nanoimprint techniques also have a variety of applications in other fields. They have been applied to the fabrication of numerous electrical, optical and magnetic devices [23, 24]. Nano-imprint technology also plays an important role in micro- and nanofluidic devices for biological and lab-on-chip applications [25, 26].

1.3.3.4 Soft-lithography

Soft-lithography is a fabrication technology based on replica molding for micro- and nano-fabrication. This non-lithographic technique offers a lot of advantages over traditional photo-lithography. The unique advantages of this process are that it is cost effective, straightforward to apply and accessible to a wide range of applications.

The fabrication process involves using an elastomeric stamp or mold. The most commonly used flexible molds are PDMS (Polydimethylsiloxane) molds. As shown in Figure 1. 6, the PDMS is poured over the surface of a master mold, then cured and peeled off. The master molds can be fabricated by conventional lithography, micromachining, or e-beam writing. The flexible PDMS molds provide a lot of advantages over hard silica or glass molds. The PDMS molds provide a surface that has low interfacial free energy (~21.6 dyn/cm) and good chemical stability; most molecules or polymers being patterned or molded do not adhere irreversibly to, or react with, the surface of PDMS. The PDMS membrane also passes gas easily, and this facilitates the imprint of solvent involving polymers. The PDMS material has good thermal stability (up to 186°C in air). The PDMS is optically transparent down to 300 nm. As the PDMS molds are flexible, they can make conformal contact with surfaces and can be released easily from rigid masters or from complex, quasi-three-dimensional structures that are being molded. Once a master mold is fabricated, it can be used many times. And the PDMS molds are cheap enough to be disposable. Therefore this method provides a very cost effective way to replicate structures.

However, some issues and problems still exist in soft-lithography techniques. This technique can replicate structures with resolution from 100nm to 100μm. Some groups are trying to increase the resolution of the replication structures to below 100nm[27]. PDMS shrinks by 1% upon curing and the cured PDMS can be readily swelled by a number of nonpolar organic solvents such as toluene and hexane. The elasticity and thermal expansion of PDMS make it difficult to get high accuracy in registration across a large area and may limit the utility of soft lithography in multilayer fabrication or nanofabrication. The softness of the PDMS limits the aspect ratio of microstructures in PDMS. When the aspect ratio (*h/l*) is too high or too low, the elastomeric character of PDMS will cause the microstructures in PDMS to deform or distort and generate defects in the pattern (Figure 1. 6). It is proven that the aspect ratio of the relief features in PDMS must be between 0.2 and 2 in order to obtain defect-free stamps or molds [28].
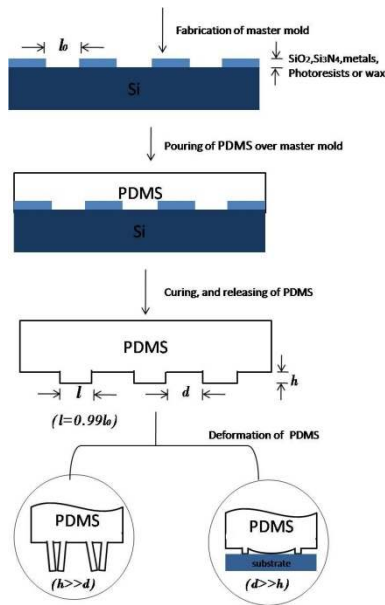
Figure 1. 6 The procedure for fabricating PDMS stamps from a master having relief structures on its surface [29]

There are several techniques based on soft-lithography, like microcontact printing (μCP) (as shown in Figure 1. 3 (d)), replica molding (REM), microtransfer mold (μCM), micromolding in capillaries (MIMIC), and solvent-assisted micromolding (SAMIM) [29].

As the dimension of the polymer waveguides is on the micrometer scale, soft-lithography perfectly suits the mold resolution requirements. A lot of methods based on soft-lithography have been explored to fabricate polymer waveguides. The most commonly used methods for fabrication of polymer waveguides are based on UV-embossing methods [6, 30] as shown in Figure 1. 7. One important aspect of this method is to control the thickness of the residual layer [31].
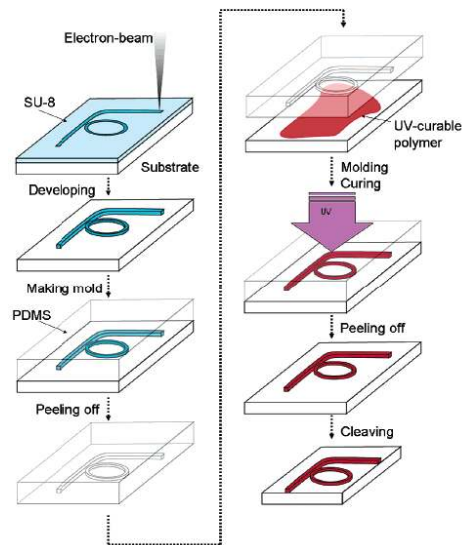
Figure 1. 7 Commonly used fabrication process for replicating polymer waveguides [32]. (The left column shows the fabrication of the soft PDMS mold. The right column shows the fabrication of the polymer waveguides.)

Various other methods based on soft-lithography are used to replicate polymer waveguides. The fabrication process also depends on the properties of the imprinted polymer. A. Flores et al use a vacuum-assisted microfluidic technique to fabricated polymer waveguides[33] (as shown in Figure 1. 8). W. C. Chuang et al use a replication method (as shown in Figure 1. 9) to replicate polymer waveguides and grating filters[34, 35].
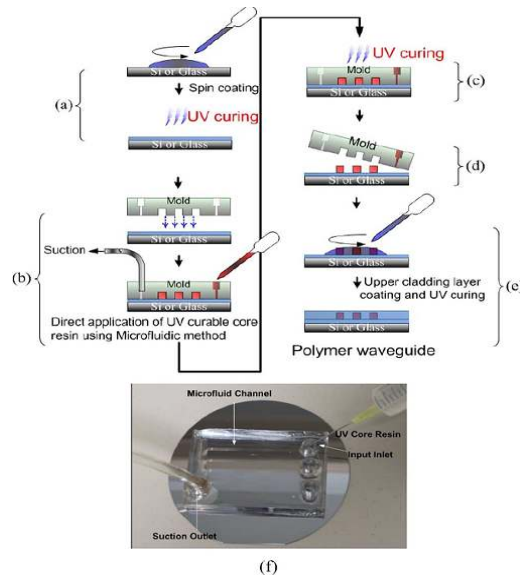
Figure 1. 8 Process flow for device replication via vacuum-assisted microfluidic technique [33]. (a) UV curable cladding layer is spin coated upon desired substrate. (b) After placing PDMS stamp over substrate, UV curable core resin drops are placed through an inlet hole. (c) Once channels are filled, the resin is cured through UV irradiation.(d) Stamp is peeled off to reveal the replicated master pattern. (e) Upper cladding is coated and cured if desired. (f) Top view of the PDMS microchannel structure along with the inlet and outlet orifices of the stamp.
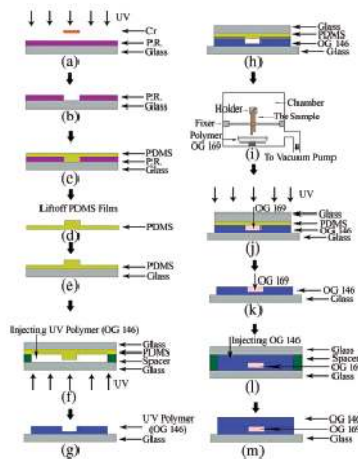
Figure 1. 9 Fabrication of a buried waveguide structure by a replication method [34]: (a)UV exposure of photoresist, (b) photoresist mold, (c) PDMS was poured into the photoresist mold, (d) PDMS mold, (e) PDMS was put on a glass substrate, (f) UV cure epoxy was injected into the space, (g) a hardened epoxy formed the cladding layer of the polymer waveguide, (h) forming a rectangular tunnel, (i) OG169 epoxy was injected into the channel,

(j) the epoxy in the tunnel was then cured by exposing the UV light, (k) the cover glass and the PDMS layer were removed from the sample, (l) OG146 epoxy was injected into the channel, (m) final waveguide.

1.3.4 Polymer-based devices and their applications

1.3.4.1 Optic interconnects

Optical interconnection methods for large data transmission have been studied to overcome electronic interconnects bottle-necks, such as data transmission speed, packaging size of electronic circuits, and power dissipation. These interconnects for computer platforms include not only on-chip interconnects, like chip-to-chip or intra-chip interconnects, but also off-chip interconnects, like interconnects on backplanes, boards and multi-chip modules (MCMs). As polymer waveguides offer a lot of advantages with CMOS compatibility and manufacturability, it has been broadly accepted as the most promising low cost electronic-friendly media for high-speed optical interconnects.

Optical interconnects of polymer waveguides between electro-optical (EO) components on printed circuits boards (PCBs) (as shown in Figure 1. 10) are commonly studied. Apart from fabrication by conventional photo-lithography or diamond blade cutting, soft-lithography and laser ablation are also used to develop low-cost interconnects[10, 36].
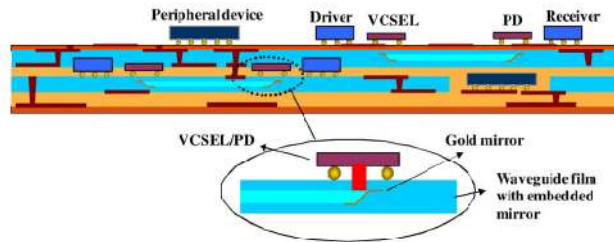
Figure 1. 10 Schematic configuration of multilayered optical-electrical hybrid PCB [36]

1.3.4.2 Planar optical components for WDM system

1.3.4.2.1 Passive devices

The simplest passive optical component is the splitter and combiner. As polymer splitters can be produced inexpensively in large volumes and high-throughput by simple stamping or embossing, fabrication of basic passive polymer splitters, typically 1×8 to 1×32 splitters are explored.

Polymer-based arrayed waveguides gratings (AWG) are widely studied as

cost-effective alternative to silica-based counterparts. As polymer materials have large thermo-optic coefficient, the polymer-based filters or AWGs are sensitive to the ambient temperature. However, athermal AWGs can be easily produced in polymer by matching the CTEs (coefficients of temperature expansion) of the substrates and thermo-optic coefficients of the materials. This type of device is needed for FTTx signal distribution in WDM passive optical networks (PON).

1.3.4.2.2 Thermo-optical dynamic devices

As polymer materials have large thermo-optic coefficients and low thermal conductivity, they are ideal candidates for thermo-optic dynamic devices. The early commercialization of polymer waveguide technology came with the introduction of thermo-optic switches. Thermo-optic N×N switches can be interferometric switches based on directional couplers or Mach-Zehnder interferometers (MZIs), or they can be digital optical switches (DOS) based on X junction, or Y junction. Dupont Company has produced commercially available 8×8 strictly non-blocking DOS-based switches [2]. In addition to switches, VOAs (variable optical attenuators) and tunable couplers that take advantages of polymers' large thermo-optic coefficient are also pursued in recent years [37].

As Bragg gratings are basic components for WDM systems, optical filters based on Bragg gratings in planar polymers have been widely explored in recent years[38, 39]. A variety of techniques such as molding, stamping, photochemical processing are used to produce polymer Bragg gratings. The large dn/dT in polymer allows tuning over a large wavelength range at moderate temperature.

1.3.4.2.3 Electro-optical dynamic devices

As polymer materials can offer high electro-optic (EO) coefficient and low electric constants compared to conventional inorganic materials, they have been proposed for electro-optic applications, especially for fast EO switches and modulations. Many labs and companies are dedicated to developing high-speed and low-voltage modulators for the last two decades [5, 40]. The major barrier for the commercialization of polymer modulators has been reliability. The most common way to achieve an EO polymer is adding a high concentration of nonlinear, optical, organic chromophore to a polymer. These polymers with EO molecules have to be poled under high external fields to achieve non-centrosysmmetry. Their long-term orientation stability is limited by the relaxation rate of the chromophores, especially in micro-and nano-structured devices. Therefore the EO coefficients of these polymers tend to reduce over time. One way to overcome the limitation of poled polymer is to use organic non-linear optical crystalline materials, which offer a stable chromophore orientation. However, these materials have problems in production and processing of single crystals. Recently, crystalline thin films are achieved [41] and EO modulated single-crystalline organic microring resonators are fabricated[42].

1.3.4.2.4 Active devices

Active polymer optical components include amplifiers, sources and detectors. The

most widely used polymer laser in the visible wavelength range is based on dye-doped polymers [43]. Organic light-emitting diodes (OLEDs) utilizing fluorescent dyes or conjugated polymers have also attracted great interest because they can emit light at all visible wavelengths with high efficiency [44]. Doping rare-earth ions like erbium or neodymium into polymer materials as active elements to provide amplification is widely studied for infrared communication windows.

1.3.4.3 Polymer waveguides for sensors

Planar optical waveguides based sensors are extensively studied in recent years. External parameters, such as temperature, pressure, refractive index change can cause modulation of light traveling within the optical waveguides. Thus the optical waveguides based sensors are useful in industrial, medical, environmental and military applications.

Polymer-based waveguide devices allow achieving low-cost optical devices, which ideally meets disposability requirements in bio-sensing and bio-chemical applications. Typical optical waveguide sensors utilize evanescent waves to probe the presence of analytes at the sensor surface or in the surrounding medium by detecting the effective index change. Such a sensing scheme is able to eliminate the need of fluorescent labeling and render label-free detection. Basic microring resonators have been applied to detect glucose concentration and surface sensing small proteins [3]. Recently, polymer ring resonators are used to detect high-frequency ultrasound as acoustic waves irradiating the polymer ring waveguide can induce strain to deform the waveguide dimensions and change the refractive index of the waveguide [45].

Other polymer optical waveguide-based sensors are also explored. Mach-Zehnder interferometers (MZI) are used to detect pressure[46]. Microring resonators made from Chromophore-containing polymer (EO polymer) are utilized to detect electric fields [4]. Some polymer waveguide based sensors are investigated to detect gas[47].

1.3.4.4 Integrated planar lightwave circuits

No single material system can achieve every function in the integrated circuits. Integrating multi-material devices to achieve highest performance is commonly applied in integrated planar lightwave circuits. Planar polymer circuits can be machined to form slots which allow chips and films of other materials being inserted. Therefore polymer circuits provide a hybrid integration platform for a variety of materials. Dupont Company has been dedicated for years to produce a polymer-based platform with hybrids of different components[2] .

Chapter 2 Development of Novel Polymer Materials

2.1 Introduction

The polymer-based planar lightwave circuits (PLCs) have advantages over their silica-based counterparts in terms of cost and tunablility. When the polymers are synthesized and processed properly, they offer high performance: transparent in the communication windows; low birefringence; wide controllability of the refractive index contrast (larger than that achievable in silica); tunablility (the thermo-optic coefficient is one order larger than that of silica); high thermal stability; ease of hybridization; high yields and low cost. Therefore a lot of effort has been devoted to develop high performance optical polymers in recent years [9, 48, 49].

Many classes of polymers like acrylates, polyamides, polycarbonates, polyesters, siloxanes, epoxy resins, sol-gels have been used in integrated optics [50-52]. However, some of the polymer properties are still unsatisfactory for some applications. Reducing the optical loss in the infrared window and enhancing the thermal stability of the polymer has always been a focus in the development of polymers for optical waveguide applications.

In this chapter, we introduce two kinds of polymer developed by Dalian University of Technology. One is a kind of inorganic-organic hybrid polymer named PSQ-L. The other is a kind of thermal plastic named PPESK. Both of them have high thermal stability. The optical properties and other properties of these two polymers have been investigated and are described here.

2.2 PSQ-L series Polymer

Polymer PSQ is a kind of inorganic-organic hybrid polymer (also known as polysiloxanes)[53, 54]. By combining the characteristics of the inorganic glass and the organic polymer, the silicate-based inorganic-organic hybrid polymer provides many advantages over traditional pure inorganic glass or organic polymer films. For instance, the hybrid material overcomes two main drawbacks of inorganic glass films: low mechanical flexibility and high temperature processing requirement (generally above 600°C). The hybrid material also provides a lot of advantages over pure organic polymer coatings, such as low optical propagation loss, extremely excellent chemical and thermal stability and good compatibility with different substrates like silicon wafer, quartz, and printed circuit board (PCB) [55, 56]. In addition, the optical properties of the hybrid materials (such as the refractive index) can be widely tuned through a combination of organic groups to modify their structures.

Based on these advantages, the liquid, UV-curable, index tunable, inorganic-organic hybrid polymer PSQ-L is synthesized. The general properties of the polymer PSQ-L are listed in Table 2. 1. The details of the PSQ-L properties are investigated in the following section.

Table 2. 1 Properties of Polymer PSQ-L

		PSQ_LL	PSQ_LH
Liquid	Colour	Colorless	
	Solubility	Soluble in methanol, ethanol, acetone, etc.	
	Viscosity (mPa·s@25°C)	~110	~140
	UV-exposure (in N_2)	120s, >2500mJ/cm^2 (180°C，2h and then 200°C, 2h)	
Film	Refractive Index @1310nm	1.456	1.517
	Refractive Index @1550nm	1.454	1.515
	Birefringence (n_{TE}-n_{TM})	<0.0005	<0.0005
	Thermo-optic coefficient (/^{o}C)	-2.2×10^{-4}	-2.4×10^{-4}
	Propagation Loss (Measured from slab waveguide)	not measured	0.8~0.9dB/cm@1550nm
		not measured	0.2~0.3dB/cm@1310nm
	Glass Transition Temp. (Tg)	not detectable	not detectable
	Degradation Temp. (1% weight loss)	322 ±10 ^{o}C (in air)	303 ±10 ^{o}C (in air)
		370 ±10 ^{o}C (in N_2)	343 ±10 ^{o}C (in N_2)
	Film Surface Roughness (AFM)	<0.5nm	<0.5nm

2.2.1 Synthesis of Polymer PSQ-L

Sol-gel processing offers a low temperature route to the development of silicate-based inorganic-organic hybrid polymer. The sol-gel reaction is a synthetic route by which metal-alkoxide monomers, silane-alkoxides in particular, are converted to ceramic/glassy materials by a sequence of hydrolysis and condensation reactions. The hydrolysis stage (Eq.(2.1)) involves reaction with water, i.e. catalyzed by an acid or a base, and formation of alcohol. The condensation stage (Eq.(2.2),(2.3)) involves formation of Si-O-Si bonds and results in siloxane macromolecules and small condensates of water or alcohol [57]. The Si-OH in the material easily condenses with -OH groups on glass, Si wafer and other inorganic material surfaces to form a laterally crosslinked layer attached to the surface by ether linkages and leads to significant enhancement of the interface strength. The Si-OH can be further eliminated by heat .

$$\equiv Si-OMe+HO-Si \longrightarrow \equiv Si-O-Si+MeOH \qquad (2.1)$$

$$\equiv Si - OH + HO - Si \equiv \rightleftharpoons Si - O - Si \equiv + H_2O \qquad (2.2)$$

$$\equiv Si - OMe + H_2O \rightleftharpoons Si - OH + MeOH \qquad (2.3)$$
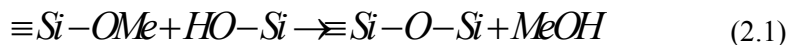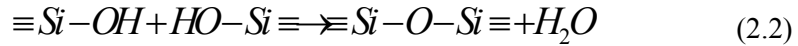
PSQ-L were synthesized by a sol-gel process from monomer methyl trimethoxysilane (MTMS), phenyl trimethoxysilane(PhTMS), and 3-(methacryloxy)propyl trimethoxysilane (MAPTMS). The optical properties of the three monomers are listed in Table 2. 2. The refractive index of the polymer PSQ-L can be adjusted by changing the molar ratio of the two monomers of MTMS and PhTMS. The high index polymer PSQ-LH and low index polymer PSQ-LL is synthesized with different molar ratio of MTMS and PhTMS. Monomer MAPTMS is added into synthesis for realizing UV-curing since it contains C=C bonds. As the monomer MAPTMS has more C-H bonds than the other two monomers, which can cause extra absorption loss in the infrared window, the molar concentration of MAPTMS is controlled between 10%-20%.

Table 2. 2 Characteristics of the precursors for synthesis of PSQ-L

	Refractive Index (20ºC)	Optical Loss (dB/cm,1310nm)	Optical Loss (dB/cm, 1550nm)	Number of C-H
MTMS	1.365	-----	-----	12
PhTMS	1.4734	0.18	0.52	14
MAPTMS	1.430	0.38	1.16	21

Figure 2. 1 shows the synthetic route of PSQ-L. Silica precursors (MTMS, PTMS, MAPTMS), in the presence of water at pH=1.0, undergo a hydrolysis reaction and subsequently a condensation reaction (

Figure 2. 1). For a hydrolytic sol-gel process, when the reaction temperature and time and the pH value of the water are fixed, the chemical structure and viscosity of the product are mainly determined by the molar ratio of water to silica precursors (set as R). Table 2. 2 shows the viscosity of PSQ-L synthesis with different water ratio. To obtain liquid resins with appropriate viscosity for spin-coating and UV curing, PSQ-LH with water ratio (R) of 1.2 and PSQ-LL with water ratio (R) of 1.3 were prepared respectively for film properties test. When the R value was higher than 1.4, the viscosity of the hybrid material would be too high to spin-coat at room temperature. While the R was lower than 1.0, the molecular weight and viscosity of the material would be too low to cure by UV light. PSQ-LH with higher PTMS feed exhibits higher viscosity (η=359 mPa·s) and the resulting film possessed higher refractive index compared with PSQ-LL with lower PTMS ratio. And the contents of MAPTMS in the resins were not more than 15 mol% due to many C-H bonds in MAPTMS.
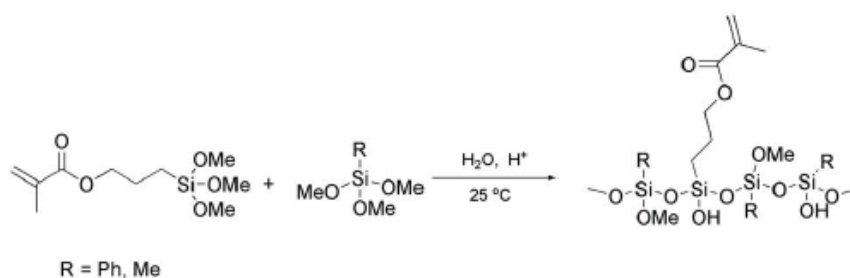
Figure 2. 1 Synthetic route of PSQ-L based on sol-gel process

Table 2. 3 Properties of PSQ-L synthesized with different monomer molar ratio

	PTMS/MTMS /MAPTMS (molar ratio)	R	Si-OMe Content[1] (%)	Molecular Weight[2] Mn	Distribution of Molecular Weight[2] PD	Viscosity η (mPa·s)
PSQ-LH1	80/5/15	1.0	36	9,660	1.10	69
PSQ-LH2	80/5/15	1.1	31	12,540	1.11	132
PSQ-LH3	80/5/15	1.2	27	14,150	1.13	359
PSQ-LH4	80/5/15	1.3	23	15,620	1.11	566
PSQ-LL1	10/75/15	1.1	28	5,660	1.12	54
PSQ-LL2	10/75/15	1.2	23	11,790	1.10	115
PSQ-LL3	10/75/15	1.3	18	16,260	1.06	166
PSQ-LL4	10/75/15	1.4	14	22,160	1.08	221
[1]-Calculated by ^{1}H-NMR. [2]-Determined by GPC						

2.2.2 Curing process of polymer PSQ-L films

By bonding photosensitive organic groups in the material, usually with unsaturated C=C bonds, the hybrid materials can be polymerized upon UV light irradiation, which allows direct patterning waveguide structures on planar substrate. The photo-initiator PI-184 (1-hydroxycyclo-hexylphenylketone) (0.8%-2%) was mixed into the liquid polymer PSQ-L to achieve photo-curing. PSQ-L can be cured by a hybrid polymerization composed of free radical polymerization of C=C from MAPTMS (Figure 2. 2), and condensation reaction of Si-OH (Figure 2. 3).
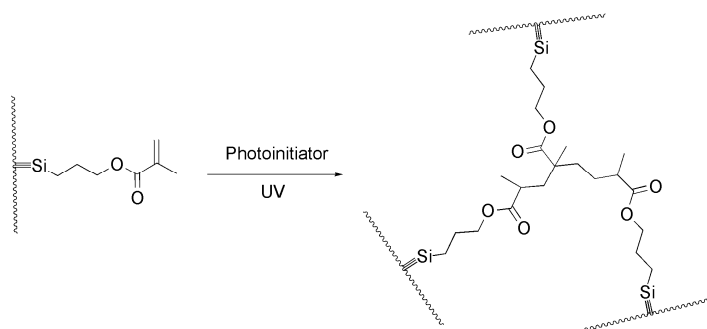
Figure 2. 2 Curing process of methacrylic groups upon UV exposure or heating
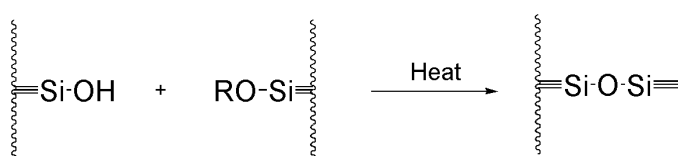
R=H or Me

Figure 2. 3 Curing process of Si-OH upon heating

The curing process of the PSQ-L film consists of two steps: first, the film is illuminated under UV light ($>2500mJ/cm^2$) during 120s (better in nitrogen); then the film is heated at 180°C for 2 hours and at 200°C for 2 hours. Upon UV exposure and in the presence of the photo-initiator PI-184, a free radical polymerization could easily occur and most C=C reacted after 120 s as shown in Figure 2. 4.

The heat treatment is carried out after the UV exposure. The residue of Si-OH in the films further is condensed with Si-OCH$_3$ or Si-OH at high temperature to form a glass-like material. The change of Si-OH and Si-OCH$_3$ during this stage was also measured by infrared spectroscopy, as shown in Figure 2. 5. The condensation degree was influenced by the thermal curing temperature. The Si-OH content decreased with increasing curing temperature, and when the temperature was up to 200 °C for 2h, there were few Si-OH left in the films as the characteristic absorption bands of Si-OH (3400cm^{-1} and 960cm^{-1}) disappeared. Optical loss would decrease as the Si-OH groups content decreases, and experimental results also prove this in the following section.
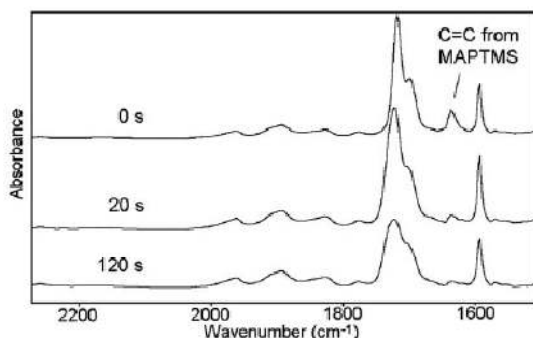
Figure 2. 4 FTIR (Fourier transform infrared spectroscopy) of PSQ-LH films after UV exposure for 0s, 20s and 120s in nitrogen.
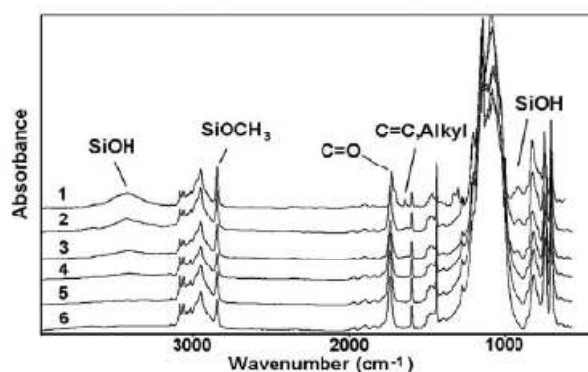
Figure 2. 5 FTIR (Fourier transform infrared spectroscopy) of PSQ-LH films with different curing conditions: 1) after UV exposure for 120 s; 2), 3), 4), 5), 6) UV exposure for 120 s, then thermal cured at 180°C, 190°C, 200°C; 210°C; 220°C for 2h respectively.

2.2.3 Film properties of polymer PSQ-L films

2.2.3.1 Film making

The polymer PSQ-L is pure liquid (solvent free). The polymer PSQ-L films are prepared by a spin-coating process. Since no solvent is involved in the spin-coating step, solvent related film defects can be avoided. The polymer PSQ-L films are prepared by spin-coating PSQ-L on bare silicon substrate. The bare silicon wafer is first washed by acetone, IPA and DI water to remove the organic materials on top.

Then it is cleaned by piranha solvent (mixing H_2SO_4 and H_2O_2 in a volume ratio of 4:1) for hydrophilic treatment of the silicon substrate. The piranha washing step is necessary for the polymer to have good adhesion to the silicon substrate.

The thickness of the PSQ-L films are measured by the prism coupler (SPA-4000) (Appendix A). The thickness of the PSQ-L film depends on several factors: the viscosity of the material, the spin-coating time and the spin-coating speed. For PSQ-L material of a certain viscosity, the thickness of the film tends to be a constant value after a certain spin-coating time (Figure 2. 6). The thickness of the polymer film can be controlled by adjusting the spin-coating speed (Figure 2. 7). The viscosity of polymer PSQ-Ls in Figure 2. 6 and Figure 2. 7 is between PSQ-Ls1 and PSQ-Ls2 in Table 2. 3.
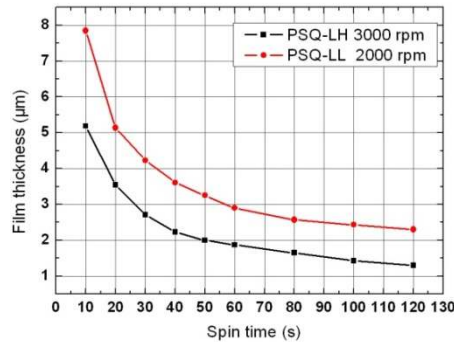
Figure 2. 6 Film thickness of PSQ-L versus spin-coating time
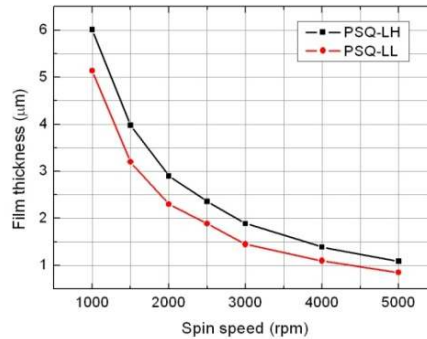
Figure 2. 7 Film thickness of PSQ-L versus spin-coating speed (spin-coating time is 60s)

2.2.3.2 Surface properties of polymer PSQ-L films
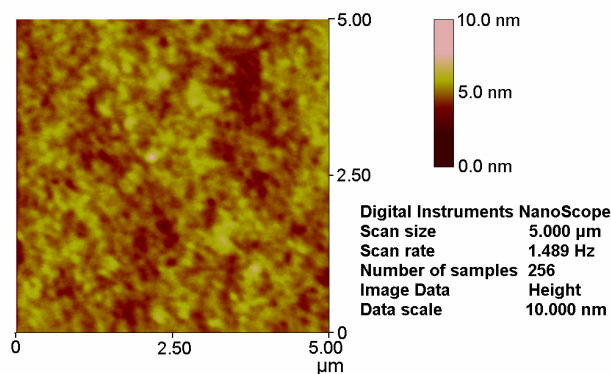
Figure 2. 8 AFM image of a PSQ-LL film spin-coated on Si wafer (The film was exposed 120s to UV in N_2 and thermally cured at 180°C for 2h and at 200°C for 2h)

Figure 2. 8 shows the AFM image of a PSQ-LL film spin-coated on silicon wafer and cured as outlined above (exposed 120s to UV in N_2 and thermally cured at 180°C for 2h and at 200°C for 2h), with a film thickness of 6.75 μm. The average surface roughness (Ra) and the root mean square roughness (Rq) (as shown in Table 2. 1) of PSQ-LL were 0.406 nm and 0.521 nm, respectively. PSQ-LH film gave a similar result. Obviously, the surface roughness of the PSQ-LL and PSQ-LH films obtained under the present processing condition were sufficiently small (less than 0.5 nm) for optical waveguide applications.

2.2.4 Optical properties of the PSQ-L films

2.2.4.1 Refractive index tuning

The refractive index of the polymer films is measured using a prism coupler (SPA-4000) (see Appendix A). As mentioned before, the index of the polymer PSQ-L can be tuned by controlling the molar ratio of the monomers during synthesis. In our case, we synthesized two types of PSQ-Ls: the one with a high index is called PSQ-LH; the one with a low index is called PSQ-LL. The refractive index of PSQ-L can be tuned between PSQ-LH (around 1.52@1550nm) and PSQ-LL (around 1.45@1550nm) by blending the two polymers with corresponding ratio (Figure 2. 9). A good linear relationship, between the refractive index of PSQ-L films and the PSQ-LL weight content was observed in Figure 2. 9. The refractive index of PSQ-L was perfectly fitted as follow,

$$n_{1310nm,TE}(x) = 1.5220 - 0.0727x$$
$$n_{1550nm,TE}(x) = 1.5200 - 0.0720x$$

(2.4)

Where x is the weight content of the mixed polymer.

The birefringence of the polymer PSQ-LH and PSQ-LL films is small (less than 0.005 for both TE and TM mode). The birefringence of PSQ-L (mixed with PSQ-LH and PSQ-LL) is also below 0.005.
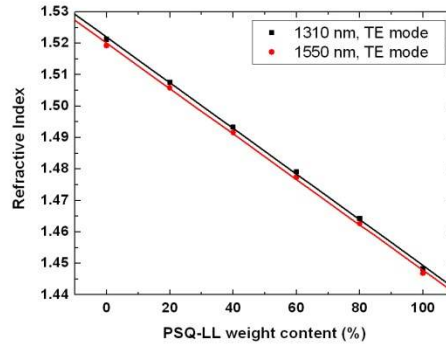
Figure 2. 9 Refractive index tuning of PSQ-L by mixing PSQ-LH and PSQ-LL with different ratios

2.2.4.2 Thermo-optic coefficient of polymer PSQ-L film

One fundamental difference between polymer materials and conventional inorganic materials (such as glass) is that they have large negative thermo-optic coefficient. The thermo-optic coefficient is extracted by measuring the refractive index of the film at different temperature. The cured PSQ-L films exhibit large thermo-optic coefficient (dn/dT): $-2.4 \times 10^{-4}/°C$ for polymer PSQ-LH at both 1310nm and 1550 nm; $-2.2 \times 10^{-4}/°C$ for polymer PSQ-LL at both 1310nm and 1550 nm. Figure 2. 10 shows the dependence of the refractive index of PSQ-LH and PSQ-LL film on the temperature.
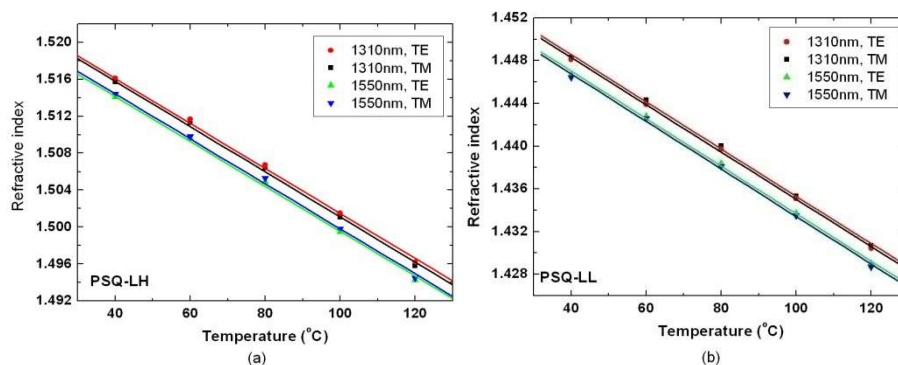
Figure 2. 10 The refractive index of PSQ-LH and PSQ-LL films at different temperatures
(a) PSQ-LH film (b)PSQ-LL film

2.2.4.3 Optical loss of PSQ-LH films

The optical loss in the communication windows is a key property of polymer materials for photonics applications. The optical loss of PSQ-L film is measured by the immersion oil method [58]. The PSQ-LH film is prepared on the silica glass substrate to form a slab waveguide. In the loss measurement, light is coupled into the slab waveguide from a prism. After propagating a certain distance in the film, the light is coupled out from the waveguide to a high-index liquid oil. The output power is measured as a function of propagation distance and thus the loss can be extracted from the linear fit of the data. Figure 2. 11 shows the loss measurement of PSQ-LH film by immersion oil technique. The film has a thickness of 8.31μm.

The PSQ-L film for loss measurement is prepared on a polished silica glass. The PSQ-L film has a thickness of 4-10μm to allow most light to be confined in the polymer film. As mentioned before, the roughness of the polymer PSQ-L film surface is small enough so that surface roughness loss can be neglected. The spin-coating process proceeds in the clean room and the material is filtered by a 0.22μm membrane filter to avoid large particles in the film. Therefore the optical loss of the PSQ-LH film is a good approximation of absorption loss of PSQ-LH film. The optical loss of the low index polymer PSQ-LL is not measured since the index is very close to that of silica glass and that PSQ-LL cannot form a slab waveguide on silica glass. The extracted loss value of the PSQ-LH film is reproducible for the film with the same curing condition. The loss measurement experiments have been done repeatedly to prove this. The optical loss of the PSQ-LH film is about 0.2~0.3dB/cm @1310nm and 0.8-0.9dB/cm @1550nm after thermal curing at 180°C for 2h and at 200°C for 2h. The influence of the curing conditions on the optical loss of the PSQ-L film is discussed in the following section.
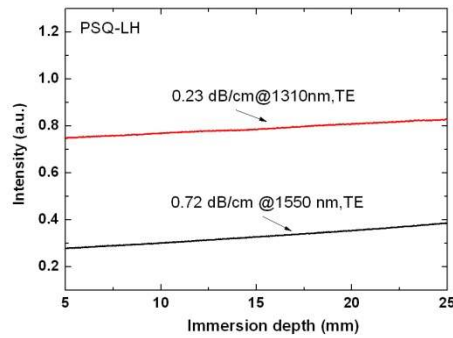
Figure 2. 11 Loss measurement of PSQ-LH slab waveguide by immersion oil technique (The film was exposed 120s to UV in N_2 and thermally cured at 180^oC for 2h and at 200^oC for 4h)

2.2.4.4 Influence of the curing condition on optical loss of

PSQ-LH films

The absorption loss of PSQ-LH in the infrared window mainly arises from vibration overtones of the aliphatic and hydroxyl groups existing in the material. The hydroxyl groups (-OH) absorption effects are more prominent at the higher wavelengths, with especially a strong absorption at the 1550nm wavelengths.

By adjusting the curing condition to further passivate the residual hydroxyl groups in the material, the optical absorption loss can be reduced. We found that higher post-baking temperature and longer heating time tend to decrease the optical loss both at 1310 nm and 1550 nm, but especially at 1550 nm.

Figure 2. 12 shows the dependence of the optical loss on the thermal curing temperature. It can be seen that, as the heat treatment temperature rises from 190 to 210 ^{o}C for 2 h respectively, the optical loss dropped from about 1.3 to 0.7 dB/cm at 1550 nm. The decrease in optical loss at 1550 nm is attributed to the reduction of Si-OH in the films as has been demonstrated previously by the FTIR analysis. As the temperatures arose above 210 ^{o}C, optical losses didn't decrease anymore at 1550 nm since the Si-OH contents in the films were already very low. At 1310 nm, the optical loss didn't show obvious drop as the thermal curing temperature rose from 180 ^{o}C to 220 ^{o}C since the absorption effect of Si-OH at 1550 nm is far stronger than at 1310 nm [59].

The relation between optical losses and thermal curing time at 200 ^{o}C is shown in Figure 2. 13. It is obvious that longer thermal treatment time also tends to decrease the optical loss both at 1310 nm and 1550 nm. The optical loss at 1550 nm is reduced from about 0.9 to 0.7 dB/cm while the loss value at 1310 nm is reduced between 0.3 and 0.2 dB/cm as the thermal curing time increased from 2 to 5 h. The condensation of

Si-OH tends to be more complete as the thermal curing time is increased. Figure 2. 11 describes the optical losses of a PSQ-LH film at 1310 nm and 1550 nm with thickness of 8.31 μm, which were thermally cured at 180 ^{o}C for 2h and at 200 ^{o}C for 4 h after UV exposure. In practise, long thermal curing time may cause some problems for the fabrication process. When thin films (with a thickness of 1-3μm for the core) are used, a curing condition of 180 ^{o}C for 2h and 200 ^{o}C for 2h after UV exposure is chosen.
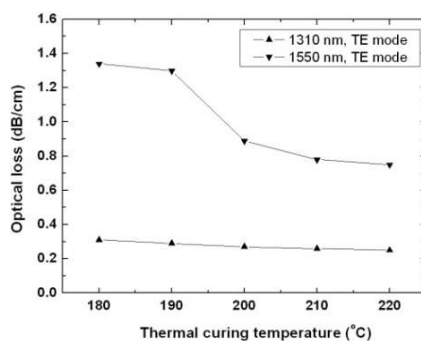
Figure 2. 12 Optical losses of PSQ-LH films under different thermal curing temperature (The films were exposed 120s to UV in N₂, baked at 180 ^{o}C for 2h and then cured at 180 ^{o}C, 190 ^{o}C , 200 ^{o}C, 210 ^{o}C and 220 ^{o}C for another 2h, respectively)
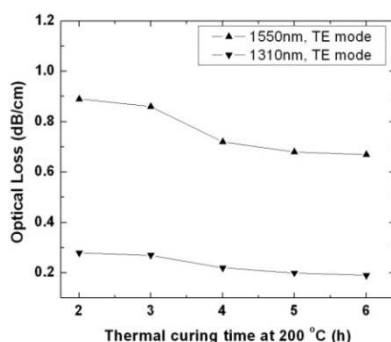
Figure 2. 13 Optical losses of PSQ-LH films with different thermal curing time at 200 ^{o}C (The films were exposed 120s to UV in N₂, baked at 180 ^{o}C for 2h and then cured at 200 ^{o}C for 2h, 3h, 4h, 5h, and 6h, respectively)

2.2.4 Thermal properties of the PSQ-L films

Polymer PSQ-L has excellent thermal stability both in inert atmospheres and in air. Figure 2. 14 shows the Thermo-Gravimetric Analysis (TGA) data of the cured PSQ-LH and PSQ-LL materials. The TGA results indicate that the thermal decomposition represented by a 1 % weight loss did not occur below 303 ^{o}C for PSQ-LH film and 322 ^{o}C for PSQ-LL film in air, and 343 ^{o}C for PSQ-LH and 370 ^{o}C for PSQ-LL film in nitrogen. These results reveal excellent thermal stability of the PSQ-L materials. The glass transition temperature (Tg) of PSQ-L is higer than the 1% decomposition temperature. The Tg of PSQ-L is not detectable because the material start to decompose before the material comes to the glass transition temperature.

(a)   (b)
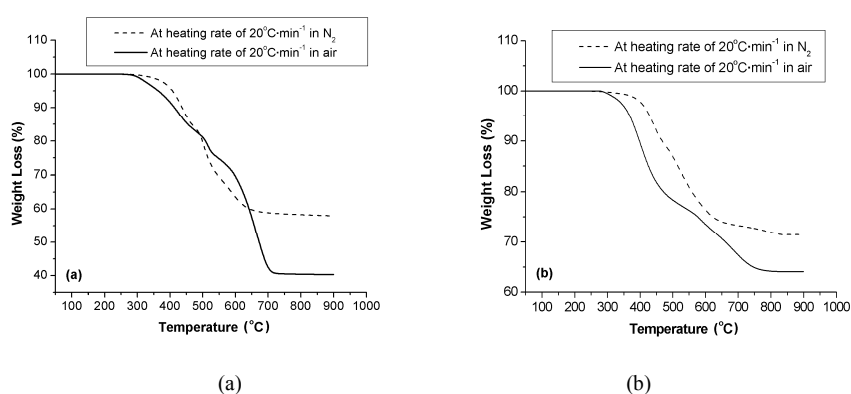
Figure 2. 14 TGA data of PSQ-LH and PSQ-LL films in N$_2$ and air
(The samples were exposed 120s to UV in N$_2$, baked at 180°C for 2h and then cured at 200°C
for 2h) (a) PSQ-LH (b)PSQ-LL

2.3 PPESK series Polymer

Polymer poly (phthalazinone ether sulfone ketone) (PPESK) is a kind of thermoplastic material. Compared with traditional thermoplastics (such as PEEK, PES, PEI), the poly(phthalazinone ether sulfone ketone) (PPESK) shows better properties in mechanical strength, chemical resistance and thermal stability (T_g:263–305°C). It has been widely used in composite materials, membranes, insulating coating and paint [60, 61]. Moreover, it can be dissolved in polar aprotic organic solvents, such as NMP (*N,N'*-dimethylacetamide, *N*-methyl-2-pyrrolidinone) and chloroform, which facilitates film making.

We apply this home-made polymer to optical applications. The optical properties of the PPESK films are investigated first. The properties of this polymer

need to be improved for further device fabrication. Since PPESK is not a cross-linked polymer, cross-linked PPESK is synthesized to strengthen the chemical strength of the polymer. To further reduce the material absorption loss in the infrared window and change the solubility of the polymer in other solvents, fluorinated PPESKs are synthesized. In this section, the film and optical properties of PPESK films are first investigated. During the PhD work, the synthesis process of fluorinated PPESK and cross-linked PPESK was not yet mature.

2.3.1 Properties of basic PPESK

2.3.1.1 Material synthesis

Poly(phthalazinone ether sulfone ketone) (PPESK) was synthesized by copolymerization of monomer DHPZ (4-(4-Hydroxyphenyl)-2,3-phthalazin-1-one), DFK(4,4'-difluorobenzophenone), and DCS(4,4'-Bis(4-chlorophenyl) sulfone). If synthesized without monomer DFK, the polymer comes to Poly(phthalazinone ether sulfone) (PPES). The molecular structure is shown in Figure 2. 15. The DFK content can enhance the solubility of the polymer while the DCS content can enhance the thermal stability of the polymer. The molar ratio of DFK and DCS is chosen to be 8:2 (PPESK-8020) considering the solubility of the polymer.
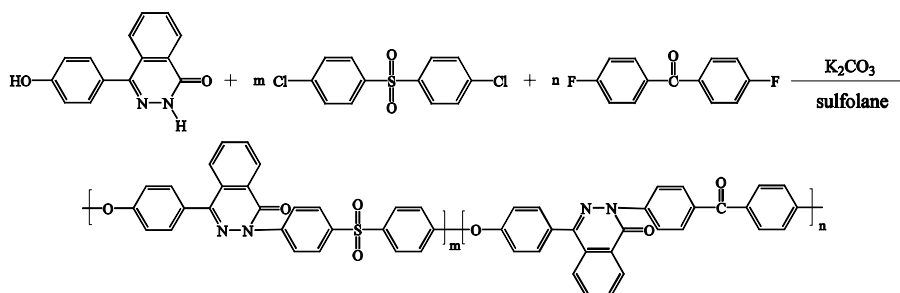
Figure 2. 15 Synthesis route of PPESK (PPESK-8020: m:n=8:2).

2.3.1.2 Film making

Due to the good solubility of PPESK in NMP solvent, the polymer film can be easily made on a silicon substrate by a spin-coating process. PPESK-8020 (m:n=8:2) is used for the spin-coating process. The PPESK films are baked at 150°C in vacuum for 6h to fully evaporate the solvent in the films. The polymer film shows good layer quality. Under a solid content of 18%, the film thickness can be controlled in a range of 1-7 μm by varying the spin velocity (Figure 2. 16).
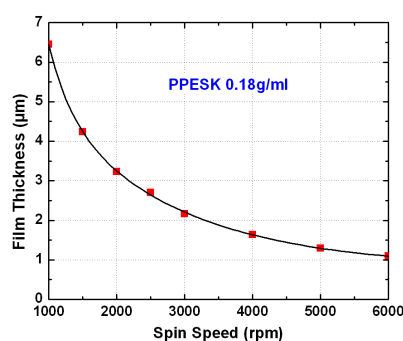
Figure 2. 16   PPESK film thickness versus spin speed

2.3.1.3 Optical and thermal properties of PPESK films

The properties of PPESK-8020 are listed in Table 2. 4. The details will be explained in the following section.

Table 2. 4 Properties of PPESK-8020

		@1310nm	@1550nm
Powder	Solubility	Soluble in organic solution, NMP, DMAC etc.	
Film	Refractive Index (TE)	1.657	1.654
	Refractive Index (TM)	1.635	1.632
	Birefringence (n_{TE}-n_{TM})	0.022	0.022
	Thermo-optic coefficient (/^{o}C) (TE)	-1.22×10^{-4}	-1.22×10^{-4}
	Thermo-optic coefficient (/^{o}C) (TM)	-1.02×10^{-4}	-1.02×10^{-4}
	Propagation Loss (TE) (Measured from slab waveguide)	0.24 dB/cm	0.52 dB/cm
	Glass Transition Temp. (Tg)	279 ^{o}C (in N_2)	
	Degradation Temp. (1 wt%)	488 ^{o}C (in N_2)	

2.3.1.1 Refractive index and birefringence

The optical properties of PPESK-8020 polymer films are measured by prism coupler (SPA-4000). As shown in Table 2. 4, the refractive index (n_{TE}=1.654@1550nm) and birefringence (Δn= n_{TE}-n_{TM}=0.022) of polymer PPESK-8020 is relatively high. This is due to the asymmetric, non-coplanar molecular structure of the DHPZ content and the molecular orientation during processing. The following experimental results prove this point.

In order to test the refractive index and birefringence dependence on the DHPZ

content, we synthesized polymer PPES with different ratio of monomer DHPZ and DCS. As shown in Figure 2. 17, the refractive index and birefringence decrease as the content of DHPZ reduces. The refractive index can be tuned in a range of 1.62~1.64 at 1550nm and the birefringence can be lowered down to 0.009.

(a)   (b)
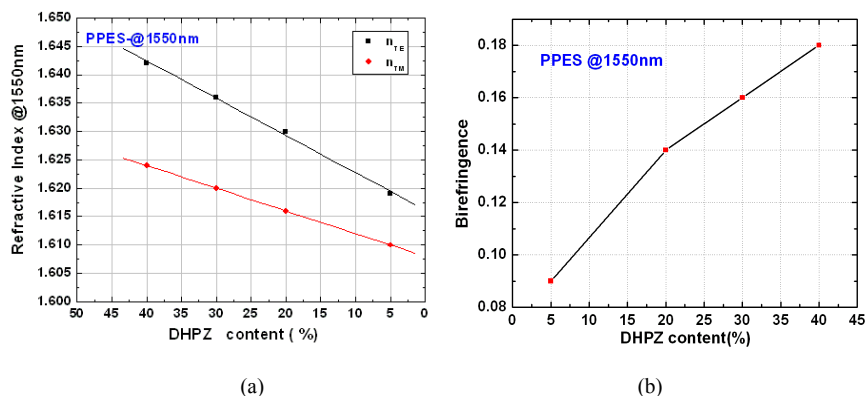
Figure 2. 17 The refractive index and birefringence of PPES versus DHPZ content
(a) The refractive index of PPES versus DHPZ content (b) The birefringence of PPES versus DHPZ content

It is also found that the birefringence of PPESK can be further reduced by a post bake process at high temperature. The birefringence of PPESK-8020 reduces as the post-bake temperature increases. The birefringence of PPESK-8020 is reduced from 0.022 to 0.006 after a post-bake at 300°C for 15min (Figure 2. 18).
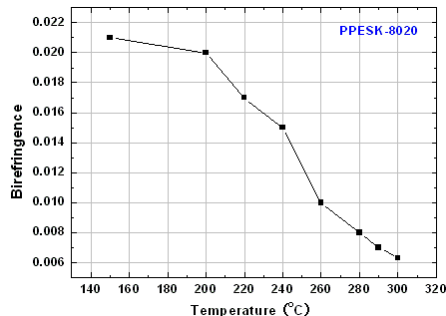
Figure 2. 18 The birefringence of PPESK-8020 after post-bake at different temperatures

The thermo-optic coefficient is calculated by measuring the refractive index at different temperature (Figure 2. 19). The thermo-optic coefficient of polymers is usually on the order of 10^{-4}/°C, much larger than that of silica-based material. The thermo-optic coefficient of PPESK-8020 is 1.22×10^{-4}/°C for the TE mode and 1.02×10^{-4}/°C for the TM mode (Figure 2. 19).
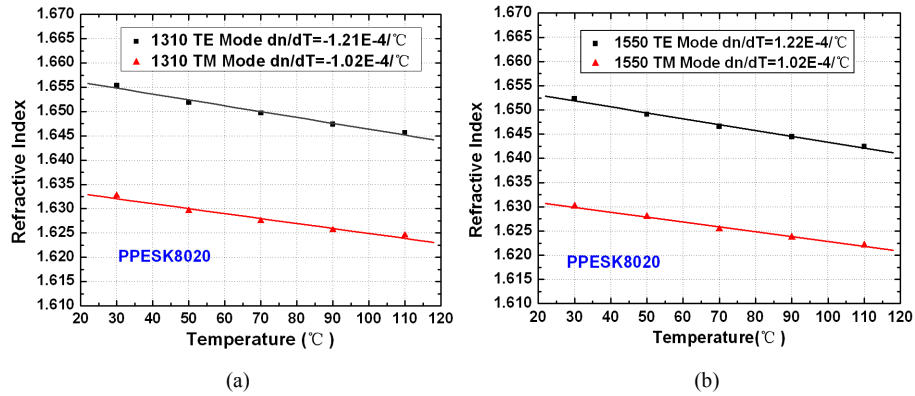
Figure 2. 19 Refractive index of PPESK-8020 versus temperature
(a) @1310nm; (b) @1550nm

2.3.1.2 Optical loss of PPESK films

One of the critical properties of polymer material is the optical loss in the communication windows. In the 1300nm~1600nm range, molecular vibration absorption mainly contributes to the optical loss, especially from C-H and -OH bonds. Our polymer, using the full C-H content, shows relatively low optical loss, less than 0.24dB/cm at 1310nm and 0.52dB/cm at 1550nm.

We measured the optical loss of a PPESK-8020 slab waveguide by the immersion oil method (Figure 2. 20). The slab waveguide is made by spin-coating PPESK-8020 on SiO_2/Si substrate. The optical loss of PPESK-8020 is expected to be relative low due to the low concentration of C-H bonds.
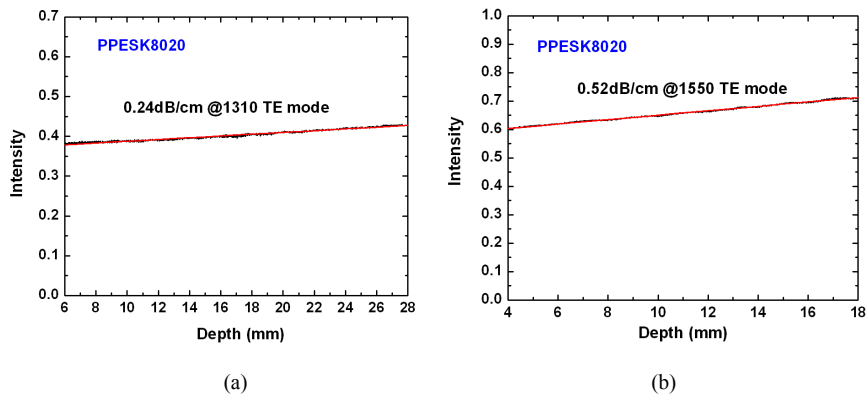
Figure 2. 20 Loss measurement of a PPESK slab waveguides by the immersion oil technique
(a) @1310nm; (b) @1550nm

2.3.1.3 Thermal properties of PPESK films

Another critical property of polymer materials is the thermal stability. PPESK polymers show good thermal stability with high glass transition temperature (279°C, in Figure 2. 21). The Thermal-Gravimetric Analysis (TGA) data of PPESK-8020 shown in Figure 2. 22 indicates temperature decomposition does not occur beyond 450°C, and 1% weight loss temperature (in Nitrogen) of PPESK-8020 is 488°C.
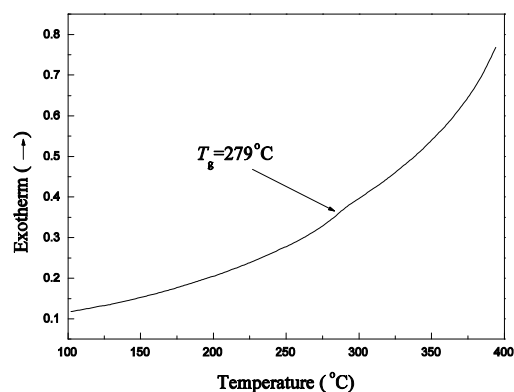
Figure 2. 21 DSC thermogram of PPESK-8020 in N_2
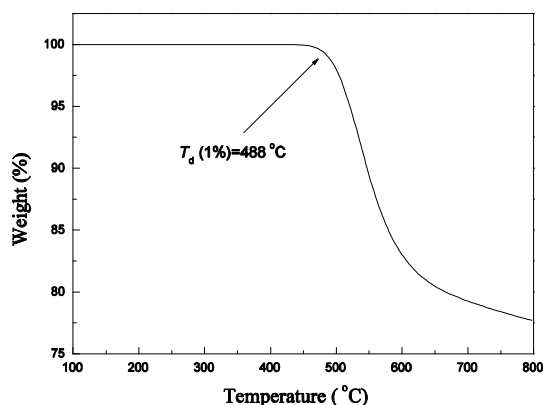
Figure 2. 22 TGA (Thermal-Gravimetric Analysis) data of PPESK-8020 in N_2

2.3.2 Improvement of PPESK series polymer

Even if polymer PPESK shows good optical properties and high thermal stability, it cannot be applied to device fabrications. The solvent used for PPESK is NMP which has a high boiling point (204.3°C) and a low volatility. This causes baking of the

films at high temperature (200°C) and long time (about 8 hours) to fully evaporate the solvent in the film. Adjusting the molecular structure to change the solubility of the materials in other solvents is necessary. It is well known that replacing C-H bonds by C-F bonds or C-D bonds can significantly reduce the absorption loss of the material. Based on this idea, fluorinated PPESK is synthesized. It is expected that the optical loss of the material can be further reduced. This also has the advantage of changing the solubility of the materials in other solvents. On the other hands, the cross-linked PPESK is desired since the polymer PPESK molecules cannot be cross-linked. Therefore we synthesized fluorinated PPESK and cross-linkable PPESK. During the PhD work, the synthesis process of this kind of polymer is still not mature. Further work has to be done later.

2.3.2.1 Fluorinated PPESK

Fluorinated PPESK (FPPEs) was synthesized by copolymerization of monomer DHPZ(4-(4-Hydroxyphenyl)-2,3-phthalazin-1-one) and two fluorinated monomers 4,40-(Hexafluoroisopropylidene) diphenol (6F-BPA) and decafluorobiphenyl (DFBP) (Figure 2. 23)[62]. The index of the FPPEs can be adjusted by the molar ratio of the monomer 6FBPA and DFBP. Figure 2. 24 shows the refractive index of FPPEs with different content ratio of 6FBPA.
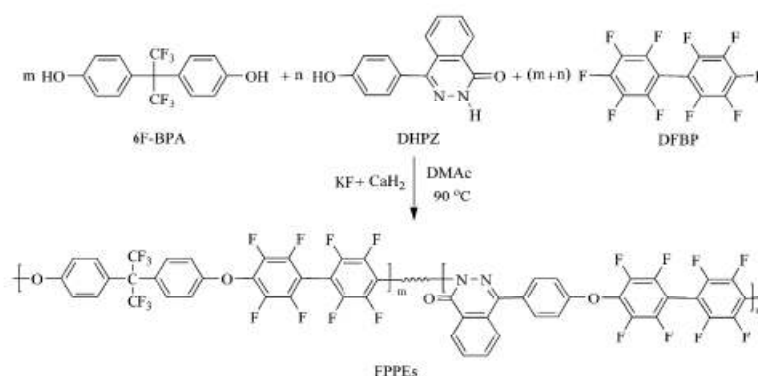
Figure 2. 23 Synthetic route of fluorinated PPESK (FPPEs)
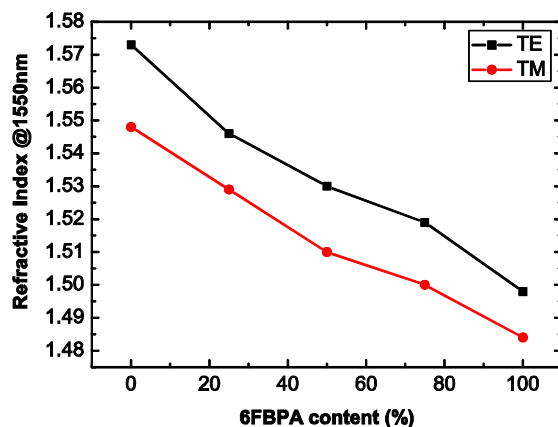
Figure 2. 24 Refractive index of FPPEs with different content ratio of 6FBPA

2.3.2.2 Cross-linkable PPESK

A novel kind of tetrafluorostyrene ended PPESK copolymer was synthesized by a two-step reaction (Figure 2. 25) [63].
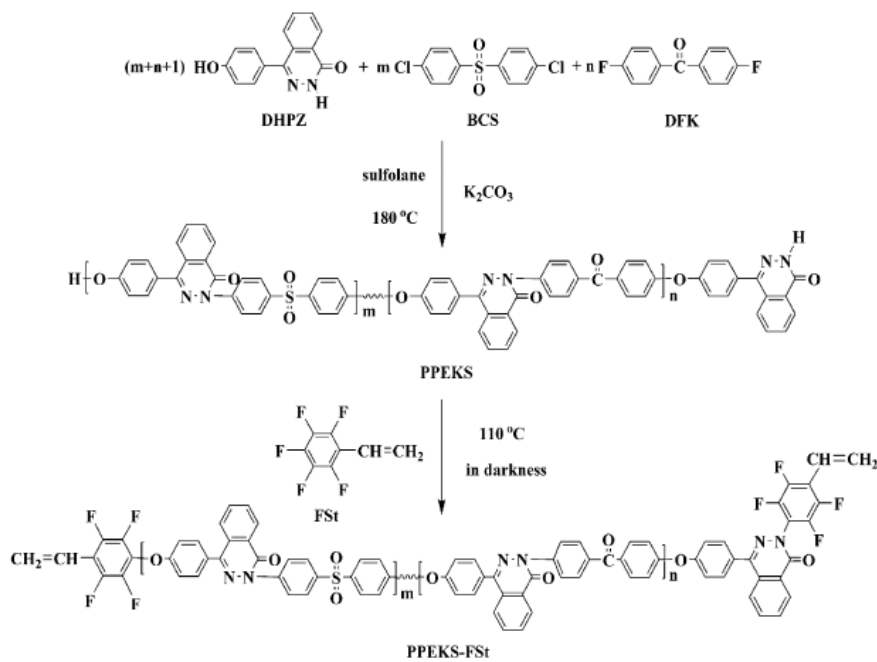
Figure 2. 25 Synthetic route of cross-linkable PPESK-FSt

2.4 Conclusion

Polymers are emerging as an important material in photonics area. Developing new materials with low cost and high performance has attracted a lot of attention in the recent years. Under this framework, we have developed two main kinds of polymer: PSQ-L series polymer and   PPESK series polymer. The optical properties and other properties of these two kinds of polymer are investigated in this chapter. Since PSQ-L series polymer can meet the basic demands for optical waveguides applications, it is chosen for the design and fabrication of polymer waveguides for the first run. However, PPESK series polymer still needs further improvement. The PPESK films are not cross-linked films and the solvent is not suitable for further device fabrication. Modification of the synthesis process has been done in the mean time.

Chapter 3 Theory and design of ring resonators

3.1 Introduction

Microring resonators are basic components in integrated optics. The compact structure and versatile wavelength-selective functionality allow using the microring resonators for a variety of applications. The basic application of microring resonators is as an optical add-drop filter. A wavelength multiplexer or demultiplexer can be realized by cascading several ring resonators with different radius [64]. Such multiplexers or demultiplexers gives more flexibility than AWGs (arrayed waveguides gratings) in DWDM (Dense Wavelength Division Multiplexing) system since each channel wavelength can be controlled by a single ring resonator. By adjusting the effective index of each ring, a reconfigurable Add-Drop Multiplexer can also be achieved in this way[65].

Other functional devices based on ring resonators, like modulators [66] and switches [67], also attract a lot attention. By detecting the shift of the resonance wavelengths or the variation of the intensity at a certain wavelength, the ring resonators can be applied to some bio-chemical sensing or other sensing applications [68].

The first sub-micrometer silicon ring resonator was achieved in 1997 [69, 70]. The silicon circuit has high compactness due to the large index contrast of silicon to air. However, polymer circuits cannot be as compact as silicon circuits due to the low index contrast to air. The polymer circuits promise to reduce the cost of the device.

In this chapter, the operation principle of the microring resonators is introduced. The factors that affect the transmission characteristics of the ring resonators are analyzed. The PSQ-L polymer based ring resonators are designed.

3.2 Operation principle of ring resonators

There are two basic structures of microring resonators. One type is composed of two straight waveguides and a ring waveguide. This kind of microring resonators with four ports for achieving add-drop filtering functions is also called add-drop filters. The other structure of microring resonators has only one straight waveguide and a ring waveguide. This kind of microring resonators can achieve large extinction ratio by adjusting the coupling efficiency and the loss. It works as a simple wavelength filter and is also called notch filters. The following will explain the principle of ring resonators and gives the basic formulation of the transmission functions.

3.2.1 Add-drop filters
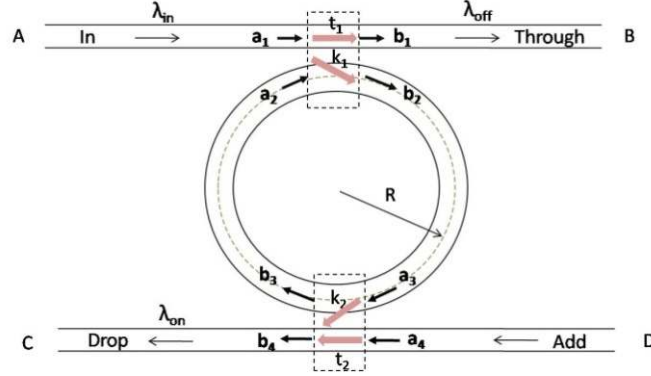
Figure 3. 1 Geometry of microring resonator (add-drop filter)

Figure 3. 1 shows the typical geometry of microring resonators. It consists of two straight waveguides and a ring waveguide. Light couples in from port A to the first coupling region and couples into the ring waveguides, then comes to the second coupling region and couples out from port C. For the certain wavelengths that satisfy the resonance condition, the light will be enhanced in the ring waveguide and all coupled out to the drop port. For the rest of the wavelengths (non-resonant wavelengths), they will be coupled out to the through port. Therefore, certain wavelengths (that satisfy the resonance condition) are filtered out at the through port (as a drop filter) and certain wavelengths (that satisfy the resonance condition) can also be uploaded from the add port.

The theoretical calculation of the intensity of the through port and drop port can be deduced from coupling theory [71]. The amplitude of the electric field coupled in and out of the straight and ring waveguides can be written as follow by transfer matrix method [72].

$$\begin{pmatrix} b_1 \\ b_2 \end{pmatrix} = \begin{pmatrix} t_1 & k_1 \\ -k_1^* & t_1^* \end{pmatrix} \begin{pmatrix} a_1 \\ a_2 \end{pmatrix} \tag{3.1}$$

$$\begin{pmatrix} b_3 \\ b_4 \end{pmatrix} = \begin{pmatrix} t_2 & k_2 \\ -k_2^* & t_2^* \end{pmatrix} \begin{pmatrix} a_3 \\ a_4 \end{pmatrix} \tag{3.2}$$

Where a_1, a_2, a_3, a_4, b_1, b_2, b_3, b_4 are the normalized electric field amplitude in the waveguides, k_1, k_2 are the coupling coefficients of the electric field amplitudes, and t_1, t_2 are the transmission coefficients of the electric field amplitude. $|k_1|^2$ stands for the coupling coefficient of the electric intensity, which means the percentage of the power coupling from the straight waveguide to the ring waveguide. Assuming the coupling loss can be neglected, the power transmitted and coupled to other waveguides should

be conserved,

$$|k_1|^2 + |t_1|^2 = 1 \tag{3.3}$$

$$|k_2|^2 + |t_2|^2 = 1 \tag{3.4}$$

Defining the loss coefficient of the amplitude as γ, and the phase propagation constant as β, and the propagation distance between the two coupling regions as L, the phase relationship of the amplitude a_2, a_3, b_2, b_3, can be written as follow,

$$a_3 = e^{-(\gamma+i\beta)L} b_2 \tag{3.5}$$

$$a_2 = e^{-(\gamma+i\beta)L} b_3 \tag{3.6}$$

$$\beta = \frac{2\pi}{\lambda} \cdot n_{eff} = k_0 \cdot n_{eff} \tag{3.7}$$

$$\theta = \beta \cdot 2L = \frac{2\pi}{\lambda} \cdot n_{eff} \cdot 2\pi R = k_0 \cdot n_{eff} \cdot 2\pi R \tag{3.8}$$

Where L is the half circumference of the ring, θ is the phase of one circumference. By taking the phase relationship of Eq.(3.5),(3.6) into Eq.(3.1)(3.2), the amplitude of through port and drop port can be expressed as,

$$b_1 = \frac{t_1 - t_2^* e^{-(\gamma+i\beta)2L}}{1 - t_1^* t_2^* e^{-(\gamma+i\beta)2L}} a_1 \tag{3.9}$$

$$b_4 = \frac{-k_1^* k_2 e^{-(\gamma+i\beta)L}}{1 - t_1^* t_2^* e^{-(\gamma+i\beta)2L}} a_1 \tag{3.10}$$

The intensity at the through port and drop port is the square of Eq.(3.9),(3.10) and can be expressed as follow,

$$I_{Through} = \left|\frac{b_1}{a_1}\right|^2 = \frac{|t_1|^2 - 2\sqrt{A} \cdot |t_1| \cdot |t_2| \cos\theta + A \cdot |t_2|^2}{1 - 2\sqrt{A} \cdot |t_1| \cdot |t_2| \cos\theta + A \cdot |t_1|^2 \cdot |t_2|^2} \tag{3.11}$$

$$I_{Drop} = \left|\frac{b_4}{a_1}\right|^2 = \frac{|k_1|^2 \cdot |k_2|^2 \cdot \sqrt{A}}{1 - 2\sqrt{A} \cdot |t_1| \cdot |t_2| \cdot \cos\theta + A \cdot |t_1|^2 \cdot |t_2|^2} \tag{3.12}$$

A is the round trip loss coefficient of the ring waveguide defined as $A = e^{-2 \cdot \gamma \cdot 2L}$. Phase

of the round trip is $\theta = \beta \cdot 2L = k_0 \cdot n_{eff} \cdot 2\pi R$. A is the round trip loss coefficient

of intensity, which means the percentage of the power left after the light propagates one round trip.

We consider a simple case, in which the coupling is symmetric for both coupling regions of the ring. That means $t_1 = t_2 = t$, $k_1 = k_2 = k$, Eq.(3.11) and (3.12) are simplified as,

$$I_{Through} = \left| \frac{b_1}{a_1} \right|^2 = \frac{|t|^2 - 2\sqrt{A} \cdot |t|^2 \cdot \cos\theta + A \cdot |t|^2}{1 - 2\sqrt{A} \cdot |t|^2 \cdot \cos\theta + A \cdot |t|^4} \qquad (3.13)$$

$$I_{Drop} = \left| \frac{b_4}{a_1} \right|^2 = \frac{(1 - |t|^2)^2 \cdot \sqrt{A}}{1 - 2\sqrt{A} \cdot |t|^2 \cdot \cos\theta + A \cdot |t|^4} \qquad (3.14)$$

Therefore for a given value of t, the intensity of through port and drop port can be plotted as a function of wavelength. The resonance conditions achieve when

$$\theta = \frac{2\pi}{\lambda} \cdot n_{eff} \cdot 2\pi R = m \cdot 2\pi \qquad (3.15)$$

Where m is an integral. The resonance condition will be further explained in the following section.

3.2.2 Notch filters

The notch filter is composed of only one straight waveguide and one ring waveguide (Figure 3. 2). The deduction of the through port intensity is similar to that of an add-drop filter.
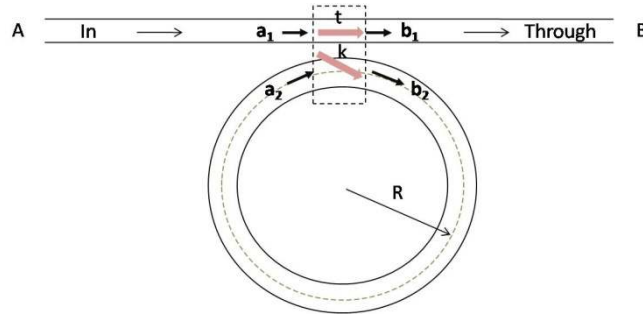
Figure 3. 2 Geometry of microring resonator (notch filter)

The small difference between the notch filter and add-drop filter is that the phase relation of the amplitudes of b_2 and a_2 is as,

$$a_2 = e^{-(\gamma + i\beta) \cdot 2L} b_2 \qquad (3.16)$$

Taking Eq.(3.16) into Eq.(3.1), the amplitude of the through port is as,

$$b_1 = \frac{t - e^{-(\gamma+i\beta)2L}}{1 - t \cdot e^{-(\gamma+i\beta)2L}} a_1$$

(3.17)

By square of Eq.(3.17), the intensity of the through port is,

$$I_{Through} = \left|\frac{b_1}{a_1}\right|^2 = \frac{|t|^2 - 2\sqrt{A} \cdot |t| \cdot \cos(2k_0 n_{eff}\pi R) + A}{1 - 2\sqrt{A} \cdot |t| \cdot \cos(2k_0 n_{eff}\pi R) + A \cdot |t|^2}$$

(3.18)

For a given t value, the intensity of through port and drop port can be plotted as a function of wavelength.

3.3 Performance parameters of ring resonators

According to Eq.(3.13),(3.14), the transmission spectrum of add-drop filters can be plotted as a function of the wavelength. The typical theoretical expected transmission spectrum of the ring resonators is shown in Figure 3. 3. The resonant wavelength is filtered out at the through port and coupled out at the drop port. In this section, we will introduce some parameters that qualify the performance of the ring resonators. The design consideration is based on taking into account the performance of the ring resonators.
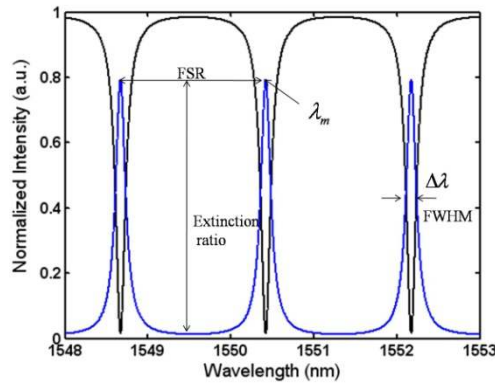
Figure 3. 3 Transmission characteristic of microring resonator
(with black line of through port, blue line of drop port)

3.3.1 Performance parameters of add-drop filters

3.3.1.1 Resonant wavelength

For certain wavelengths, the intensity in the ring cavity can be enhanced. In this case, the round trip phase is an integer multiple of 2π (Eq.(3.15)). These wavelengths are called resonant wavelengths. They satisfy the resonant condition,

$$m \cdot \lambda_m = n_{eff} \cdot 2\pi R \tag{3.19}$$

Where m is an integer, λ_m is the resonant wavelength, n_{eff} is the effective index of the ring waveguide, R is the radius of the ring.

3.3.1.2 Free spectral range (FSR)

The free spectral range (FSR) is one of the key parameters of the ring resonators. It is the wavelength spacing between two adjacent resonance peaks. From Eq.(3.19), the FSR can be written as,

$$FSR = \lambda_{m+1} - \lambda_m = \frac{\lambda^2}{2\pi R \cdot (n_{eff} - \lambda \cdot \frac{dn_{eff}}{d\lambda})} = \frac{\lambda^2}{2\pi R \cdot n_g} \tag{3.20}$$

Where n_g is the group index of the waveguides, defined as

$$n_g = n_{eff} - \lambda \cdot \frac{dn_{eff}}{d\lambda} \tag{3.21}$$

From Eq.(3.20), we can see that the FSR is inversely proportional to the radius of the ring. In order to achieve a large free spectral range, the radius of the ring must be small enough. For instance, if a 5nm FSR is needed, the radius of the ring should be about 51 μm, assuming using polymer waveguide with an effective index of 1.5 at 1550nm.

3.3.1.3 FWHM (full bandwidth at half-maximum)

FWHM is defined as the full bandwidth at half-maximum of the transmission spectrum peak (Figure 3. 3). For symmetric coupling, the intensity of the through port can also be written as,

$$I_{Through} = 1 - \frac{(1 - A \cdot |t|^2) \cdot (1 - |t|^2)}{(1 - \sqrt{A} \cdot |t|^2)^2 + 4 \cdot \sqrt{A} \cdot |t|^2 \cdot \sin^2(\theta / 2)} \tag{3.22}$$

And,

$$\theta = \frac{2\pi}{\lambda} \cdot n_{eff} \cdot 2\pi R \tag{3.23}$$

The intensity of the through port follows a Lorenz function (regarding to the variable $\sin(\theta/2)$), the FWHM of Eq.(3.22) is,

$$\Delta\theta_{FWHM} = \Delta(\sin\frac{\theta}{2}) = \frac{1-\sqrt{A}\cdot|t|^2}{A^{1/4}\cdot|t|} \tag{3.24}$$

For a small bandwidth, $\sin(\theta/2)$ can be approximated as $\theta/2$. The deviation of Eq.(3.23) is as,

$$\Delta\theta = 2\pi\cdot\Delta(\frac{n_{eff}}{\lambda})\cdot 2\pi R = 2\pi\cdot\frac{n_g}{\lambda^2}\cdot 2\pi R\cdot\Delta\lambda = \frac{2\pi}{FSR}\cdot\Delta\lambda \tag{3.25}$$

Therefore taking Eq.(3.25) into Eq.(3.24), the FWHM of wavelength is expressed as,

$$\Delta\lambda_{FWHM} = \frac{\lambda^2}{2\pi^2 n_g R}\cdot\frac{1-\sqrt{A}\cdot|t|^2}{A^{1/4}\cdot|t|} = \frac{FSR}{\pi}\cdot\frac{1-\sqrt{A}\cdot|t|^2}{A^{1/4}\cdot|t|} \tag{3.26}$$

The round trip loss and the coupling efficiency both have an effect on the FWHM, and it will be discussed in the following part.

3.3.1.4 Q-factor

The Q factor is an important factor for the ring resonator, defined as the ratio of the resonance wavelength and FWHM,

$$Q = \frac{\lambda_m}{\Delta\lambda_{FWHM}} = \frac{2\pi^2 n_g R}{\lambda_m}\cdot\frac{A^{1/4}\cdot|t|}{1-\sqrt{A}\cdot|t|^2} \tag{3.27}$$

3.3.1.5 Finesse

Finesse is defined as the ratio of the free spectral range and the FWHM,

$$F = \frac{FSR}{\Delta\lambda_{FWHM}} = \frac{\pi\cdot A^{1/4}\cdot|t|}{1-\sqrt{A}\cdot|t|^2} \tag{3.28}$$

3.4.1.6 Extinction ratio

The extinction ratio of through port and drop port is defined as the ratio of the maximum intensity and minimum intensity of the resonance peak. For a symmetric coupling case, the extinction ratio of the through port is as,

$$EX(Through) = \frac{I_{max}}{I_{min}} = \left(\frac{1+\sqrt{A}}{1-\sqrt{A}}\right)^2 \cdot \left(\frac{1-\sqrt{A}\cdot|t|^2}{1+\sqrt{A}\cdot|t|^2}\right)^2 \tag{3.29}$$

The extinction ratio of the drop port is as,

$$EX(Drop) = \frac{I_{max}}{I_{min}} = \left(\frac{1+\sqrt{A}\cdot|t|^2}{1-\sqrt{A}\cdot|t|^2}\right)^2 \tag{3.30}$$

3.3.2 Performance parameters of notch filters

The performance parameters of the notch filter are similar to those of add-drop filters. Resonance condition and the expression of FSR are the same as for add-drop filters. Only the expressions of FWHM, Q factor and Finesse are a little different from that of the add-drop filters.

3.3.2.1 FWHM (full bandwidth at half-maximum)

For symmetric coupling, the intensity of the through port can also be written as,

$$I_{Through} = 1 - \frac{(1-|t|^2)\cdot(1-A)}{(1-\sqrt{A}\cdot|t|)^2 + 4\cdot\sqrt{A}\cdot|t|\cdot\sin^2(\theta/2)} \tag{3.31}$$

Similar to that of add-drop filter,

$$\Delta\lambda_{FWHM} = \frac{\lambda^2}{2\pi^2 n_g R} \cdot \frac{1-\sqrt{A}\cdot|t|}{A^{1/4}\cdot|t|^{1/2}} = \frac{FSR}{\pi} \cdot \frac{1-\sqrt{A}\cdot|t|}{A^{1/4}\cdot|t|^{1/2}} \tag{3.32}$$

3.3.2.2 Q-factor

The Q factor is defined as the ratio of the resonance wavelength and FWHM,

$$Q = \frac{\lambda_m}{\Delta\lambda_{FWHM}} = \frac{2\pi^2 n_g R}{\lambda_m} \cdot \frac{A^{1/4}\cdot|t|^{1/2}}{1-\sqrt{A}\cdot|t|} \tag{3.33}$$

3.3.2.3 Finesse

The finesse is defined as the ratio of the free spectral range and FWHM,

$$F = \frac{FSR}{\Delta\lambda_{FWHM}} = \frac{\pi \cdot A^{1/4} \cdot |t|^{1/2}}{1 - \sqrt{A} \cdot |t|} \tag{3.34}$$

3.3.2.4 Extinction ratio

One difference between a notch filter and an add-drop filter is that the through port intensity of the notch filter can go to zero when $A = |t|^2$, i.e. the round trip loss equals the transmission coefficient. It is also called critical coupling condition. The extinction ratio of the through becomes infinite at the critical coupling condition, as can be seen from the following expression,

$$EX(Through) = \frac{I_{max}}{I_{min}} = \left(\frac{|t| + \sqrt{A}}{|t| - \sqrt{A}}\right)^2 \cdot \left(\frac{1 - \sqrt{A} \cdot |t|}{1 + \sqrt{A} \cdot |t|}\right)^2 \tag{3.35}$$

3.4 Design considerations

For most applications, ring resonators with small bandwidth, high Q factor and large extinction ratio are desirable. In this section, we will discuss some universal relationship of the effect of loss coefficient and coupling efficiency on the transmission spectrum of add-drop filters.

According to Eq.(3.26), the bandwidth depends on the radius of the ring, the round trip loss coefficient and transmission efficiency (coupling efficiency) of the ring. The radius of the ring is normally chosen by considering the FSR that needs to be achieved and to what extent the bending loss is tolerant. The coupling efficiency can be adjusted by changing the gap distance between the ring and the straight waveguides or changing the coupling length for racetrack ring resonators. The loss of the ring resonators originates from several aspects: material absorption loss, waveguide bending loss, substrate leakage loss, surface roughness scattering loss, and the loss due to modal mismatch at the junctions of straight and curved waveguides. The losses due to waveguide bending, substrate leakage and modal mismatch can be negligible with improved waveguide and device design.

For a given ring radius and coupling efficiency, the bandwidth (FWHM) of the transmission spectrum will increase as the loss increases. The Q-factor, Finesse and extinction ratio of both ports will all decrease as the loss increases. A calculated example is plotted in Figure 3. 4. The transmission spectrum of both ports is plotted with different loss coefficient. The performance of the ring resonators is deteriorated as the loss increases. This demands that the total loss of the ring waveguides should be minimized as much as possible from design.

On the other hand, for a given ring radius and round trip loss coefficient, the bandwidth of the transmission spectrum will decrease as the coupling efficiency decreases. The Q-factor and Finesse will all increase as the coupling efficiency decreases. The extinction ratio of the through port will decrease as the coupling

efficiency decreases while the extinction ratio of the drop port will increase as the coupling efficiency decrease. A calculated example is shown in Figure 3. 5. The transmission spectrum of both ports is plotted with coupling efficiency. So you can achieve narrow bandwidth by decreasing the coupling efficiency, but it also decreases the extinction ratio of the through port.
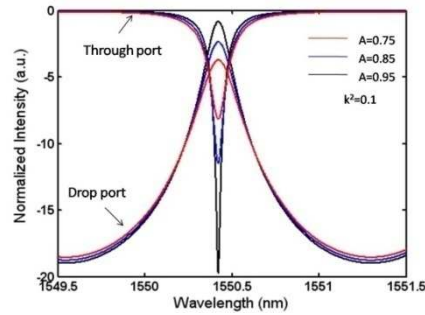
Figure 3. 4 Calculated transmission spectrum of ring resonators with different loss coefficient value
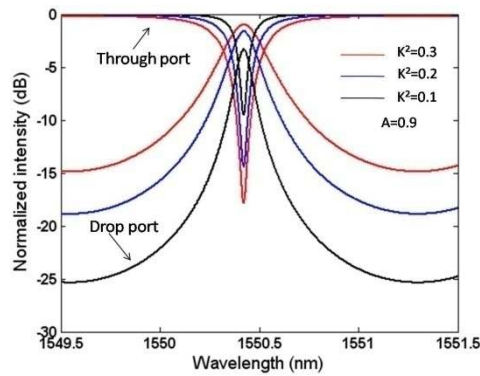
Figure 3. 5 Calculated transmission spectrum of ring resonators with different coupling coefficient

3.5 Design of polymer PSQ-L ring resonators

As polymer PSQ-L has good film properties, optical properties and high thermal stability, it is chosen to fabricate polymer waveguides for the first test. The high index polymer PSQ-LH is used as core material and the low index polymer PSQ-LL is used as cladding material. Our aim for the first run is to test the material in optical applications and to develop the fabrication technology compatible with the materials. The design considerations come along with the aim of the first run. In this section, we

describe the considerations of the design of the PSQ-L ring resonators for the first run.

3.5.1 Cross-section design

The cross-section of the waveguide is designed as buried channel waveguides (Figure 3. 6(b)). High index polymer PSQ-LH (n=1.515@1550nm) is used as core material and low index polymer PSQ-LH (n=1454@1550nm) is used as cladding material. Theoretically, to support a single mode in the PSQ-LH waveguide, the width and height should be both less than 2.2μm. For the first test, we choose the waveguide with width of 3μm and height of 1.8μm considering the fabrication process possibility. The first order mode in the straight waveguides will be evanescent after light propagating through the bend region and therefore only the fundamental mode exists in the ring waveguides.
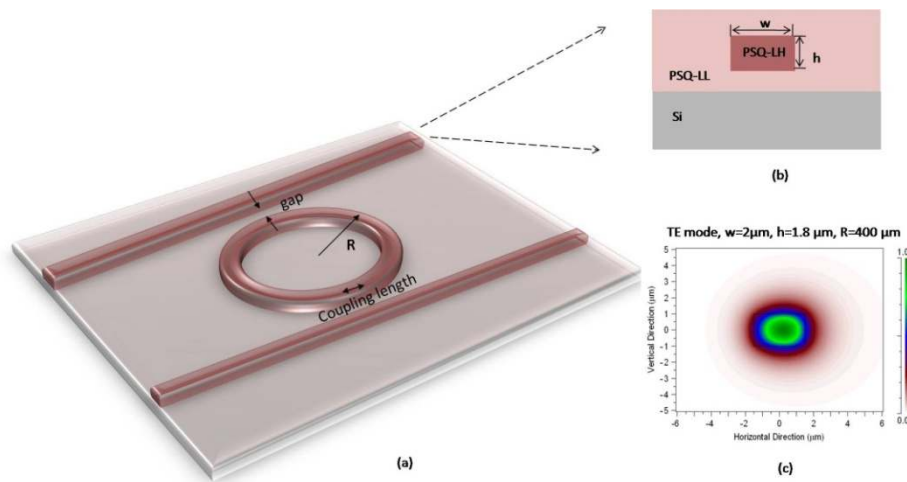
Figure 3. 6 Structure of ring resonators (a) Structure of ring resonators (b) cross-section of the waveguides (c) calculated TE mode profile (for waveguide with w=3μm,h=1.8μm,R=400μm)

3.5.2 Choosing the radius

Two aspects have to be taken into account when choosing the radius of the ring. One is the FSR and the other is the bending loss of the ring. According to Eq.(3.20), the FSR of the ring is inversely proportional to the radius of the ring. To get a large FSR, the radius of the ring should be a small value. Taking polymer waveguide as an example, Figure 3. 7 shows the calculated FSR as a function of the ring radius. The group index is set as 1.48 for polymer waveguides. For a 2.5nm FSR, the radius of the ring should be around 100μm and for a 1nm FSR, the radius of the ring should be around 250μm.
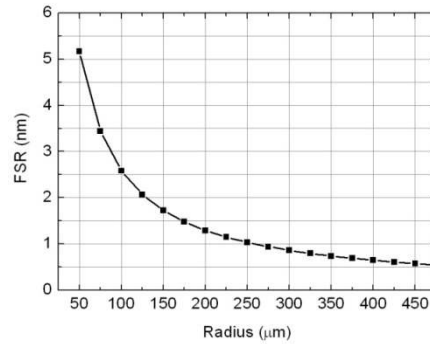
Figure 3. 7 Calculated FSR as a function of ring radius
(the group index is set as 1.48 for polymer waveguides)

Actually, the radius of the ring is limited by the bending loss and mode mismatch loss between the straight waveguides and the bend waveguides (in case of racetrack ring resonators). Extra loss should be avoided since it will deteriorate the performance of the ring. Figure 3. 8 shows the calculated bend loss of the buried PSQ-LH waveguide (TE mode) as a function of ring radius with different waveguide width (the height of the waveguide is fixed to be 1.8μm). Figure 3. 9 shows the calculated mode mismatch loss (TE mode) between the straight waveguides and the bending waveguides with different ring radius. The bending loss and mode mismatch loss are calculated by BPM method (to calculate the mode overlap between two mode profiles). As can be seen from Figure 3. 8, the bending loss increases exponentially as the ring radius decreases. The mode mismatch loss also increases as the ring radius decreases (Figure 3. 9). As we do not care about the value of the FSR for the first run and to minimize the extra loss caused by design, the radius of the ring is chosen to be 400μm for safety.
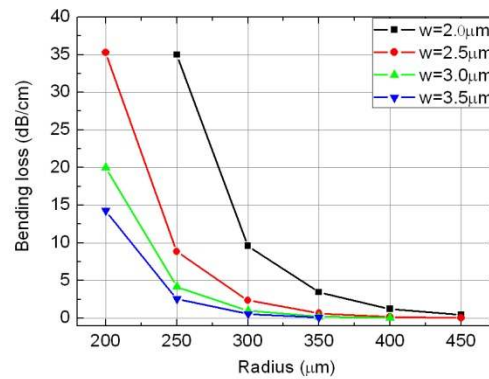
Figure 3. 8 Calculated bending loss as a function of ring radius with different waveguide width (TE mode)
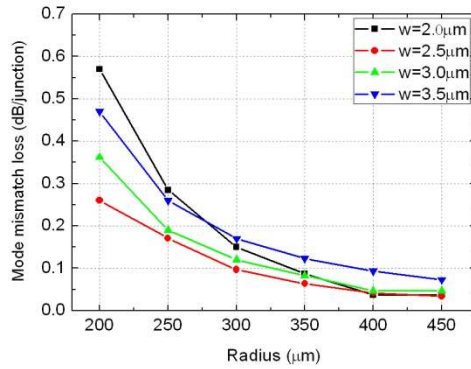
Figure 3. 9 Calculated mode mismatch loss as a function of ring radius with different waveguide width (TE mode)

3.5.3 The dimension of the coupling length and gap distance

The coupling efficiency between the straight waveguides and the ring is controlled by the gap distance (between the straight waveguide and the ring waveguide) and the coupling length (Figure 3. 6(a)). In order to increase the coupling efficiency, the ring is designed as a racetrack ring resonator. Decreasing the gap distance will increase the coupling efficiency, but it also imposes challenges on fabrication technology. Figure 3. 10 shows the calculated coupling efficiency with different gap distance and coupling length (TE mode).

(a)   (b)

(c)   (d)
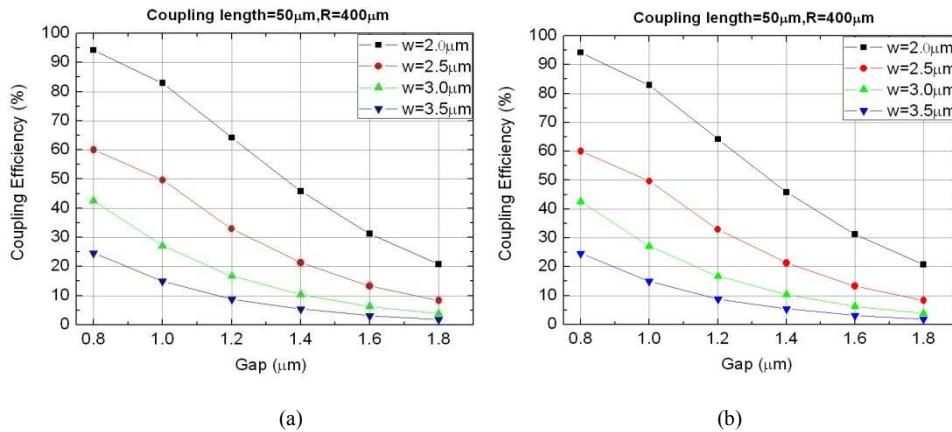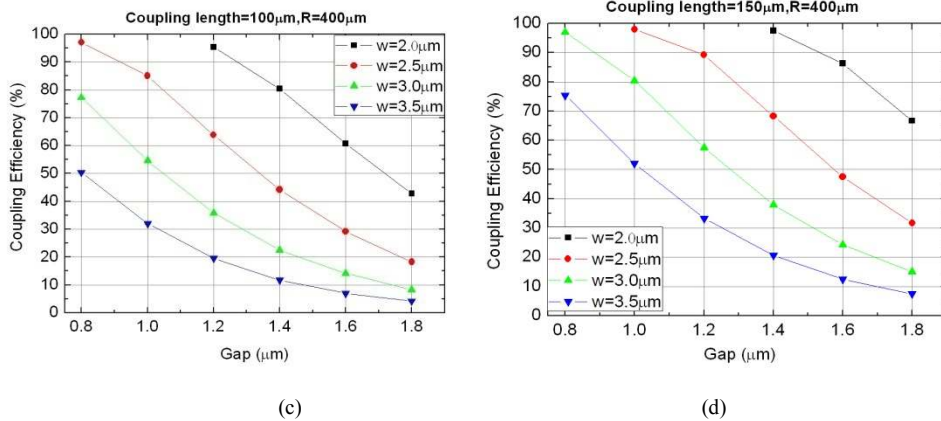
Figure 3. 10 Calculated coupling efficiency with different gap distance and coupling length
for different waveguide width (TE mode)
(a) with a coupling length of 0μm (b) with a coupling length of 50μm (c) with a coupling
length for 100μm (d) with a coupling length of 150μm

The performance of the ring resonators, like bandwidth (FWHM), Q factor, extinction ratio of both ports all depends on the coupling efficiency and loss coefficient of the ring resonator. According to Eq.(3.29),(3.30), we can theoretically calculate the extinction ratio of both ports with a given coupling efficiency and loss attenuation factor. Figure 3. 11 gives an example of the calculated extinction ratio of the through port and drop port as a function of the coupling efficiency with different loss coefficient. To get a small bandwidth and high Q value, the coupling efficiency should be kept as small as possible. But this also causes a tradeoff, a decrease of the extinction ratio of the through port. Therefore the coupling efficiency should be chosen as a moderate value. In our case, the aim of the design is to realize the resonance phenomenon of the ring resonators. Therefore the extinction ratio of both ports is expected to have a similar level. Assuming the loss of the ring waveguides is several dB/cm, from Figure 3. 11, the coupling power efficiency is chosen to be 30%-40% in order to have above 10dB extinction ratio for both ports. The bandwidth and Q-factor are considered less important than the extinction ratio of both ports. From Figure 3. 10, in order to achieve 30%-40% coupling efficiency, the coupling length should be larger than 100μm for a width of 3μm. The mask layout includes racetrack ring resonators with different coupling length and gap distance.
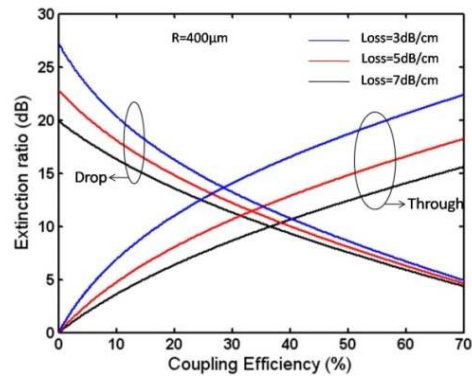
Figure 3. 11 The extinction ratio of the through port and drop port as a function of the coupling efficiency with different loss coefficient (the radius of the ring is set as 400μm)

It is hard to foresee the loss caused by fabrication even if the scattering loss of the waveguide can be theoretically calculated [73]. We choose the dimension of the PSQ-L ring resonators mainly by considering the extinction ratio of both ports. The ring resonators with little variation of dimensions are drawn on the mask.

For the notch filter, different coupling lengths are chosen to ensure the coupling conditions can be satisfied. The mask layout includes notch filters with different coupling length and gap distance.

3.6 Conclusion

In this chapter, the operation principle of the microring resonators is first introduced. The polymer PSQ-L based microring resonators are designed. The parameters of the ring resonators are optimized and analyzed on the basis of the aim of this design. The idea behind this design is also explained here.

Chapter 4 Fabrication of polymer waveguides

The polymer PSQ-L is used for fabrication of polymer waveguides. The high index polymer PSQ-LH is used as the core material and the low index polymer PSQ-LL is used as the cladding material. Our aim is to develop suitable fabrication processes compatible with this kind of material. Both conventional lithography and nanoimprint technology are tried to fabricate PSQ-L waveguides. In this chapter, the detailed fabrication processes are described. Different fabrication processes are tried and investigated. Suitable fabrication processes are developed for fabrication of PSQ-L waveguides.

4.1 Fabrication of polymer PSQ-L waveguides by photo-lithography and etching process

4.1.1 Introduction

Photo-lithography and ICP (Inductively Coupled Plasma) etching or RIE (Reactive Ion Etching) is a conventional technology to fabricate inorganic-material based waveguides. The patterns are transferred to the substrate from the mask by a photo-lithography process. The minimum transferred pattern resolution is limited by the light diffraction limit. For the UV lamp with a central wavelength of 365nm, the minimum resolution is about 0.6μm.

To transfer the patterns from the mask to the polymer layer, the simplest way is to first transfer the patterns to the photo-resist layer and then use the patterned photo-resist as a mask to do the etching process (as shown in Figure 4. 1). The patterns are transferred to the photo-resist layer by a UV-exposure (photo-lithography) process and a develop process (developing in the resist developer). To use the patterned photo-resist to transfer the patterns is quite simple and no further process is needed. However, the sidewall of the photo-resist can also be etched during the etching process. Using a partly etched photo-resist pattern is like using a partly damaged mask, therefore the pattern transferred to the substrate is also damaged to some degree. Some fabrication is tolerant to this (e.g. very short etching time results in very low sidewall roughness). But it is a problem for our fabrication which demands smooth sidewalls. In this case a hard mask is needed to protect the resist patterns identical to the mask (Figure 4. 2). The hard mask can be made by depositing a metal layer on the resist or epitaxially growing a layer of silica

by MOCVD (Metal organic vapour phase epitaxy). We use a metal mask as a hard mask. After metal deposition, a lift-off process is done. A thin gold layer on a titanium layer is used as a mask. Because the gold layer does not have a good adhesion to the polymer layer, the titanium layer is the first deposited.
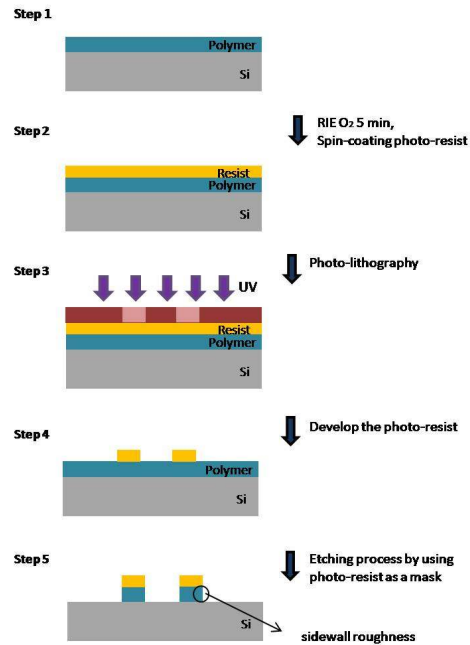
Figure 4. 1 Transfer of patterns to the substrate by using photo-resist as a mask
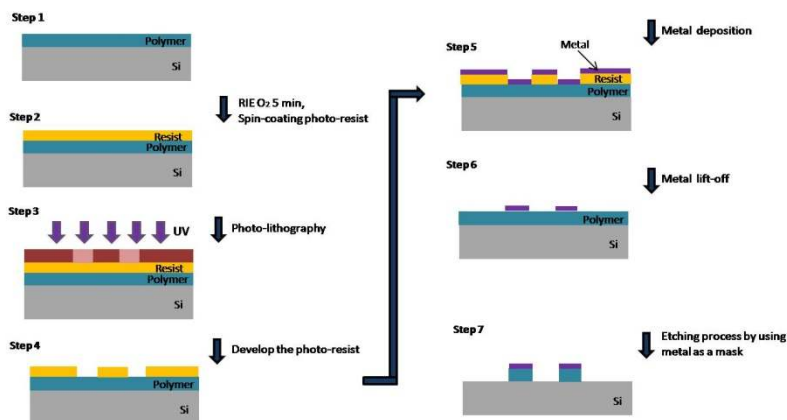
Figure 4. 2 Transfer of patterns to the substrate by using metal as a hard mask

4.1.2 Fabrication process and results

The cross-section of the polymer PSQ-L waveguides is designed as a buried waveguide. The high index polymer PSQ-LH is used as the core material and the low index polymer PSQ-LL is used both as under-cladding and upper-cladding.

There are two optional fabrication processes for fabrication of the buried channel waveguides (as shown in Figure 4. 3) by using conventional lithography and ICP etching. The first option (Figure 4. 3 (a)) is to do the lithography and etching on the core PSQ-LH layer. The thickness of the polymer PSQ-LH film is controlled by the spin-coating speed. The thickness of the under-cladding and upper-cladding don't need to be controlled accurately. Only the thickness of the under-cladding layer should be large enough to avoid extra substrate leakage (in our case it should be thicker than 2.5μm) and the upper-cladding needs to be thicker than the etch depth (for Figure 4. 3 (a)).

To accurately control the thickness of the core layer is quite important for waveguide fabrication since a thinner core layer (compared to the standard film thickness) can cause extra bending losses and substrate leakage losses while the thicker core layer can cause multimode behavior in the waveguides. In our case, the thickness of the core layer PSQ-LH should be controlled between 1.3-2.2μm. It is experimentally found that the thickness of PSQ-LH films is not very reproducible by spin-coating. With the same spin-coating speed and other conditions, the core film thickness has a variation of about 400 nm. To avoid this problem, a second fabrication process is proposed in Figure 4. 3 (b). The waveguide trenches are etched on the under-cladding layer and the core layer is then spin-coated on top. Since the etching depth of the waveguide trenches can be controlled accurately by the monitor on an ICP etching machine, this process easily allows controlling the thickness of the core layer. The core layer is spin-coated on the etched structures. The residual layer of the core layer is etched away and the thickness can also be controlled by the monitor on ICP etching machine (there will be a difference when etching to the cladding layer, (step 4 in Figure 4. 3 (b)). In this section, we will give a detailed description of the two fabrication processes. However, the process of Figure 4. 3 (b) seems not successful.
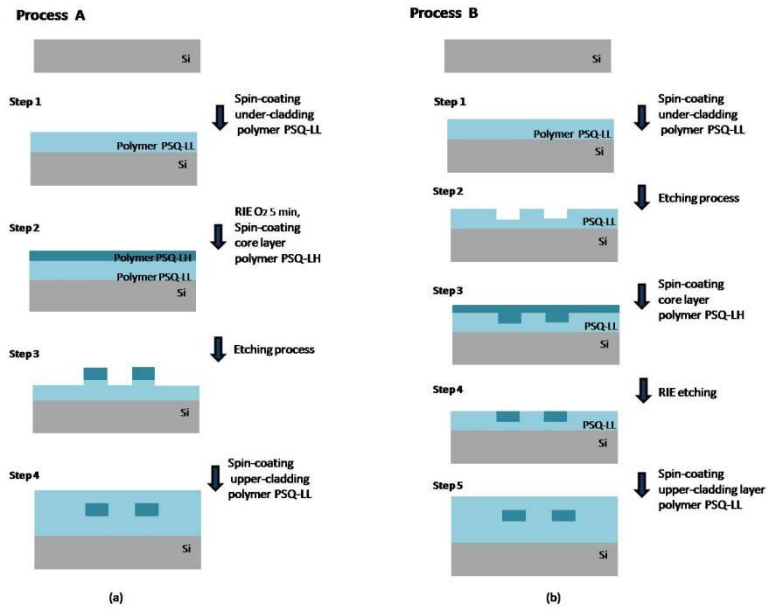
Figure 4. 3 Two optional processes for fabrication of buried polymer PSQ-L waveguide

➢ **Process A**
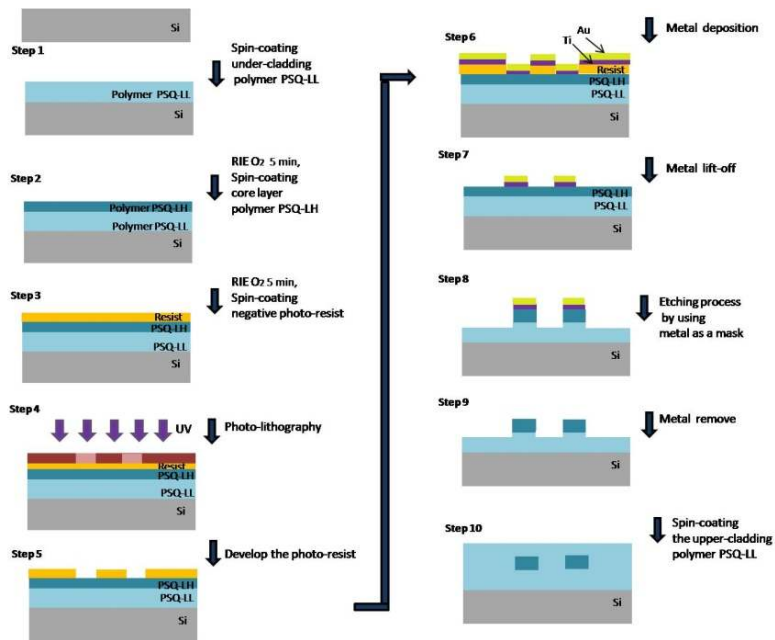
Figure 4. 4 Process A: Fabrication process for buried polymer PSQ-L waveguides

The detailed fabrication process A for PSQ-L waveguides is shown in Figure 4. 4.

The polymer PSQ-L ring resonators are fabricated by a conventional lithography and ICP etching process. First, a lower index layer (PSQ-LL) is spin-coated on the silicon substrate and cured (UV exposure 2min, at 180°C for 2h and 200°C for 2h). After Oxygen Plasma Etching for 5 minutes (to improve the adhesion to the second layer), a high index polymer layer (PSQ-LH) is spin-coated on and cured as a core layer. In order to protect the sidewall from being destroyed during the etching process, hard metal masks have to be used. Therefore, a reverse pattern is first transferred to the negative photoresist and followed by depositing a metal mask of Ti/Au. After a metal lift-off process, the waveguide pattern is transferred to the metal mask. Then an ICP dry etching process (SF_4: 4sccm, O_2: 40sccm, ratio:1:10, etch by 15mTorr) is carried out. After that, the metal mask is removed (Au by gold etching solvent, Ti by diluted HF solvent). Finally, an upper cladding PSQ-LL is spin-coated on top of the waveguides and cured. Figure 4. 5 and Figure 4. 6 show the SEM pictures and microscope pictures of the PSQ-L waveguides after the ICP etching process. Optimization of the ICP etching parameters has been carried out to achieve such rectangle waveguides and smooth sidewalls.

(a)   (b)

(c)   (d)
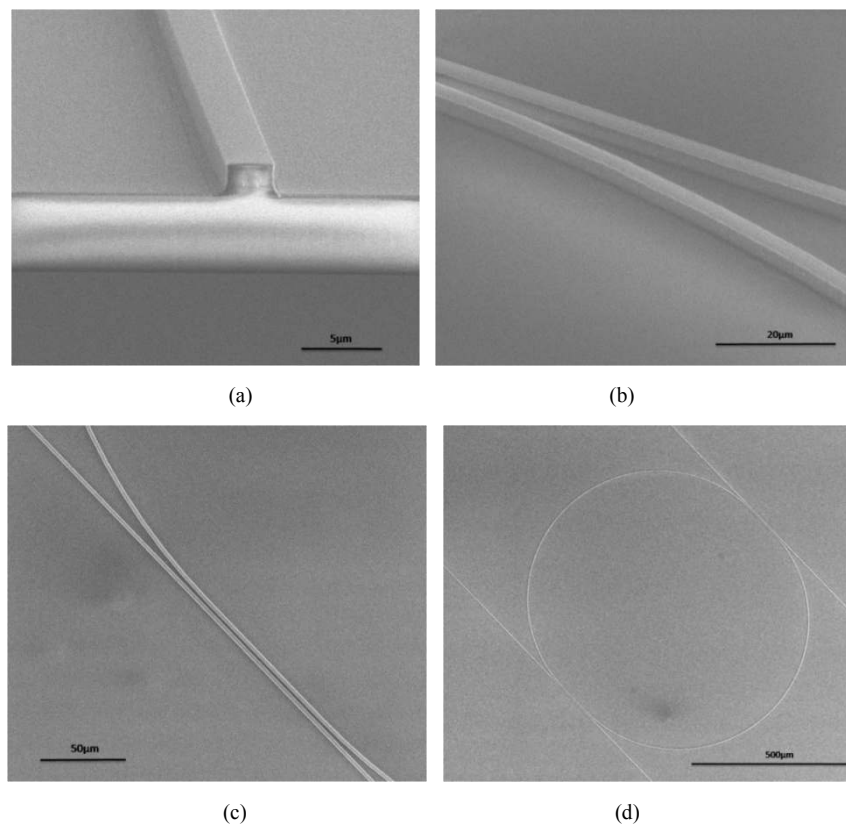
Figure 4. 5 SEM pictures of PSQ-L waveguides fabricated by conventional lithography and ICP etching (a) Cross-section of the waveguide (b) side view of the coupling region of the ring resonator (c) top view of the coupling region (d) top view of ring resonator

(a)

(b)

(c)

(d)
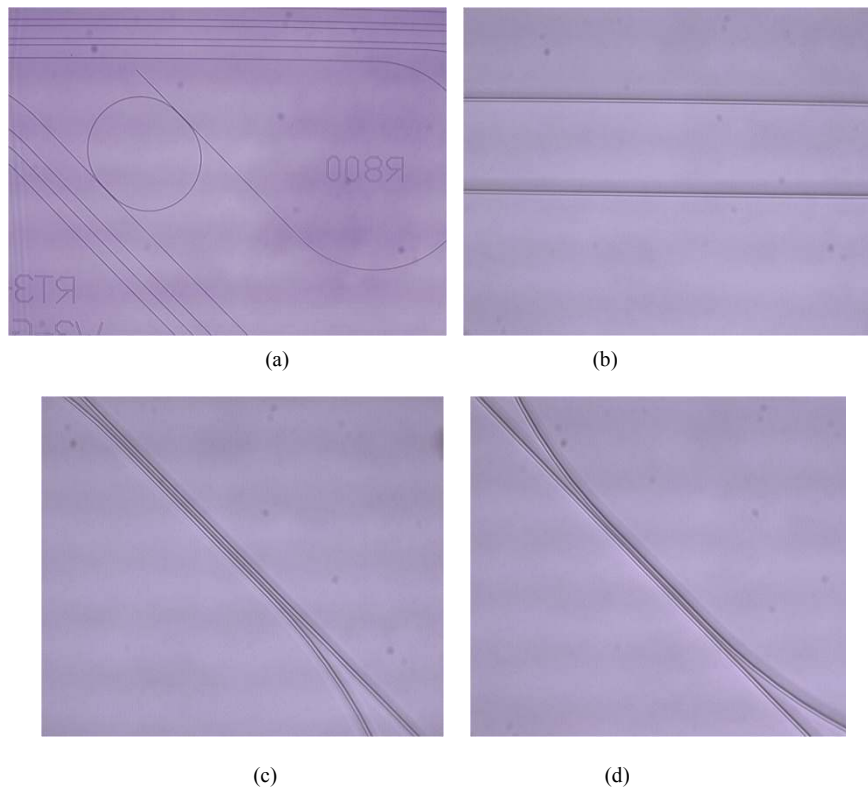
Figure 4. 6 Microscope pictures of PSQ-L waveguides fabricated by conventional lithography and ICP etching (a) ring resonator (b) straight waveguides (c) (d) coupling region of the ring resonators

➢ **Process B**
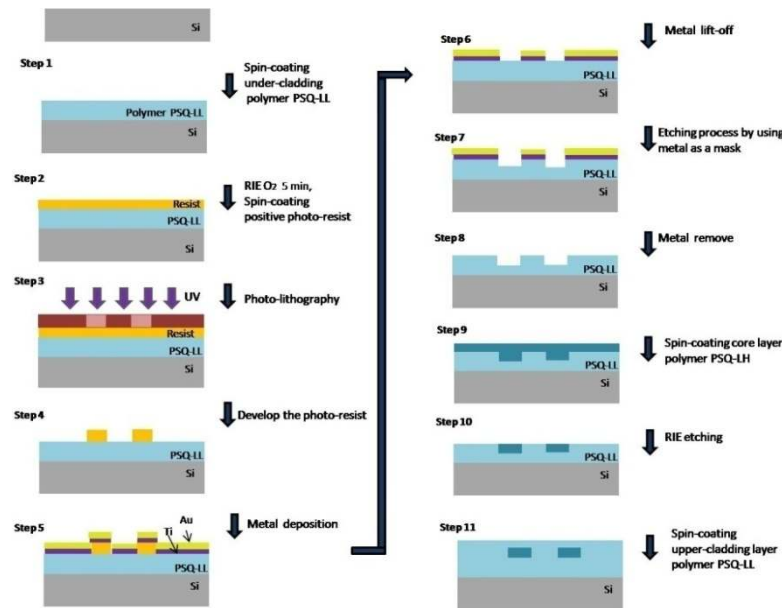
Figure 4. 7 Process B: fabrication process for buried polymer PSQ-L waveguides

The other option is to do the etching on the lower index layer. The detailed fabrication process is shown in Figure 4. 7. First, the low index layer PSQ-LL is spin-coated on the silicon wafer and cured (UV exposure 2min, at 180°C for 2h and 200°C for 2h). After the patterns are transferred to the low index layer, an etching process is carried out and the core layer of PSQ-LH is then spin-coated on the patterned low index layer. A further etching process is necessary to etch away the residual core layer. After that an upper cladding is spin-coated on top and cured.

However, this fabrication process seems not successful. The bottoms of the etched waveguides trenches are contaminated by the evaporated gold (Figure 4. 8) during the ICP etching process. This is because gold is a very soft metal and most of the surface is covered with metal masks for this reverse pattern. More detail will be given in the next section.
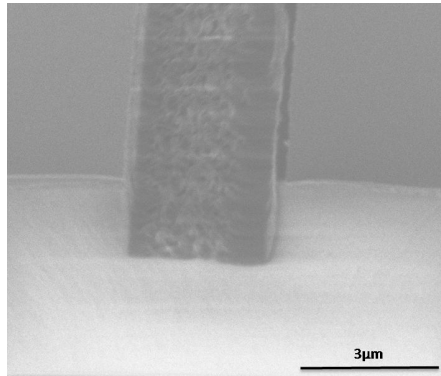
Figure 4. 8 SEM picture of cross-section of the waveguide trench etched on the lower cladding layer

4.1.3 Problems with existing fabrication processes

Even though we can get some nice results for PSQ-L waveguides fabricated by lithography and ICP etching, we still have some problems in some fabrication steps. As can be seen from the fabrication flow of Figure 4. 4 and Figure 4. 7, the polymer PSQ-L is exposed to some solvents (like acetone solvent in the metal lift-off step and the development step) during the process. This will cause some problems for the films since PSQ-L cannot resist some solvents for a long time. The following will give a further explanation.

1) The most important problem we met at first is that it is hard to accurately control the film thickness. It is also difficult for us to accurately measure the thickness of the polymer film without the prism coupler (the fabrication is done in Gent where the lab does not have a prism coupler). So the fabrication process of Figure 4. 3 (b) is proposed in order to replace the process of Figure 4. 3 (a). Even though the process of Figure 4. 3 (a) has one more step than the process of Figure 4. 3 (b), in fact it uses a positive resist which is more convenient than using the negative resist.

2) The second most important problem we face is that the cured polymer PSQ-L film cannot resist the acetone solvent for a long time. As we can see in both processes in Figure 4. 4 and Figure 4. 7, the sample needs to be immerged in acetone solvent in the developing step and the metal lift-off step. We found that the surface of the polymer layer seems a little bit cracked after immerging in acetone for a long time (e.g. 5 min). This is not much of a problem in process A (Figure 4. 4) since the little destroyed under-cladding layer does not have much influence on the core layer. But it is a big problem for the process B (Figure 4. 7). Because the little cracked surface leads to a deposited metal on top which is also cracked. That is also the reason why the gold is evaporated out in the etching process and makes the fabrication process in Figure 4. 3 (b) not successful.

3) Another challenge is how to successfully remove the metal mask on the polymer layer after etching (Step 9 in Figure 4. 4). The gold can be easily removed

without destroying the under-layer because of the titanium layer protecting the waveguide core layer. But how to completely remove the titanium layer without destroying the polymer waveguide is quite critical for this fabrication process. The titanium layer is removed in the diluted HF acid. Immerging the sample in the diluted HF acid for a long time can make the core layer flow away while immerging for a short time cannot completely remove the Ti layer and can cause metal absorption loss for the waveguides. So the time of immerging in the diluted HF acid to remove Ti layer should be well controlled.

4)   The last problem we met is that   the film tends to be cracked after baking a long time or many times at high temperature. As can be seen from Figure 4. 3, the under-cladding layer is baked three times together with the core layer and the upper-cladding layer. This problem can be solved by adjusting the curing time of each layer or add more photo-initiator into the polymer to harden the films.

4.2 Fabrication of polymer PSQ-L waveguides by using nanoimprint process

The conventional lithography and ICP etching process to fabricate polymer waveguides is complicated and requires a lot of experience. Exploring other methods to simplify the fabrication process and reduce the cost is quite necessary for the application of polymer-based devices. Therefore we try to use nanoimprint technology to fabricate polymer PSQ-L waveguides. Several different imprint processes are investigated here.

The imprint processes can be divided into two groups depending on the different mold materials: hard mold imprint and soft-lithography (soft-mold imprint). The hard mold imprint uses hard molds, like silicon, glass and metals. The soft mold imprint uses soft, flexible molds, like PDMS molds.

Our aim is to develop a simple imprint process compatible with polymer PSQ-L. Several different imprint processes are tested. Silicon molds are easy to be fabricated since silicon is easier to be etched than glass. So we first use silicon molds and silicon substrates to test the imprint technology. However, this method has problems in demolding. We tried another imprint process by using silicon molds and quartz glass (transparent) substrates and this method doesn't show any problems in demolding. However, using quartz glasses as molds or substrates is not practical since glass molds are difficult to fabricate and quartz glass substrates are difficult to be cleaved. Therefore we switched to another imprint process: soft-lithography, which uses transparent soft molds and silicon substrates. PSQ-L waveguides are successfully fabricated in this way. In the remainder of this section, the detailed imprint processes and the problems met will be described.

4.2.1 Hard mold imprint

4.2.1.1 Imprint with silicon molds and silicon substrates
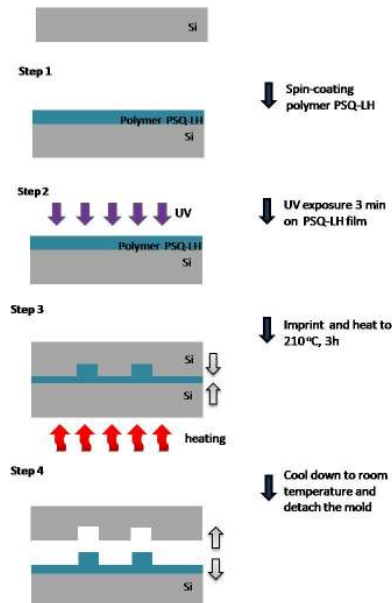
Figure 4. 9 Hard mold imprint process using silicon molds and silicon substrates

Since silicon molds are easy to be fabricated and silicon substrates are easy to be cleaved, we tested the imprint technology with silicon molds and silicon substrates first. The molds we used to test the imprint technology are SOI wafers of 1.22μm deep and minimum resolution of 500nm. This kind of SOI mold is not designed for polymer PSQ-L waveguides and is just for testing the fabrication technique. The imprint process is shown in Figure 4. 9 . The SOI molds are anti-adhesion treated before doing the imprint by solvent (0.1 % trideca-fluoro-(1,1,2,2)-tetrahydrooctyltrichlorosilane (C8H4Cl3F13Si, ABCR GmbH) in pentane). The silicon substrates are subjected to a hydrophilic treatment using a piranha solvent. The polymer PSQ-LH films are first spin-coated on the silicon substrates with a thickness of 1-2μm. Since the purpose of this experiment is to test the fabrication technique, no under-cladding layer is spin-coated first. After spin-coating, the film is exposed to a UV lamp for 3 minutes (this polymer is photo-initiated). The imprint process is done by using a home-made imprint machine. The imprint pressure is about 1 atmosphere. During the imprint process, the sample is heated to 210ºC to obtain full polymerization. After 2-3 hours, the sample is cooled down to room temperature and the mold is detached from the substrate.
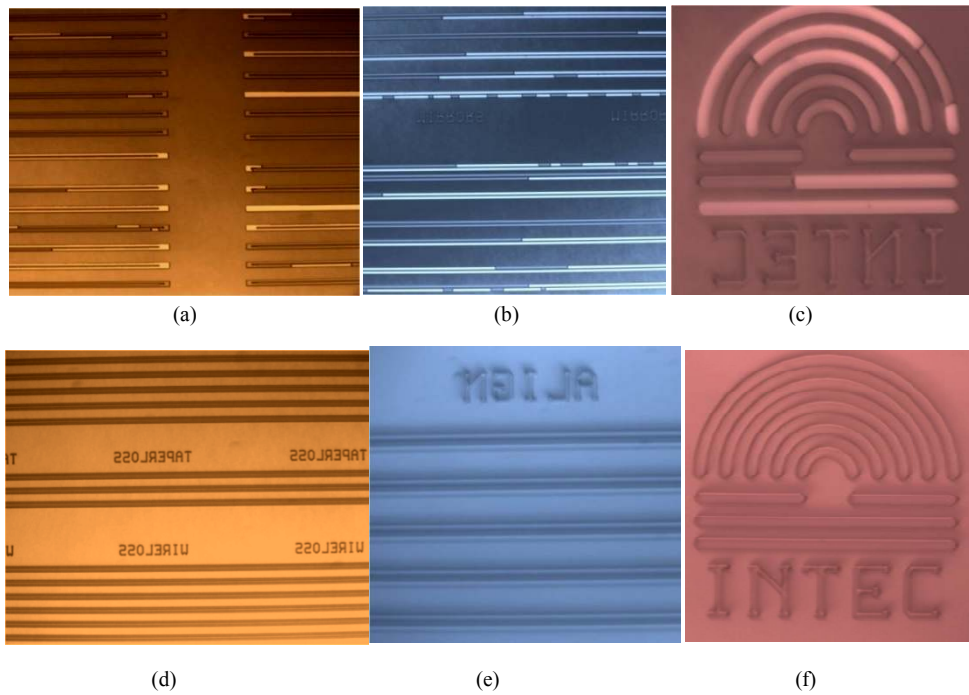
Figure 4. 10   Microscope pictures of the PSQ-L layer imprinted by silicon molds and on silicon substrates (a)(b)(c)with incomplete features (d)(e)(f) with intact features
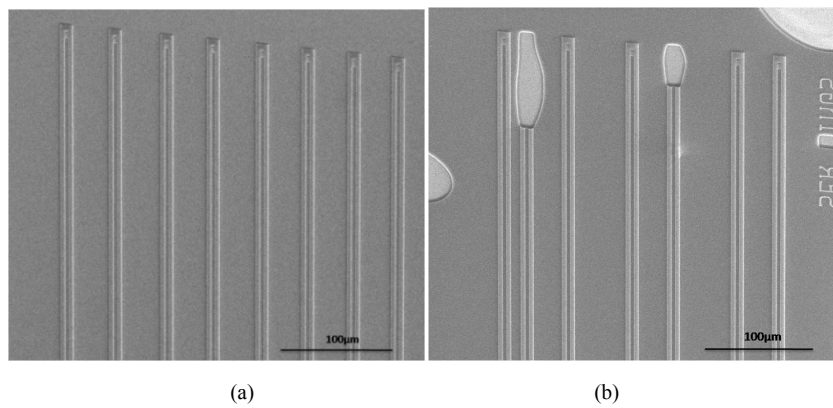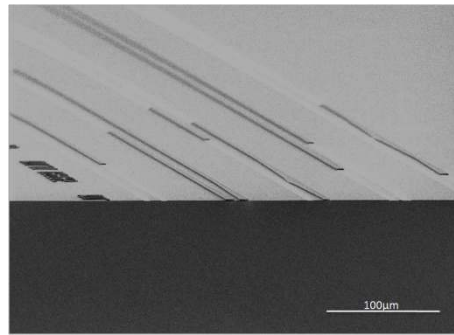
(c)

Figure 4. 11 SEM pictures of the imprinted PSQ-L layer using silicon molds and silicon substrates (a) with intact features (b) (c)with incomplete features

For a good imprint process, the patterns on the mold should be fully transferred to the substrate without much distortion. The microscope pictures of the imprinted PSQ-LH films after detaching the mold are shown in Figure 4. 10. Apparently, this imprint process is not suitable for this kind of material. Some features on the molds are missing on the imprinted layer. The missing parts are expected to have sticked on the molds. The SEM pictures of the imprinted PSQ-LH films prove (Figure 4. 11) this point. This imprint process is done many times. Even though sometimes we can have some good imprinted features; we can never avoid the incomplete imprinted features. The imprinted results (some parts stick to the mold) indicate that one side (the mold or the substrate surface) has more surface power than the other side. So we expect that the hydrophobic treatment of the mold surface or the hydrophilic treatment of the substrate is not enough. The reasons for this phenomenon are expected to be the following:

  a)   in step 2 of Figure 4. 9, the UV curing time is not enough;
  b)   the mold is partly not clean and causes a partly bad hydrophobic treatment;
  c)   the anti-adhesion treatment of the mold is not uniform;
  d)   the hydrophilic treatment of the substrate is not uniform;
  e)   the surface of the polymer is not cured completed because of the existence of the air

    We try to improve the imprint process by taking the following measures,
→ a) try to increase the curing time
→ b) try to clean the mold completely
→ c) try to use a gaseous anti-adhesion treatment (which is more uniform than wet method)
→ d) try a hydrophilic treatment of the substrate surface by oxygen RIE (reactive ion etching) to make the substrate more uniformly hydrophilic
→ e) try to cure the polymer layer in nitrogen

       However, none of the above measures above solve the problem. The real reason is found when doing the imprint by using silicon molds and quartz glass substrates and it will be explained in the next section.

(a)   (b)   (c)
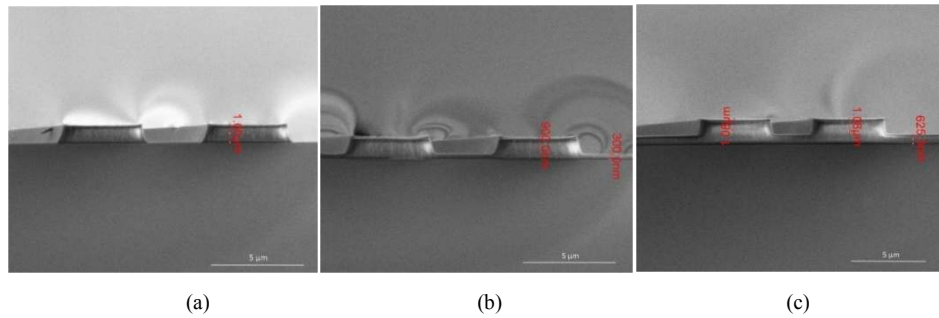
Figure 4. 12 SEM pictures of the cross-section of the imprinted PSQ-LH layer using silicon molds and silicon substrates

The other aspect we need to consider for the imprinted waveguides is the uniformity of the imprinted features on the whole sample. The uniformity of the residual layer thickness reflects this property. Figure 4. 12 shows the SEM pictures of the cross-section of the PSQ-LH layer imprinted by silicon molds on silicon substrates. Figure 4. 12 (a),(b),(c) are from different regions of the sample. After UV curing, the polymer PSQ-L is still in a liquid state and can easily be deformed. So the patterns on the molds can be transferred completely to the polymer PSQ-LH layer. The residual layer of the ridge waveguide depends on the pressure applied on the mold during the imprint process. Because the home made imprint machine cannot provide a uniform pressure on the whole sample substrate, the thickness of the residual layer in Figure 4. 12 (a),(b),(c) is not identical and some parts get almost zero residual layers (Figure 4. 12 (a)). A uniform residual layer is expected to be obtained by using a professional imprint machine.

4.2.1.2 Imprint with silicon mold and quartz glass substrate
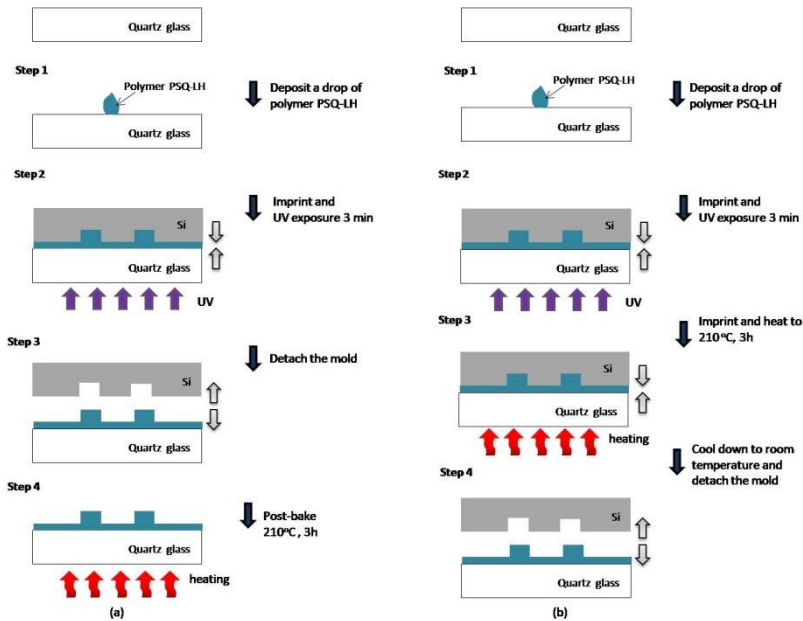
Figure 4. 13 Hard mold imprint process by using silicon molds and quartz glass substrates (a) post-bake after detaching the mold (a) post-bake before detaching the mold

The polymer PSQ-L has two steps of curing (first UV curing, and then thermal curing). The imprint process can also be done by S-FIL (Step-and-flash imprint lithography process) using a silicon mold and quartz glass substrates. We tried this way of imprint process. The imprint process is shown in Figure 4. 13 (a). The imprint procedure is as follow: First the quartz glass gets a hydrophilic treatment by a piranha solvent and the mold is anti-adhesion treated; then a small drop of polymer PSQ-L is deposited on the quartz glass substrate; then the silicon mold is pressed to the substrate under 1 atmosphere pressure; the UV light illuminates from the quartz glass side to cure the polymer. After 5 minutes exposure, the mold is detached from the substrate. The imprinted PSQ-L film needs to be post-baked for 3 hours at 210°C to be fully polymerized. The same kind of SOI mold (as mentioned in the previous section) is used to test the fabrication techniques. The imprint process is done by the Mask aligner (Suss MA 6). The quartz glass acts as a mask and the mold acts as a substrate when doing imprint process by the mask aligner.

The imprinted pattern on the PSQ-LH film shows that the features on the molds are fully transferred to the substrate (Figure 4. 14, Figure 4. 15). The problems of the polymer partly sticking on the mold haven't been met in this process. Figure 4. 15 (a)(b) shows the imprinted grating on the PSQ-LH film. The mold is an SOI wafer with a depth of 220nm (etched only to the silicon layer on top). The SEM pictures of the cross-section of the imprinted grating are shown in Figure 4. 15(c)(d). The small tilt of the sidewall is due to the insufficient power of the UV lamp on the mask aligner machine. In Figure 4. 15 (c)(d) the depth of the grating is about 135nm (compared to

the mold depth of 220nm) which means the material shrinks during the UV curing process. The exact percentage of the shrinkage after UV exposure has not been studied yet.

(a)   (b)   (c)
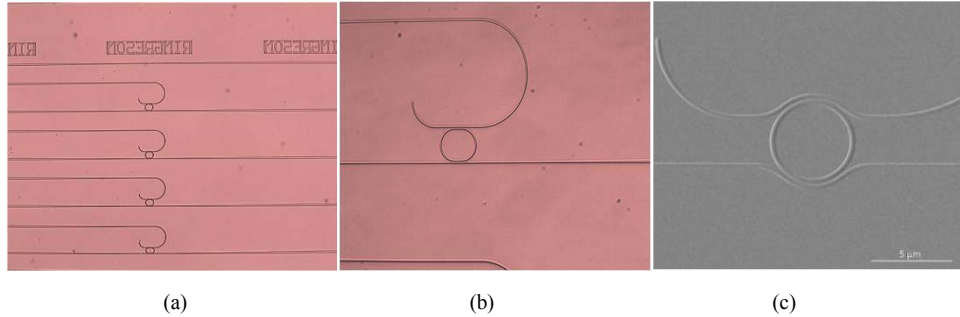
Figure 4. 14 Pictures of the imprinted PSQ-LH layer by silicon mold and quartz glass substrate   (a)(b) microscope pictures (c)SEM pictures

(a)   (b)

(c)   (d)
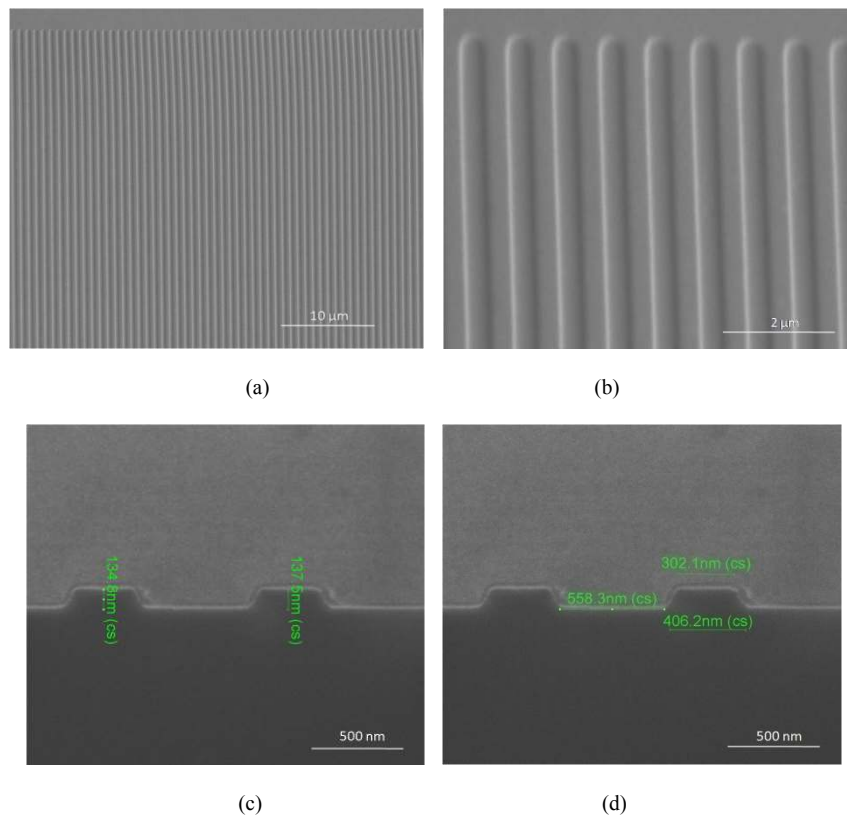
Figure 4. 15 SEM pictures of the imprinted grating on PSQ-LH layer by silicon molds and quartz glass substrates (a)(b)top view (c)(d) cross-section

(a)   (b)
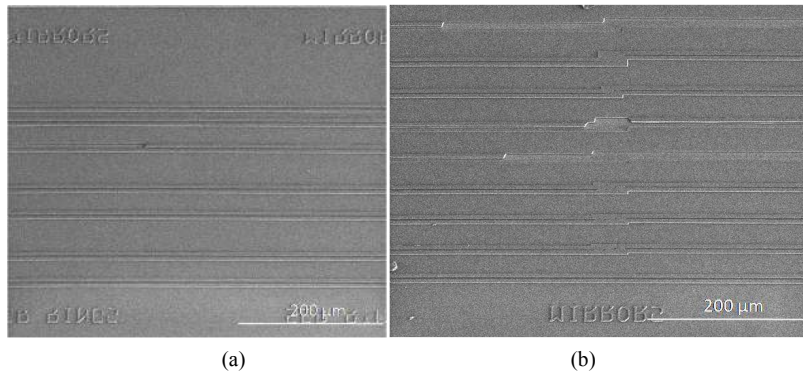
Figure 4. 16 SEM pictures of the imprinted PSQ-LH layer by silicon molds and quartz glass substrates with a post-bake process without detaching the mold

The imprint process in Figure 4. 13 (a) never has the problem of the polymer sticking on the silicon molds. So we speculate that the real reason for the sticking is the little methanol produced in the polymer thermal curing process or the little solvent inside the material. These small molecules cannot come out of the silicon molds. The process in Figure 4. 13(b) is proposed to prove this point. The only difference between Figure 4. 13 (a) and (b) is only in step 3 and step 4: (a) is first detaching the mold and then doing the post-bake; (b) is imprinting while heating and then detaching the mold. The problem of the polymer partly sticking on the silicon mold occurs again in the process of Figure 4. 13 (b). As shown in Figure 4. 16, some parts of the structures are missing after detaching the mold. So the real reason for the problem of polymer sticking on the silicon molds is the little methanol produced in the polymer thermal curing process or the little solvent inside of the polymer PSQ-L.

4.2.2 Soft-lithography

As discussed in the previous section, it seems impossible to imprint the polymer PSQ-L waveguides using silicon molds and silicon substrates. Transparent molds or transparent substrates are more preferable for this kind of polymer. Compared to silicon substrates, quartz glass substrates are difficult to be cleaved. Quartz glass molds are also difficult to be fabricated (to be etched). Therefore we resort to a kind of transparent and flexible molds: PDMS molds. The imprint process by using this kind of soft molds is also called soft-lithography [6, 19].

For fabrication of submicron structures, PDMS molds have more advantages than UV-transparent silica glass molds. The cost of PDMS molds is quite low. Once a master mold is made, it can be used many times. Soft-lithography has been proved an effective way to fabricate polymer waveguide circuits. The process includes three steps: first fabricating master molds; then pouring PDMS on top to fabricate PDMS molds, and finally doing the imprint process. A detailed fabrication process will be explained in the following section.

4.2.2.1 Master molds fabrication and PDMS molds fabrication
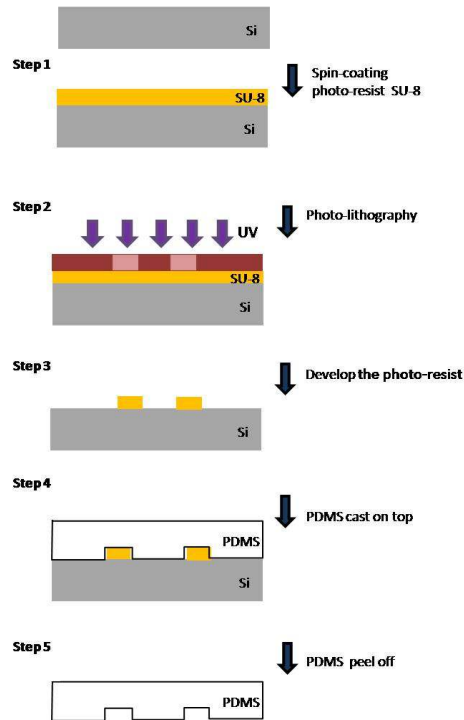
Figure 4. 17 Master molds and PDMS molds fabrication process

The fabrication processes of master molds and PDMS molds are shown in Figure 4. 17. First we need to fabricate a master mold by the conventional-lithography. Then the PDMS is poured on top to replicate the pattern and form the PDMS molds. The master molds for soft-lithography can be made from silicon or a photo-definable resist. The negative resist SU-8 is a commonly used resist for fabrication of master molds. For us, the pattern's minimum resolution is 1μm, which is sufficient for using photo-definable resist to fabricate master molds.

SU-8(2) (purchased from MicroChem Corp.,which has the lowest viscosity in the SU-8 series) is used for the fabrication of the master mold. The steps for fabricating the master mold are shown in Figure 4. 17. First, the SU-8(2) is spin-coated on the silicon substrate. Referring to the product instruction from MicroChem Corp., the spin-coating speed is 2000prm to control the film thickness to be about 2μm. After spin-coating, a pre-exposure bake of 90 seconds is necessary to evaporate the solvent in SU-8. The exposure process is done by the mask aligner and the exposure is optimized to be 10 seconds for this thickness. A post-exposure bake of

90s follows after lithography to fully cure the exposed part. The development time of 30s in SU-8 developer is optimized to fabricate straight sidewalls. Finally, the sample is post-baked at 170°C for 3 minutes to let the resist fully harden. The lithography exposure time and develop time are optimized for defining a straight and smooth side-wall.
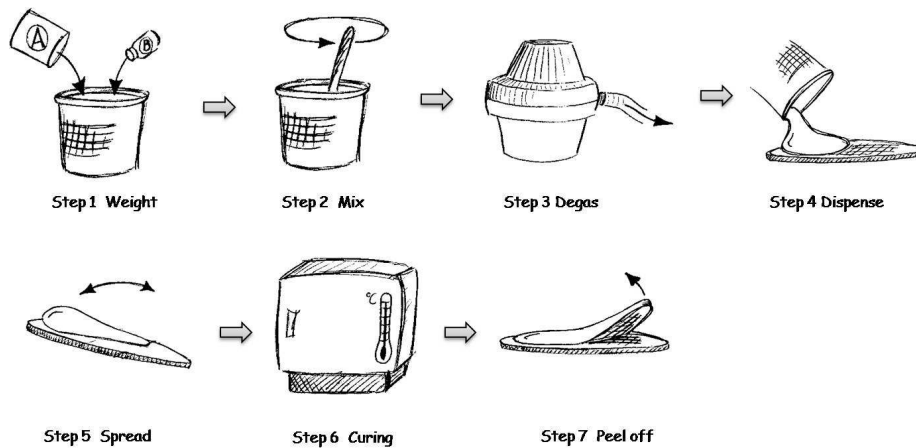
Figure 4. 18 Preparation procedure of PDMS molds

After fabrication of the master mold, the PDMS molds are fabricated. The PDMS (polydimethylsiloxane) is a kind of silicone. PDMS (Sylgard 184, purchased from Dow Corning) is UV-transparent and has low viscosity. PDMS (Sylgard 184) has two components: a base part and a curing agent part. The detailed procedure for preparing a PDMS mold is shown in Figure 4. 18. The procedures are as follow:

1. Take the curing agent and base part with a ratio of 1:10 (by weight).

2. Use a plastic spoon to mix the base and the curing agent.

3. After the mixing the silicone mixture will be full of air bubbles and needs degassing. This is done in an exsiccator using vacuum.

4. Dispensing the silicone on to the template and also degassing in exsiccator.

5. Tilting the sample in different directions to make PDMS to cover the whole template by silicone.

6. PDMS (Sylgard 184) is thermally curable. The curing temperatures vary from room temperature to over 150°C. The curing time depends on the curing temperature. In our case, we use a curing time of 10 minutes at 150°C.

7. Peel off the stamp from the template

The surface of the SU-8 master mold is not specifically treated since the polymer

surface is already hydrophobic. The master molds can be reused many times. This is also one of the advantages of using PDMS molds. Once a complicated master mold is fabricated, it can be used many times. Moreover, the PDMS molds can be easily peeled off from the substrate without destroying the substrates. In the next section, the imprint process using the PDMS molds will be described.

4.2.2.2 Imprint fabrication of polymer PSQ-L waveguides

As we have the PDMS molds, we first try to do the imprint on the core layer as other works[6]. The imprint process is shown in Figure 4. 19. First, an under-cladding layer PSQ-LL is spin-coated on the silicon substrate. After oxygen RIE of 5 minutes, a core layer PSQ-LH is spin-coated on top or a drop of PSQ-LH is deposited on top. Then the PDMS mold is put on top. After some time, it is exposed to the UV lamp for 3 minutes. After that, the PDMS mold is peeled off and the polymer is baked for 2h at 200°C to allow further solidification after UV exposure.

An important aspect in this fabrication process for polymer waveguides is to minimize the residual layer thickness. A thick residual layer should be avoided because it can cause extra bending loss and cross-talk between adjacent waveguides. Conventionally, RIE etching is carried out after the imprint to etch through the residual layer. However, RIE etching is not an ideal solution as it causes sidewall roughness and may even destroy the optical properties of the polymer waveguides.

The thickness of the residual layer is related to the imprint time, imprint pressure and viscosity of the imprint material [74]. There are several ways to reduce the thickness of the residual layer [74] to a tolerant extent, like high pressure [75] or dilution of the polymer solution to reduce the viscosity [31]. High pressure can cause deformation of the mold. For us, it is hard to employ high uniform pressure on the PDMS molds. So we try to dilute the PSQ-LH with the solvent acetone to reduce the thickness of the residual layer. Experimental results show that we can reduce the thickness of the residual layer in this way only to 1µm since a highly diluted polymer has problems in UV-curing. So we resort to another imprint process.
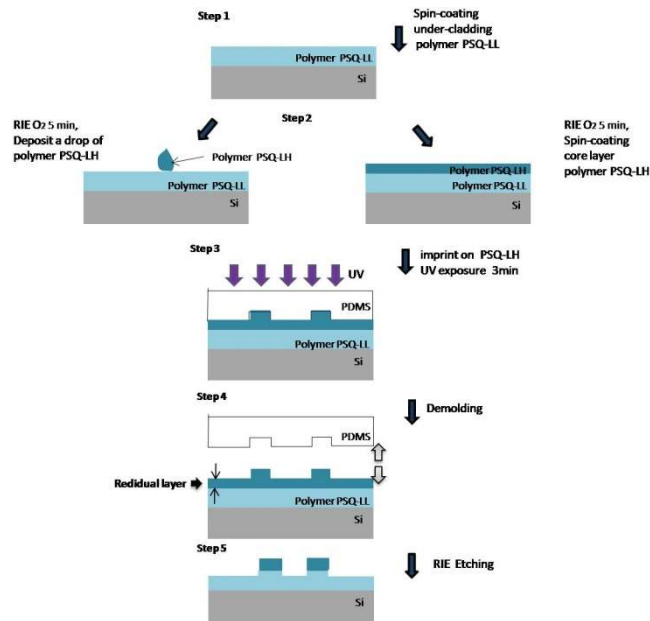
Figure 4. 19 Imprint process A for fabrication of PSQ-L waveguides by using PDMS molds
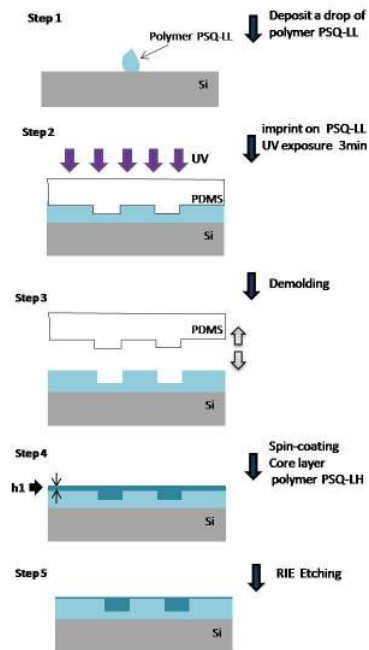
Figure 4. 20 Imprint process B for fabrication of PSQ-L waveguides by using PDMS molds

Unlike in conventional imprint processes, the imprint step for structuring in this paper is done first on the cladding layer rather than on the core layer and is followed

by a spin-coating step to fill the imprinted features with core layer material. This approach smartly avoids controlling the thickness of the residual core layer. The imprint process is carried out as follows (Figure 4. 20). First, a drop of pure PSQ-LL is deposited on the silicon wafer, and then the PDMS mold is put on top. After 20 minutes imprint time, it is exposed to the UV lamp for 3 minutes. After that, the PDMS mold is peeled off and the polymer is baked for 1h at 180°C to allow for solidification after UV exposure. To improve the adhesion to the second layer, 5 minutes of oxygen plasma etching is done on the first layer. Then the core layer PSQ-LH is spin-coated on the first layer with high speed (9500rpm). Finally, the sample is post baked at 180°C for 2h and at 200°C for another 2h to allow for full polymerization. We use a high spin-coating speed to avoid further RIE etching of the residual core layer.

Since the residual cladding layer thickness does not need to be controlled accurately as long as it is thick enough to eliminate the substrate leakage loss, this process smartly avoids the difficulties related to controlling the thickness of the residual core layer. This method also has the advantage of being compatible with other core material.

(a) (b)

(c) (d)
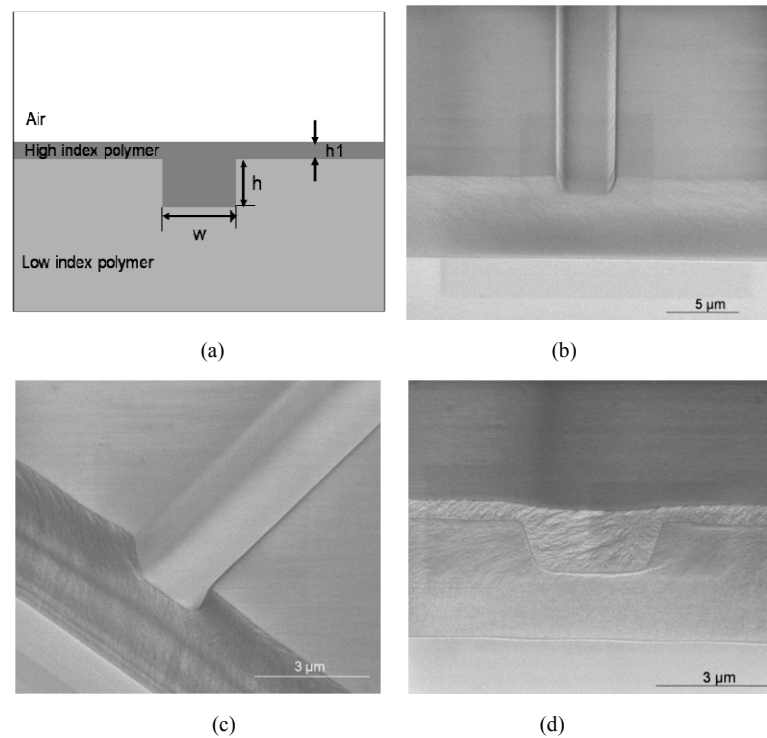
Figure 4. 21 (a) cross-section of the waveguide (b) (c) SEM picture of the imprinted low index PSQ-LL layer (d) SEM picture of the waveguide cross-section (after spin-coating the high index PSQ-LH layer)

The designed cross-section of the imprinted waveguide is shown in Figure 4. 21(a). The width and the height of the buried waveguide are designed as 3μm and 2μm. SEM pictures of the imprinted waveguide trench on the low index layer PSQ-LL are shown in Figure 4. 21 (b),(c). The cross section of the waveguide (after spin-coating the high index layer PSQ-LH) is shown in Figure 4. 21 (d). The residual layer (h1) is minimized by spin coating PSQ-LH with a high speed to about 800nm. Due to the high spin-coating speed, the core layer forms a shallow trench on the waveguide surface. It has no influence on the performance of the device since most light is confined in the ridge of the core layer. The small roughness on the sidewalls originates from the SU-8 mold.

The sidewall shape of the trench is a little collapsed, which is expected to be improved by a higher power UV lamp to achieve a better polymerization. Figure 4. 22 proves this point, which shows the imprinted cross-section of PSQ-LL layer with lower UV exposure power.
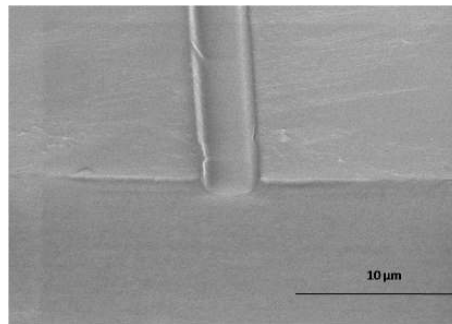
Figure 4. 22 Cross-section of the imprinted PSQ-LL layer (with low UV exposure power)

4.3 Conclusion

We have successfully fabricated polymer PSQ-L based polymer waveguides. Both fabrication technologies: the conventional lithography (and ICP etching process) and the nanoimprint process are tried and investigated. The conventional lithography and ICP etching process is more complicated than nanoimprint process. The fabrication parameters of ICP etching have been optimized for fabrication of PSQ-L waveguides. For nanoimprint technology, different imprint processes are also tried for fabrication of PSQ-L waveguides. A suitable imprint process by using soft, flexible PDMS molds is found to have good compatibility with this kind of material. Simple ring resonators and straight waveguides are fabricated by both methods. Compared to conventional lithography and ICP etching process, the imprint process for fabrication of polymer waveguides is much simpler and more promising for further applications.

Chapter 5 Measurement results

5.1 Measurement setup

There are two main kinds of basic setups for measuring the response spectrum of the optical devices over a range of wavelengths. One is using a broadband light source at the input port, like a SLED (super-luminescent light-emitting diode), and using an optical spectrum analyser to collect light at the output port (Figure 5. 1(a)). The other method is to use a tubale laser as a light source and using a power meter to detect power at the output port (Figure 5. 1 (b)). The tunable laser sweeps a range of wavelengths to get response over the whole spectrum. For data collection, the optical spectrum analyser is connected to the computer by a GPIB cable. The tunable laser and power meter are conneted to the computer by GPIB cable to collect data.

(a)

(b)
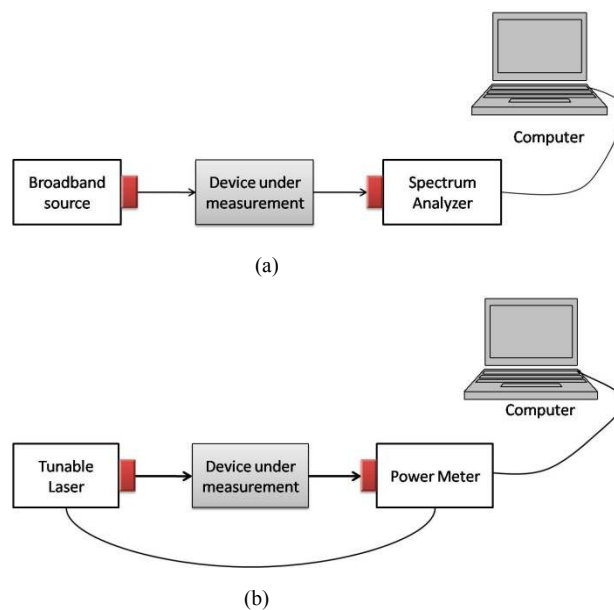
Figure 5. 1 Measurement schemes for measuring transmission spectrum
(a) By using broadband light source and spectrum analyzer
(b) By using tunable laser and power meter

Both setups in Figure 5. 1 can be used to measure the transmission spectrum of optical devices. One aspect has to be taken into account when doing the measurement

of the transmission spectrum. For the transmission spectra with narrow bandwidth, a tunable laser is more preferable than an optical spectrum analyzer, because it gives higher resolution. Take the polymer ring resonators designed in the previous chapter for example, the FSR of the ring resonator is expected to be around 0.6nm. The minimum resolution of our spectrum analyser (Agilent 86140B) is 0.06nm. The optical spectrum analyzer can not be used to get enough resolution for this case. A tunable laser (Santec TSL-510 with a minimum resolution of 1pm) and a detector must be used in this case.

(a)

(b)
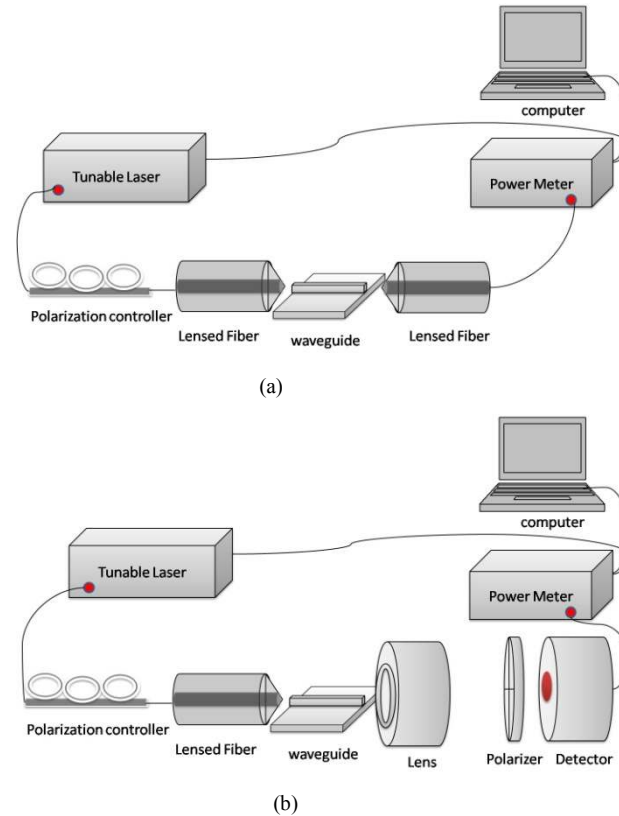
Figure 5. 2 Measurement setup for end-fire measurements (a) Using lensd fiber to couple light in and out (b) using lensed fiber and objective lens to couple light in and out

Another aspect is how to couple light from fiber into polymer waveguides for the measurement. As the polymer waveguide has a core of several micrometers wide, the light can be coupled into the waveguides horizontally by aligning a lensed fiber (Ozoptics) or a single mode fiber with polymer waveguide facets. This type of coupling mechanism for measurements is also called end-fire measurements (as shown in Figure 5. 2). The light is launched into the waveguide through a lensed fiber

and collected by another lensed fiber (Figure 5. 2 (a)) or a lens (Figure 5. 2 (b)). The designed polymer waveguides support a single mode. And the lensed fiber in Figure 5. 2 can also be replaced by a single mode fiber.

In Figure 5. 2, the lensed fiber is mounted on a 3-dimension translation stage and the sample is mounted by the vacuum chunk on a 2-dimension translation stage. (Figure 5. 3) Since the polymer material is transparent to visible light, the alignment between the lensed fiber and the polymer waveguide can be easily done by launching red light (from the red laser). For the out coupling part when using a lens in Figure 5. 2 (b), the infrared camera and TV monitor are used for alignment.
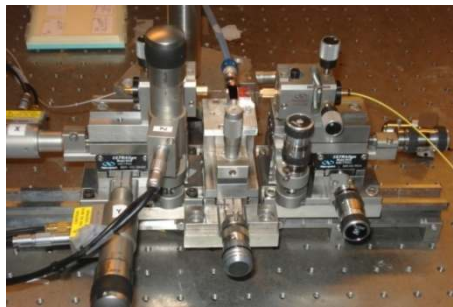
(a)
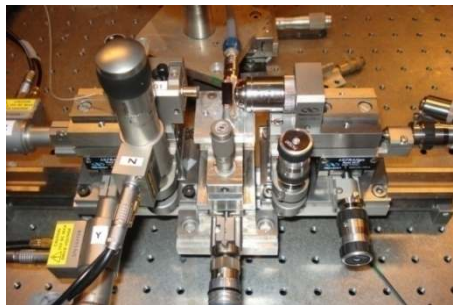
(b)

Figure 5. 3 Photos of measurement setup (a) using lensed fiber to couple light in and out (b) using lensed fiber and lens to couple light in and out

In order to separate the TE and TM mode in the polymer waveguides, either single polarization light (TE or TM) should be launched into waveguides or a polarizer (acting as a polarization filter) should be used at the output port. Since a lensed fiber cannot maintain the polarization from the polarization maintaining fiber connected from the tunable laser, a polarization controller is inserted in the input port to provide different polarizations (Figure 5. 2). It has to be mentioned that the polarization controller cannot provide very accurate polarization. For more accurate polarization control, a polarizer can be inserted between the Detector and Objective lens to provide different polarizations (Figure 5. 2 (b)). Some tricks of how to separate TE and TM

mode will be discussed in the following section.

5.2 Measurement results

This section gives straightforward measurement results for PSQ-L ring resonators fabricated by soft-lithography and conventional lithography. The transmission spectra are measured by using the setup in Figure 5. 2. The detailed analysis of the transmission spectra is also given in this section.

5.2.1 Racetrack ring resonators fabricated by soft-lithography

5.2.1.1 Typical transmission spectrum

The transmission spectrum of the ring resonator is measured by coupling light from a tunable laser to the waveguide via a lensed fiber. The transmitted light is collected by a single mode fiber to the power meter. A polarization controller is used at the input port to select the polarization (as shown in Figure 5. 2 (a)). Figure 5.4 (c) (d) shows the measured TE and TM mode transmission spectrum of racetrack ring resonators fabricated by soft-lithography. The waveguide has a width of 3μm and a height of 2μm. The ring resonator has a radius of 400μm, gap of 1.4μm, and coupling length of 150μm. The little parasitical peak (more obvious at the drop port for dBm scale) is due to inaccurate control of the polarization of the input light and therefore comes from the resonance peaks of the TM mode. Since the TM mode shows similar response as the TE mode, the following analysis is therefore done first for TE polarization. It is expected that by optimizing the waveguides dimension polarization independent waveguides can be fabricated.

The transmission spectrum of the ring resonators is expected to follow the Lorentz function as mentioned in Chapter 3,

$$I_{TH} = \frac{T - 2A^{1/2} \cdot T \cdot \cos(2\pi / \lambda \cdot n_{eff} \cdot 2\pi R) + A \cdot T}{1 - 2A^{1/2} \cdot T \cdot \cos(2\pi / \lambda \cdot n_{eff} \cdot 2\pi R) + A \cdot T^2} \qquad (5.1)$$

$$I_{DR} = \frac{(1 - T)^2 \cdot A^{1/2}}{1 - 2A^{1/2} \cdot T \cdot \cos(2\pi / \lambda \cdot n_{eff} \cdot 2\pi R) + A \cdot T^2} \qquad (5.2)$$

Where A is the power attenuation coefficient per round trip; T is the power transmission coefficient; n_{eff} is the effective index of the bend waveguide; R is the radius of the ring. The ring is on resonance when $n_{eff} \cdot 2\pi R = m \cdot \lambda$, where m is an integer.

For TE polarization mode, the FSR of the ring is about 0.57nm as expected due to the large ring radius. The FWHM (Full Width of Half Maximum) is about 0.042nm. By taking the ratio between the resonance wavelength and FWHM, a Q factor of about 3.7×10^4 is calculated. 6dB extinction ratio at the through port and 18dB

extinction ratio at the drop port is obtained. By fitting the data, A and T in Eq.(5.1) can be extracted. A is about 0.80, which means 80% of the power is maintained after light propagation per round trip; T is about 0.89, which means that 11% of the power is coupled from the straight waveguide into the ring.

The per round trip power attenuation corresponds to a loss of 3.4 dB/cm of the ring waveguide. The material absorption loss is about 0.9 dB/cm (Chapter 2) and the loss due to mode mismatch between the straight waveguide and the bent ring waveguide is calculated to be about 0.05dB per section (corresponding to 0.7 dB/cm). From calculation, we find that the bend loss and the substrate leakage loss can be neglected. Therefore the scattering loss of the ring waveguide is estimated to be about 1.8 dB/cm.

The TM mode shows similar results as the TE mode. The attenuation factor A is extracted to be 0.79 and the transmission factor T is extracted to be 0.90. Further explanation is omitted since the results are similar to TE mode.
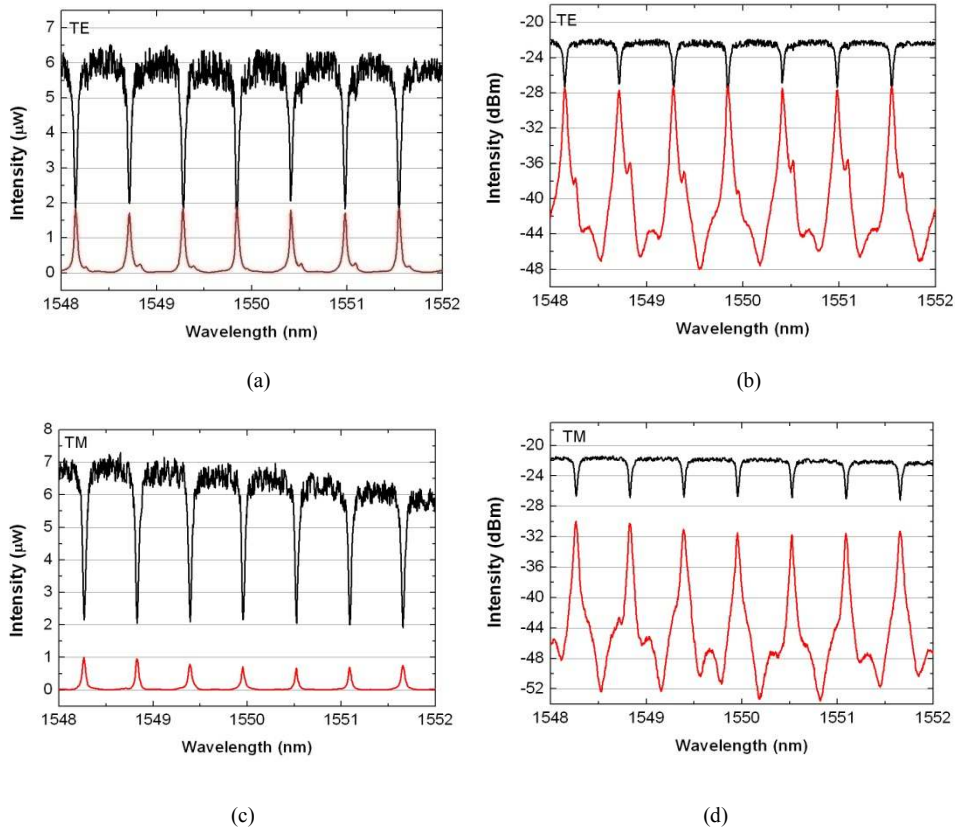
Figure 5. 4 Transmission spectrum of ring resonator fabricated by soft-lithograhy (a) TE mode with µW scale (b) TE mode with dBm scale (c) TM mode with µW scale (d) TM mode with dBm scale (Dimension parameters of the racetrack ring resonator: R=400µm, Gap=1.4µm, L=150 µm)

5.2.1.2 Discussion

This part gives more details about the analysis of the transmission spectrum of the ring resonators. The transmission spectrum of the through port is fitted by the Lorenz function of Eq.(5.1). The attenuation factor A and the transmission factor T are extracted from it. To validate the fitted results, the extracted parameters (A and T) are put back into Eq.(5.2) to calculate the theoretically expected extinction ratio of the drop port and compare that to the measurement results. The following gives an example of the analysis of the TE mode transmission spectrum of Figure 5.4.
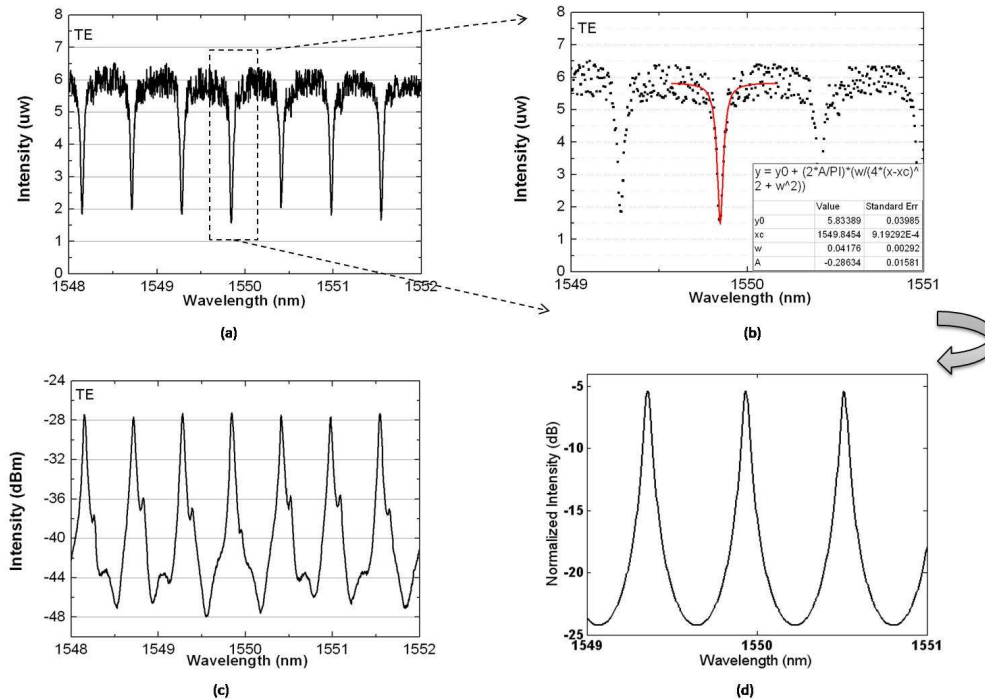
Figure 5. 5 Fitting of the transmission spectrum (a) Through port transmission spectrum of TE mode (b) Fitting of a certain transmission peak (c) Drop port transmission spectrum of TE mode (d) Theoretically calculated drop port transmission peak using the parameters extracted from (Dimensions of the racetrack ring resonator: R=400μm, Gap=1.4μm, L=150 μm)

There are two parameters that must be extracted from Eq.(5.1) and therefore two equations as a function of A and T are necessary for extracting the parameters. The equation for FWHM and extiction ratio calculated from the measured transmission

spectrum are used for extracting the parameters.

Theoretically, the transmission spectrum of the through port of the ring resonators should follow Eq.(5.1). Eq.(5.1) can also be written as a Lorentz function,

$$
\begin{aligned}
I_{TH} &= \frac{T - 2A^{1/2} \cdot T \cdot \cos\theta + A \cdot T}{1 - 2A^{1/2} \cdot T \cdot \cos\theta + A \cdot T^2} \\
&= 1 - \frac{\left(1 - A \cdot T\right) \cdot \left(1 - T\right)}{\left(1 - A^{1/2} \cdot T\right)^2 + 4 \cdot A^{1/2} \cdot T \cdot \sin^2(\theta/2)}
\end{aligned}
\tag{5.3}
$$

Where θ is defined as $\theta = \dfrac{2\pi}{\lambda} \cdot n_{eff} \cdot 2\pi R$. The ring is on resonance when

$\theta = \dfrac{2\pi}{\lambda_c} \cdot n_{eff} \cdot 2\pi R = m \cdot 2\pi$, where m is an integer. For a transmission spectrum

with a small bandwidth, $\sin\dfrac{\theta}{2} \approx \dfrac{\theta}{2}$, and,

$$
d(\frac{\theta}{2}) = \pi \cdot 2\pi R \cdot d(\frac{n_{eff}}{\lambda}) = \frac{\pi}{FSR} \cdot d\lambda
\tag{5.4}
$$

Therefore taking Eq.(5.4) into Eq.(5.3), I$_{TH}$ can be expressed as,

$$
\begin{aligned}
I_{TH} &= 1 - \frac{\left(1 - A \cdot T\right) \cdot \left(1 - T\right)}{\left(1 - A^{1/2} \cdot T\right)^2 + 4 \cdot A^{1/2} \cdot T \cdot \sin^2(\theta/2)} \\
&= 1 - \frac{\left(1 - A \cdot T\right) \cdot \left(1 - T\right)}{\left(1 - A^{1/2} \cdot T\right)^2 + 4 \cdot A^{1/2} \cdot T \cdot (\theta/2)^2} \\
&= 1 - \frac{\left(1 - A \cdot T\right) \cdot \left(1 - T\right)}{\left(1 - A^{1/2} \cdot T\right)^2 + 4 \cdot A^{1/2} \cdot T \cdot (\pi/FSR)^2 \cdot \left(\lambda - \lambda_C\right)^2}
\end{aligned}
\tag{5.5}
$$

Where FSR is the free spectral range of the ring resonator.

A normalized Lorentz function is expressed as,

$$
y = y_0 + \frac{(2A_0/\pi) \cdot w}{4\left(x - x_c\right)^2 + w^2}
\tag{5.6}
$$

Where w is the FWHM (full width of half maximum) of the Lorentz function.

Comparing Eq.(5.5) with a normalized Lorentz function of Eq.(5.6), the FWHM of the transmission sepctrum is a function of A and T,

$$
w = \frac{FSR}{\pi} \cdot \frac{1 - A^{1/2} \cdot T}{\sqrt{A^{1/2} \cdot T}}
\tag{5.7}
$$

Since w can be extracted by Lorentz fit of the transmission spectrum, $A^{1/2} \cdot T$

can be calculated from Eq.(5.7).

The other function of A and T is the extinction ratio of the through port. The extinction ratio of the transmission spectrum can be calculated from the ratio of the maximum and minimum of the fitted Lorentz function,

$$Ex = \frac{1+A^{1/2}}{1-A^{1/2}} \cdot \frac{1+A^{1/2} \cdot T}{1-A^{1/2} \cdot T} \approx \frac{y_0}{y_0 + 2A_0 / \pi / w} \qquad (5.8)$$

Therefore A and T can be extracted from Eq.(5.7) and Eq.(5.8).

As shown in Figure 5. 5, the through port of the transmission spectrum is first fit by a normalized Lorentz function. The FWHM, A and T are extracted to be 0.042, 0.80, 0.89. By taking the value A and T back into the Eq.(5.2), a drop port spectrum is theoretically calculated and plotted in Figure 5. 5 (d). The theoretically calculated extinction ratio of the drop port in Figure 5. 5(d) is almost the same as the one measured in Figure 5. 5(c), which gives a good conformity of the theoretical calculation and measurement results.

5.2.2 Notch filters fabricated by soft-lithography

5.2.2.1 Typical transmission spectrum

Figure 5. 6 shows the measured transmission spectrum of the polymer notch filter at critical coupling condition fabricated by soft-lithography. The light is coupled into the waveguide from a tunable laser by a lensed fiber and collected by a lens at the output port (Figure 5. 2(b)). The TE and TM mode is seperated by a polarizer in front of the detector. The critical coupling condition of the notch filter is achieved when the round trip attenuation factor A equals the transmission factor T. As mentioned above, the round trip attenuation factor A of a 400μm radius ring is about 0.80, therefore 20% of coupling effciency is needed to satisfy critical coupling condition. The notch filters are designed with the same coupling length of 50μm and different coupling gaps from 1μm to 1.4μm. Experimental results show that the notch filter with a gap of 1μm satisfies the coupling condition. As shown in Figure 5. 6, the TE and TM mode have maximum extinction ratio of 20 and 13 dB, respectively, illustrating that the critical coupling condition is essentially satisfied. The resonators have a free spectral range (FSR) of 0.6 nm, a 3-dB bandwidth of 0.045 nm and 0.035nm, Q factor of 3.4×10^4 and 4.4×10^4 respectively for TE and TM mode.

Similar to racetrack ring resoantors, the transmission spectrum of notch filters is fitted by a Lorentz function. The round trip attenuation factor A and the transmission factor T are extracted: for TE mode, T=85%, A=0.81; for TM mode, T=87%, A=0.79.

It should be mentioned that the transmission spectrum of a notch filter is sensitive to both the round trip attenuation coefficient A and transmission coefficient T. So even a small change of T or A will cause a big difference in the transmission spectrum, especially for the case of near critical coupling.

(a)   (b)
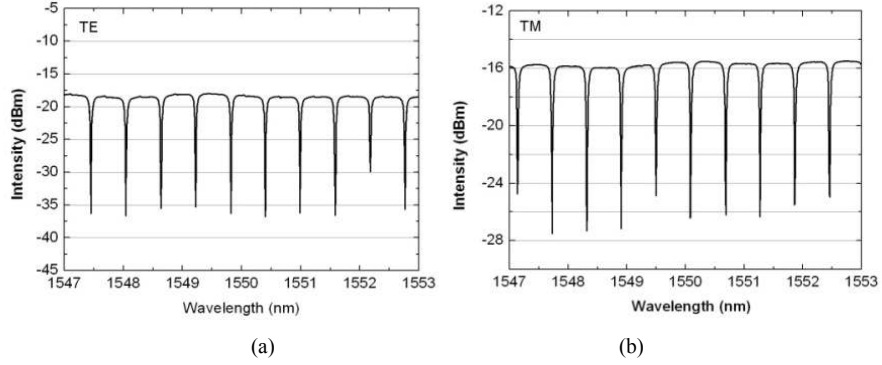
Figure 5. 6 Transmission spectrum of notch filter at critical coupling condition
(a) TE mode (b) TM mode
(Dimension parameters of the notch filter: R=400µm, Gap=1µm, L=50 µm)

5.2.2.2 Discussion

The fitting of the transmission spectrum is similar to that of the racetrack ring resonators. Here we just illustrate the formulation difference for the fitting of the spectrum.

Theoretically, the transmission intensity of the notch filter is expressed as,

$$
\begin{aligned}
I &= 1 - \frac{(1-A)\cdot(1-T)}{\left(1-\sqrt{A\cdot T}\right)^2 + 4\cdot\sqrt{A\cdot T}\cdot\sin^2(\theta/2)} \\
&= 1 - \frac{(1-A)\cdot(1-T)}{\left(1-\sqrt{A\cdot T}\right)^2 + 4\cdot\sqrt{A\cdot T}\cdot\pi/FSR\cdot(\lambda-\lambda_C)^2}
\end{aligned}
\tag{5.9}
$$

Comparing Eq.(5.9) with the normalized Lorentz function of Eq.(5.6), the FWHM of the transmission sepctrum can be expressed as,

$$
w = \frac{\pi}{FSR}\cdot\frac{1-\sqrt{A\cdot T}}{\sqrt[4]{A\cdot T}}
\tag{5.10}
$$

Since w can be extracted by a Lorentz fit of the transmission spectrum, $A\cdot T$ can be calculated from Eq.(5.10).

The extinction ratio of the through port is also related to A and T. The extinction ratio of the transmission spectrum can be calculated from the ratio of the maximum and minimum of the measured transmission spectrum,

$$
Ex = \left|\frac{\sqrt{T}-\sqrt{A}}{\sqrt{T}+\sqrt{A}}\right|\cdot\frac{1+\sqrt{A\cdot T}}{1-\sqrt{A\cdot T}}
\tag{5.11}
$$

Therefore A and T can be extracted from Eq.(5.10) and Eq.(5.11).

5.2.3   Racetrack   ring   resonators   fabricated   by

photo-lithography

The ring resonators fabricated by conventional photo-lithography and ICP etching are characterized. The transmission spectrum of the ring resonators is measured by the setup shown in Figure 5. 2 (a). Light is coupled from a tunable laser into the waveguide via a lensed fiber. The transmitted light is collected by a single mode fiber to the power meter. A polarization controller is used at the input port to select the polarization. Figure 5.7 (c)(d) shows the measured transmission spectrum of the ring resonator for TE mode and TM mode on both linear scale and dBm scale. This ring has a radius of 400μm, a gap of 1.8μm and a coupling length of 150μm. The TM mode shows similar response as the TE mode. Taking the TE mode as example, the FSR of the ring is about 0.56nm as expected due to the large ring radius. The FWHM (Full Width of Half Maximum) is about 0.027nm. By taking the ratio between the resonance wavelength and the FWHM, a Q factor of about 5.7×10^4 is calculated. About 2.5dB extinction ratio at the through port and 23dB extinction ratio at the drop port is obtained.

The measured spectrum of the ring resonators is fitted by using Eq.(5.5). Parameters of A and T are extracted. For TE mode, A is about 0.81, which means 81% of the power is maintained after light propagation per round trip; T is about 0.96, which means that 4% of the power is coupled from the straight waveguide into the ring. The low coupling efficiency is due to the large gap between the ring and the straight waveguides.

The per round trip power attenuation coefficient corresponds to a loss of 3.2 dB/cm of the bend waveguide. The material absorption loss is about 0.9 dB/cm and the loss due to mode mismatch between the straight waveguide and the bent ring waveguide is about 0.7 dB/cm, which follows from theoretical calculations. Assuming the bend loss and substrate leakage loss can be neglected, a scattering loss of the ring waveguide of 1.6 dB/cm is estimated for both TE and TM mode, which is quite low compared to other polymer ring resonators [6, 21, 76].

The TM mode shows similar results as the TE modes. The attenuation factor A is extracted to be 0.81 and the transmission factor T is extracted to be 0.965. Further explanation is avoided since the results are similar to the TE mode.
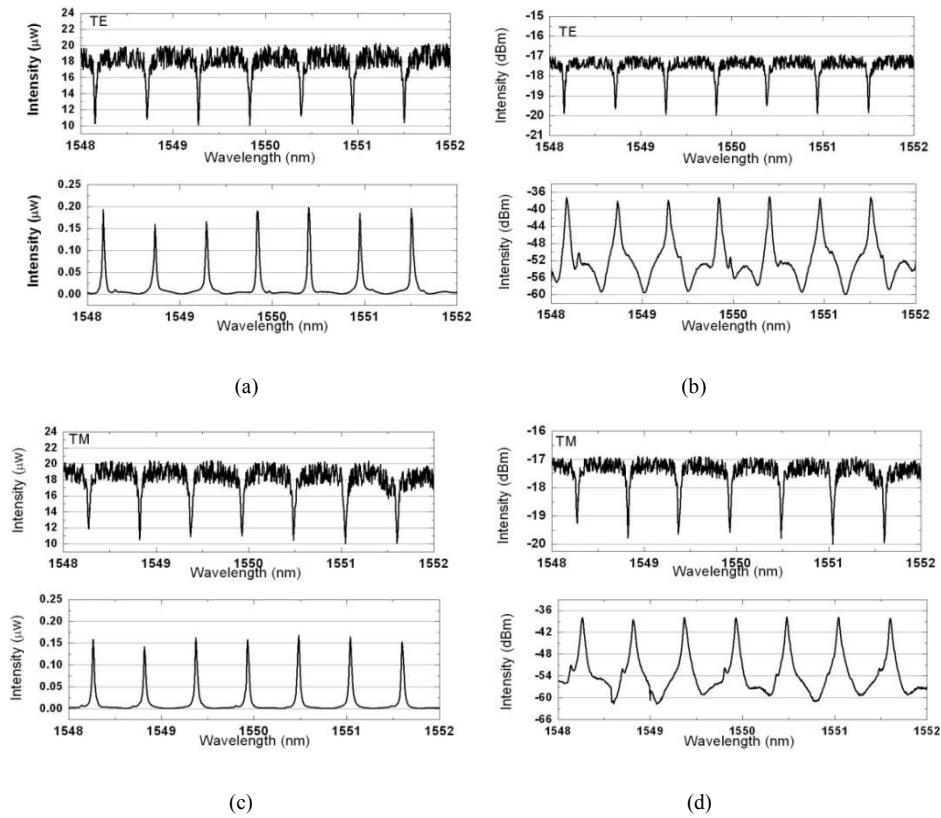
Figure 5. 7 Transmission spectrum of ring resonator fabricated by photo-lithograhy and ICP etching (a) TE mode with μw scale (b) TE mode with dBm scale (c) TM mode with μw scale (d) TM mode with dBm scale (Dimension parameters of the racetrack ring resonator: R=400μm, Gap=1.8μm, L=150 μm)

5.2.4 Loss measurement of straight waveguide

The optical loss of the waveguides is an important factor for optical devices. The loss of the bent waveguides can be extracted from the transmission spectrum of the ring resonators. However, the bent waveguides normally have a larger loss than straight waveguides and the loss also varies for different radius. It is necessary to measure the loss of the straight waveguides to evaluate the fabrication technology.

The cut-back method is most commonly used for evaluating the loss of the straight waveguides [77, 78]. However, this method is not so accurate since the coupling loss between the lensed fiber and the waveguides is not reproducible each time. The coupling loss depends on both the waveguides facets and the alignment between the lensed fiber and the waveguides facets.

The Fabry-Perot resonance method is a simple and accurate way to evaluate the loss of the straight waveguides. One important aspect of using this method is that the

facets of the waveguides have to be good enough to provide efficient reflection to the waveguides. Otherwise, imperfect reflection leads to larger evaluated loss value than the true value.

The optical loss of the straight waveguides can be extracted by using the following equation [79],

$$\alpha = -\frac{1}{L} \cdot 10 \cdot \log\frac{K}{2R} \qquad (5.12)$$

Where α is the loss of the waveguides given in dB/cm; L is the length of the waveguides; K is the contrast factor of the Fabry-Perot resonance spectrum, defined

as $K = \dfrac{I_{max} - I_{min}}{I_{max} + I_{min}}$; R is the perfect reflectivity of the facet between the core and air,

defined as $R = (\dfrac{n_{eff} - 1}{n_{eff} + 1})^2$. In an actual situation, the waveguide facet is never perfect

and thus the real R value is always smaller than the perfect facet reflectivity. Therefore the extracted value α is an upper limit of the waveguide loss.

For polymer waveguides, the facet reflection between the core and air is quite low, which results in low extinction ratio of the transmission spectrum. Considering a perfect reflection condition, the reflection of the facet between the core and air is only 4% (given that the index of polymer is 1.5 and the index of air is 1). Imperfect facets may easily lead to failure measurements of the resonant phenomenon. To our knowledge, we are the first one to use this method to measure the loss of polymer waveguides fabricated by soft-lithography.

The polymer PSQ-L waveguides are cut with the cleavage of silicon wafer. No polishing is done on the facet of the polymer waveguides. Light from a tunable laser is launched into the polymer waveguides via a lensed fiber and collected by a lens to a power meter. A polarizer is inserted in front of the detector to control TE and TM mode of the waveguides (Figure 5. 2). Figure 5. 8 shows the transmission spectrum of the straight waveguides with a length of 6.8mm.

(a)   (b)
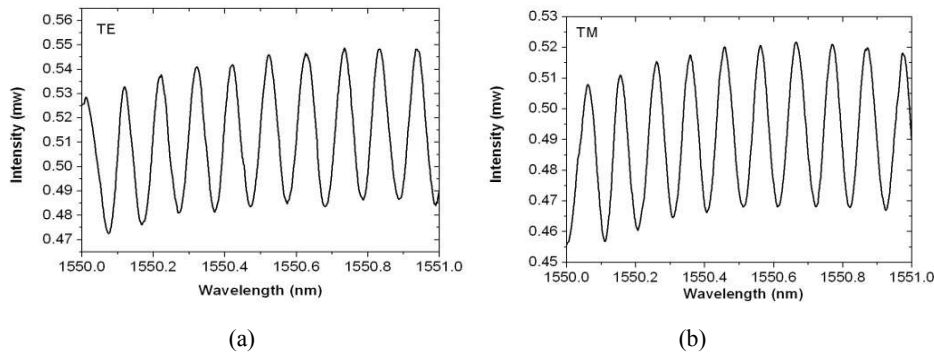
Figure 5. 8 Fabry-Perot resonance spectrum for measuring the loss of polymer PSQ-LH waveguides (a) TE polarization (b) TM polarization

By using Eq.(5.12), the extracted loss of the straight waveguides in Figure 5. 8 is 1.7dB/cm for TE mode and 2.2dB/cm for TM mode. Assuming the substrate leakage loss can be neglected and subtracting the material absorption loss of 0.9 dB/cm @1550nm, the scattering loss of the straight waveguide is less than 0.8 dB/cm for TE mode and 1.3dB/cm for TM mode. The real value of the scattering loss should be much lower than this value since the facet is below perfect facet reflectivity.

This method for the loss measurement is quite dependent on the facets of the waveguides. For not so good facets or not so good alignment, the extracted loss value of the straight waveguides is larger than the value extracted from the ring resonators. The straight waveguides fabricated by conventional-lithography are not measured by this method.

The low scattering loss of PSQ-L waveguides proves soft-lithography to be a good fabrication process for the fabrication of polymer waveguides.

5.3 Measurement tricks

5.3.1 How to split TE and TM mode

As the polymer waveguides are not designed as polarization independent waveguides, both TE and TM mode exist in the waveguide. Because TE and TM mode have different effective index and thus different resonant peak, it is necessary to distinguish the two modes when measuring the transmission spectrum.

A polarization controller is inserted in the input port to provide single polarization (Figure 5. 2) light. The polarization of the input light can be tuned by manually rotating the three wheels of the polarization controller at input port. This is a manual way to change the input polarization and the polarization of the light cannot be controlled very accurately in this way. A much better way to distinguish TE and TM mode is to use a lens to couple light out of the waveguides (Figure 5. 2(b)), the polarization is controlled by the polarizer inserted infront of the detector at the output port.

It is very difficult to accurately control the input polarization by a polarization controller. A trick is found to separate two modes by a using polarization controller if TE and TM mode have different propagation loss in the waveguide. For example, a high power (like 5 mW) is lauched into the waveguide, the detected power will change when manually rotating the wheels of the polarization controller. So if we know which mode has a larger loss beforehand, manually rotating the wheels of the polarization controller to get a the maxium or minimum power is a simple way to distingusish TE and TM mode.

5.3.2 Pros and cons of using two out-coupling elements

The pros and cons of using the two out-coupling elements (in Figure 5. 2(a) (b)) to measure the transmission spectrum of the ring resonators will be discussed here.

We take two examples of the transmission spectrum illustrated above, which are measured by both setups in Figure 5. 2(a) (b). Figure 5. 9 (a) (b) shows the transmission spectrum of the same ring resonator as in Figure 5.4 (c) (d) fabricated by soft-lithography and measured by both setups. Figure 5. 10 (a) (b) shows the transmission spectrum of the same ring resonator as in Figure 5.7 (c) (d) fabricated by photo-lithography and measured by both setups.

When using a lensed fiber or single mode fiber to collect the light at the output port (Figure 5. 2 (a)), it is not easy to accurate control the polarization of the input light. Therefore the TM mode resonance peak appears in the transmission spectrum (more obvious in the drop port, see Figure 5. 9 (b)).

When using a lens to collect the light at the output port (Figure 5. 2 (b)), it is easy to separate the TE and TM mode at the output port and obtain nice transmission spectrum for both ports (see Figure 5. 9 (a)). But for measuring the drop port with a high extinction ratio, this setup is less effective. For example, the drop port (in Figure 5. 9) should have an extinction ratio of 18dB according to the theoretical calculation, but using a lens to collect light, only an extinction ratio of about 14dB is obtained. This is more obvious when the light of the drop port is very weak, like the transmission spectrum of the ring fabricated by photo-lithography (Figure 5. 10). Only 5-6db extinction ratio is obtained by a using lens to collect light at the output port while about 20dB extinction ratio is obtained by using a single mode fiber at the output port. Therefore, for a weak light spot and a high extinction ratio, using a lens to collect the light for measuring the transmission spectrum is less effective than using a single mode fiber.

(a)   (b)
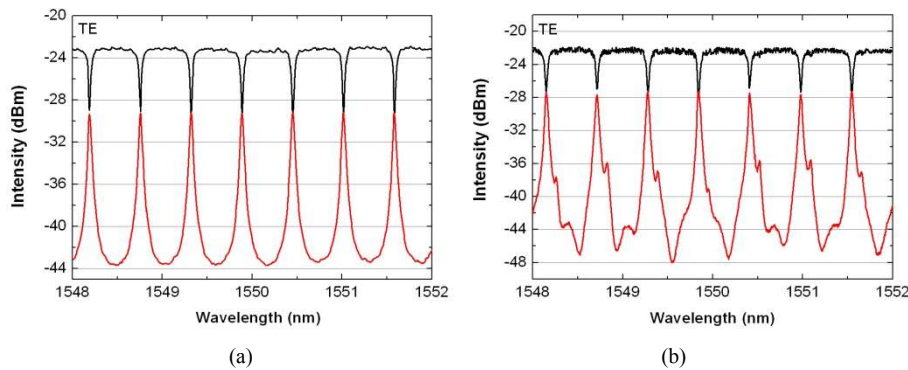
Figure 5. 9 Transmission spectrum of ring resonator measured by two setups (a) Using lens to collect light at the output port (b) Using single mode fiber to collect light at the output port (Fabricated by soft-lithography, Parameters of the racetrack ring resonator: R=400μm, Gap=1.4μm, L=150 μm)

(a)   (b)
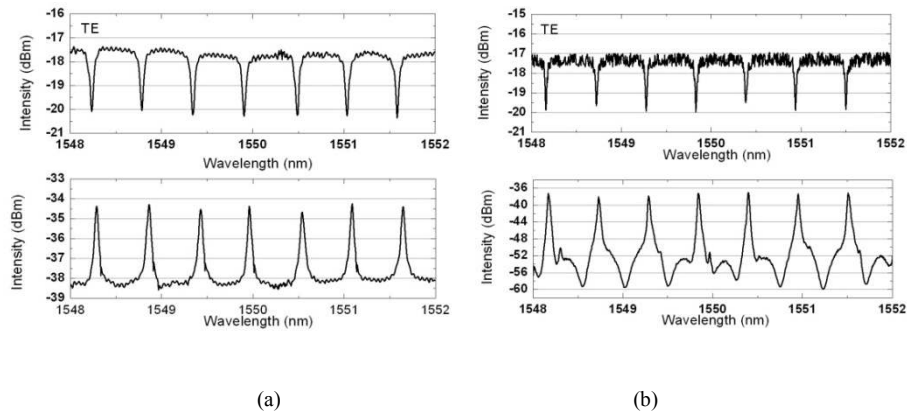
Figure 5. 10 Transmission spectrum of ring resonator measured by two setups (a) Using lens to collect light at the output port (b) Using single mode fiber to collect light at the output port (Fabricated by photo-lithograhy and ICP etching, Dimension parameters of the racetrack ring resonator: R=400μm, Gap=1.8μm, L=150 μm)

5.3.3 The influence of the tunable laser sweeping step on measured spectrum

In order to get a uniform extinction ratio in the measured transmission spectrum, the sweeping step of the tunable laser, used as light souce for the input port of the waveguides, should be much smaller than FWHM. Figure 5.11 shows the transmission spectrum of the notch filter at critical coupling condition, measured with different sweeping intervals of the tunable laser. As shown in Figure 5.11 (c) (d), with large sweeping intervals of 20pm, the transmission peak extinction ratio is not uniform. By reducing the sweeping intervals of the tunable laser, a more uniform transmission peak is obtained. However, the smaller the sweeping interval is, the longer sweeping time it takes. A compromise between the sweeping time and transmission specrum resolution must be made when doing the measurement.
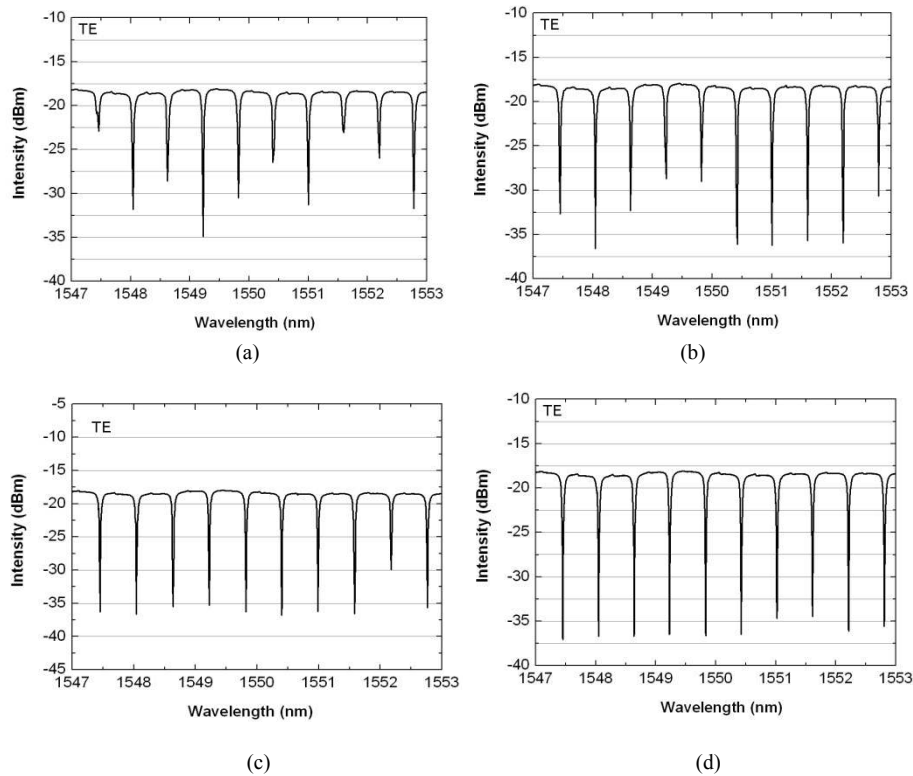
Figure 5. 11 Notch filter transmission spectrum measured with different sweeping interval of tunable laser (a) with 20pm sweeping interval (b) with 10pm sweeping interval (c) with 5pm sweeping interval (d) with 2pm sweeping interval

5.4 Experimental results analysis and outlook

This part gives insight into the measurement results. The optical loss and coupling efficiency extracted from the transmission spectrum are important parameters for ring resonator-based devices. Therefore the factors that influence the optical loss of the waveguides and the coupling efficiency between the ring and straight waveguides are analyzed. Existing problems are emphasized in the following section.

Since the fabrication process of soft-lithography is simpler and more promising than conventional-lithography, this part is mainly dedicated to the analysis of the waveguides fabricated by soft-lithography.

5.4.1 Optical loss of polymer waveguides

For microring waveguide devices, there are five possible factors contributing to the cavity loss: absorption loss from the material itself, waveguide bend loss, substrate leakage loss, surface roughness scattering loss, and the loss due to modal mismatch at the junctions of straight and curved waveguides. Among them, experiments have

shown that the surface roughness scattering loss dominates the entire loss. Theoretically, the bend loss could be suppressed by using curved waveguides with sufficiently large radius of curvature. Substrate leakage loss can be reduced by using a thicker under-cladding layer. In addition, the modal mismatch could be further reduced by using waveguide offsets at the junctions [80]. Therefore, it is possible that the losses due to waveguide bending, substrate leakage and modal mismatch can be negligible with improved waveguide and device design.

The sidewall scattering loss originates from the fabrication process. It will be extensively discussed in this section. The quality of the contact mask also has an important influence on fabricated waveguides as the defects on the mask can be transferred to the imprinted waveguides.

5.4.1.1 Waveguides fabricated by conventional lithography

The surface roughness of the waveguides fabricated by conventional lithography originates from ICP etching process. The parameters of the ICP etching process (like the pressure, the ratio of the gas) will influence the roughness of the sidewall. By optimizing the ICP etching process parameters, the loss of the waveguides can be minimized.

On the other hand, the defects on the mask also have some influence on the fabricated waveguides. The estimated scattering loss of the bent waveguides mentioned above is from early ICP etching work. Experimental results show that after regular usage of the contact mask, the loss of the fabricated waveguides increases a lot. Some defects on the contact mask may come from the mask shop during fabrication. Cleaning the mask after usage can also cause some defects on the mask.

5.4.1.2 Waveguides fabricated by soft-lithography

Several factors contribute to the scattering loss of the imprinted waveguides. The roughness of the waveguide trenches may originate from several aspects when taking a close look at the fabrication flow: 1) the contact mask defects; 2) SU-8 master mold roughness from lithography process; 3) PDMS mold; 4) cross-section structure of imprinted waveguides after spin-coating the core layer. The following will specify the several aspects.

1) the contact mask defects

There are some defects on the contact mask especially on the bending region as shown in Figure 5.12(microscope pictures). These defects may come from the mask shop during fabrication or caused by cleaning of the mask after usage. It is expected that these defects are the main cause of the scattering loss of the imprinted waveguides. Because these defects can be fully transferred to the SU-8 master mold and further to the imprinted waveguide. A second run should be done by checking the original mask beforehand and improving the quality of the mask.
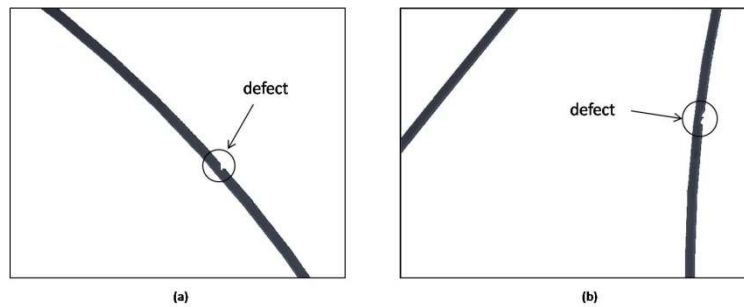
Figure 5. 12 Defects on the contact mask (microscope pictures)

Few defects are observed on the straight waveguides and it is expected that the straight waveguides have very low scattering loss. That is also the reason why we can use Fabry-Perot resonance method to measure the loss of the straight waveguides even with imperfect facets.

2)   SU-8 master mold

The sidewall roughness of the SU-8 molds from the lithography and developing process can also cause roughness of the imprinted trenches. It is expected this roughness is not the main reason of the scattering loss compared to the loss caused by mask defects. The sidewall roughness cannot be seen clearly from SEM pictures in Chapter 4.

3)   PDMS mold

One PDMS mold can be used several times. Repeated use of the PDMS mold is not recommended since it may be contaminated from the UV-lithography process (as some polymer is not fully polymerized due to the non-uniform intensity of the UV lamp). PDMS material is cheap and it can be disposed each time. Experiments also indicate that after multiple usage of the same PDMS mold, it can cause larger losses in the imprinted waveguides.

4)   Cross-section of the imprinted waveguides

The cross-section of the waveguides (after spin-coating the core layer) has an influence on the optical loss of the waveguides. For a thin residual layer (Figure 5. 13(a)), the loss of the waveguides is similar to that of channel waveguides as the light is most confined into the under cladding layer (Figure 5. 13(c)). For a thicker residual layer (Figure 5. 13(b)), the waveguides can be viewed as a ridge waveguides and most light is confined in the slab waveguides (Figure 5. 13(d), with a residual layer of 0.8μm and waveguide height of 2μm), which means the sidewall roughness has less influence than in the channel waveguides. Since the imprint process is a manual process and does not resort to any imprint machine, the thickness of the under cladding layer is not completely uniform. Even with a high spin-coating speed,

the residual layer varies from position to position of the wafer. Experiments prove this point. For waveguides with cross-section of Figure 5. 13(a), the extracted loss of TE and TM mode is more or less the same; for waveguides with cross-section of Figure 5. 13(b), the extracted loss of TE and TM mode is not the same and normally smaller than that of Figure 5. 13(a).
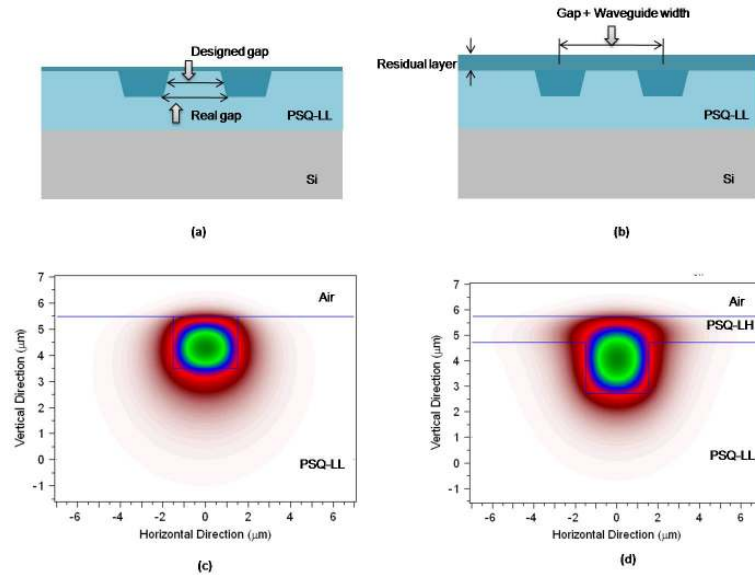
Figure 5. 13 Cross-section of imprinted waveguides
(a)with a thin residual layer (b) with a thick residual layer (c) calculated TE mode profile of structure (a), (d) calculated TE mode profile of structure (b)

5.4.2 Coupling efficiency between the straight waveguides and the ring

The coupling efficiency between the straight waveguides and the ring depends on the gap distance and the coupling length of racetrack ring resonators. However, as the sidewall of the imprinted waveguides trench is not vertical, the coupling efficiency also depends on the cross-section of the waveguides. For the waveguide cross-section with a thin residual layer ((Figure 5. 13(a)), the real gap is larger than the designed gap due to the non-vertical sidewall of the imprinted waveguides trench. Therefore the coupling efficiency is not sensitive to the coupling gap. Experimental results show that for the waveguides with a thin residual layer (Figure 5. 13(a)), the coupling efficiency is more or less the same with different gaps (for a coupling length of 150μm with different gaps of 1.2μm, 1.4μm, 1.6μm, the extracted coupling efficiency is

10 %).For the ridge waveguides with a thicker residual layer (as shown in Figure 5. 13(b)), the coupling is proportional to the gap as the light is mostly confined in the slab waveguides (Figure 5. 13(b)). Experimental results also prove this point: for a coupling length of 150μm with a gap of 1.2μm, the extracted coupling efficiency is about 30%; with a gap of 1.4μm, the extracted coupling efficiency is about 20 %.

5.4.3 Existing problems

1) Defects on the mask

The defects on the mask are expected to be the main source of the scattering loss. In the next run, a new mask will be fabricated to compare with the previous results. On the other hand, the surface roughness of the core layer also has an influence on the total scattering loss. For soft-lithography process, after spin-coating the high index polymer PSQ-LH with high speed, it is observed that the surface of the thin PSQ-LH layer (around 800nm) doesn't look flat. This may be caused by small molecules forming in the UV curing process. As the film is very thin, it looks especially more obvious.

2) Coupling efficiency controll

Accurate control of the coupling efficiency between the ring and the straight waveguides is quite important. For a given loss factor, by adjusting the coupling efficiency between the ring and straight waveguides, the extinction ratio of the through and drop ports can be adjusted to satisfy different applications.

For the ring resonators fabricated by soft-lithography, we have problems to accurately control the coupling efficiency. As mentioned before, the cross-section of the waveguides has an effect on the coupling efficiency (Figure 5. 13). This problem can be solved by using an imprint machine instead of manual imprint. It is expected that the flatness of the under cladding layer will be improved and thus the residual core layer. The sidewall of the imprinted trenches will be more vertical by using a UV lamp with higher power. Thus the coupling efficiency can be controlled more accurately by controlling the gap distance.

3) Polarization dependence

As the polymer waveguides are not designed as polarization independent waveguide, the waveguides fabricated by the two fabrication processes are both polarization dependent. This may cause some inconvenience in the application of polymer devices since a polarizer has to be inserted. In the future polarization independent polymer waveguides will be designed and fabricated.

4) Wavelength temperature sensitivity

As polymer has a large thermo-optic coefficient ($-1\sim3\times10^{-4}$/°C), the resonance wavelength of polymer ring resonators has a large dependence on the temperature. Some groups have successfully achieved athermal polymer waveguides on the

polymer substrate by using the polymer's positive substrate expansion coefficient to counterbalance the polymer's negative thermal-optic coefficient.

5)   Polymer material

The polymer PSQ-L needs to be post-baked at high temperature (200°C for 2h) for full polymerization. The high temperature curing is not suitable for some applications, especially when using a polymer substrate. Further exploration and improvement of the polymer is important in the future work.

5.5 Conclusion

The transmission spectrum of polymer PSQ-L ring resonators fabricated by both conventional lithography and soft-lithography process has been measured. The theoretically expected transmission spectra are obtained. Parameters such as the optical loss of the waveguides and the coupling efficiency are extracted from the transmission spectrum of ring resonators. The estimated scattering loss of bent waveguides (with a radius of 400μm) is about 1.6dB/cm for waveguides fabricated by conventional lithography and 1.8dB/cm for waveguides fabricated by soft-lithography. Different measurement setups are used and the results are compared and discussed. The factors that influence the loss and coupling efficiency are analyzed.

Chapter 6 Athermal SOI devices

6.1 Introduction

Silicon based devices with high index contrast have been widely used for various applications in recent years. With mature CMOS (Complementary Metal Oxide Semiconductor) fabrication technology, silicon based devices have the potential to provide highly compact circuits with low cost, multifunctionality and enhanced performance. The future roadmap is to integrate sensing functions, photonic functions, electronic functions and thermal control elements on one single chip. Better power efficiency of the whole chip is highly desired. The problem of the heat dissipation of the chip has to be considered during packaging since the temperature stability is quite important.

However, silicon has a quite large thermo-optic coefficient (TO_Si: $1.8 \times 10^{-4}/°C$), almost twenty times larger than silica material. The high temperature dependence of silicon material degrades the performance of silicon-based devices. To stabilize the chip temperature to a constant level, external heaters or coolers have to be employed. This element takes extra space and reduces the power efficiency of the whole chip.

In the past, a lot of research has been done on suppression of the temperature dependence of the silica-based devices [30, 81, 82]. Various methods have been employed to achieve athermal silica-based devices [81-83]. Some specific methods for athermal silica-based AWG (arrayed waveguides grating) for the application of WDM (Wavelength Demultiplexing) have been extensively studied in recent years [84-86]. However, due to the large thermo-optic coefficient and high refractive index of silicon material, most methods that successfully achieved athermal silica-based devices are not applicable to silicon-based devices.

Among those methods, the simplest one and applicable to most devices (e.g. ring resonator, Mach-Zehnder interferometer, AWG etc.) is to overlay a polymer cladding on the circuit using the polymer's negative thermo-optical (TO) coefficient to counterbalance the waveguide core's positive TO coefficient. The biggest obstacle for silicon waveguides to use this method is that silicon has a quite large thermo-optic coefficient, of the same order of magnitude as for the polymer material ($10^{-4}/°C$) and almost twenty times larger than that of silica. This requires almost half of the light to penetrate out of the silicon core into the polymer cladding to achieve the athermal condition.

Recently, some groups experimentally demonstrated the possibility of achieving athermal silicon waveguides by using this method [87-89]. In order to have more light into the polymer cladding, the dimension of the silicon waveguides is highly reduced either by narrowing the core width [87] or by thinning the core height [89], or by using a slot waveguide structure [88]. Narrowed waveguides and slot waveguides impose big challenges for fabrication. E-beam writing is employed in

[87, 89] and results in large losses.

In this chapter, we first give an overview of the methods to achieve athermal waveguides. We propose the possible way to achieve athermal silicon waveguides. By overlaying a polymer PSQ-LH cladding on uniform narrowed silicon waveguides, athermal silicon ring resonators and Mach-Zehnder interferometers are successfully achieved.

6.1.1 General methods to achieve athermal waveguides

There are many methods to achieve athermal waveguide devices. Some methods are based on the thermo-optic properties of some specific materials. To be more universal, we first explore the general formula of temperature dependence for the resonant devices.

The resonant wavelength of the devices (e.g. ring resonator, MZ interferometer, AWG etc.) can be expressed as follow,

$$S = n_{eff}(\lambda_m) \cdot L = m\lambda_m \tag{6.1}$$

Where S is the optical path, n_{eff} is the effective index of the waveguide at resonant wavelength λ_m, L is the length of the ring or the length difference of different paths for multipath interferometric devices. By taking the derivative with respect to the temperature of Eq.(6.1), the temperature dependence of the resonant wavelength is as follow,

$$\begin{aligned}
\frac{d\lambda_m}{dT} &= \frac{L}{m} \cdot \frac{dn_{eff}}{dT} + \frac{n_{eff}}{m} \cdot \frac{dL}{dT} \\
&= \frac{\lambda_m}{n_{eff}} \cdot \frac{dn_{eff}}{dT} + \frac{\lambda_m}{L} \cdot \frac{dL}{dT} \\
&= \frac{\lambda_m}{n_{eff}} \cdot \frac{dn_{eff}}{dT} + \lambda_m \cdot \alpha_{sub}
\end{aligned} \tag{6.2}$$

Where α_{sub} is the thermal expansion coefficient of the substrate, defined as $\alpha_{sub} = \frac{1}{L} \cdot \frac{dL}{dT}$. Since the thickness of the substrate is much larger than that of the waveguide layer, the thermal expansion of waveguide layer is determined by the thermal expansion of the substrate. Most devices use silicon substrates and $\alpha_{sub} = \alpha_{Si} = 2.63 \times 10^{-6}$ [90].

The athermal condition is achieved when Eq.(6.2) equals zero. The temperature dependence of the effective index is determined by the dn/dT of both core and cladding material,

$$\frac{dn_{eff}}{dT} \approx \Gamma_{core} \cdot \frac{dn_{core}}{dT} + (1 - \Gamma_{core}) \cdot \frac{dn_{cladding}}{dT} \qquad (6.3)$$

Where Γ_{core} is the confinement factor of the core waveguide. For a highly confined waveguide ($\Gamma_{core} \gg 1 - \Gamma_{core}$), dn_{eff}/dT is the same order as dn/dT of the core material.

Most semiconductor materials have a positive thermo-optic coefficient while polymer has a negative thermo-optic coefficient. Therefore there are some methods developed to use some material's specific thermo-optic properties to achieve athermal devices [91-93].

The substrate thermal expansion coefficient is normally positive. As referred to Eq.(6.2), if the term of dn_{eff}/dT is negative, it is possible to achieve athermal condition by use of the material themselves.

In this section, we introduce several general methods to achieve athermal waveguides based on the thermo-optic properties of materials and applicable to most devices (e.g. ring resonator, MZ interferometer, AWG etc.).

➢ **Athermal all polymer-based devices**
  Polymer material has a negative thermo-optic coefficient and a large positive thermal expansion coefficient. The thermo-optic coefficient and the thermal expansion coefficient of polymer are both on the same order of 10^{-4}. Therefore, the temperature dependence of a polymer waveguide can be suppressed by carefully choosing the core polymer for waveguides and substrate to counterbalance those two terms in Eq.(6.2). An athermal all-polymer AWG has been successfully realized by this way [94].

➢ **Athermal TiO$_2$-SiO$_2$-based devices**
  The thermo-optic coefficient of TiO$_2$-SiO$_2$ glass is negative at a TiO$_2$ concentration of more than 50mol%, which makes it possible to achieve athermal TiO$_2$-SiO$_2$-based devices. An athermal AWG has been achieved in this way [93].

➢ **Athermal silica-based devices by overlaying a polymer cladding on top**
  In addition to using the negative thermo-optic coefficient of some specific material, there is another way to achieve negative dn_{eff}/dT. Referring to Eq.(6.3), the temperature dependence of the waveguide effective index depends on dn/dT of both core and cladding materials. Polymer material has a large negative thermo-optic coefficient (-1-3×10^{-4}/°C) while silica material has a positive thermo-optic coefficient (1×10^{-5}/°C) [81, 95]. By using a polymer's negative thermo-optic coefficient to counterbalance the waveguide core's positive thermo-optic coefficient, athermal silica-polymer hybrid waveguides have been successfully achieved by overlaying a polymer cladding on silica circuits. This method was first proposed by Kokubun. Y et al in 1993 [90]. Later athermal optical filters and AWG were successfully achieved by this method [30, 92].

6.1.2 Several specific methods for athermal silica-based AWGs

The arrayed waveguide grating (AWG) is a key component for wavelength-division multiplexing (WDM). The change of the core index with temperature results in a

wavelength shift of each channel. This wavelength limits the channel resolution and density. An extra electronic heater or cooler has to be used to stabilize the chip temperature. Therefore, temperature control is crucial to AWG devices and the overall chip.

Since silica-based devices are quite commercial with mature fabrication technology, a lot of effort has been dedicated to the development of athermal silica-based AWG in the past few years [83, 86, 96].

In this section, we introduce several specific ways dedicated to achieve athermal AWGs. Some athermal AWG modules are already commercial available [84, 85, 96]. Some methods have already been adopted for athermal silica-based AWG products.

6.1.2.1 Athermal silica-based AWG by inserting a groove filled with silicone
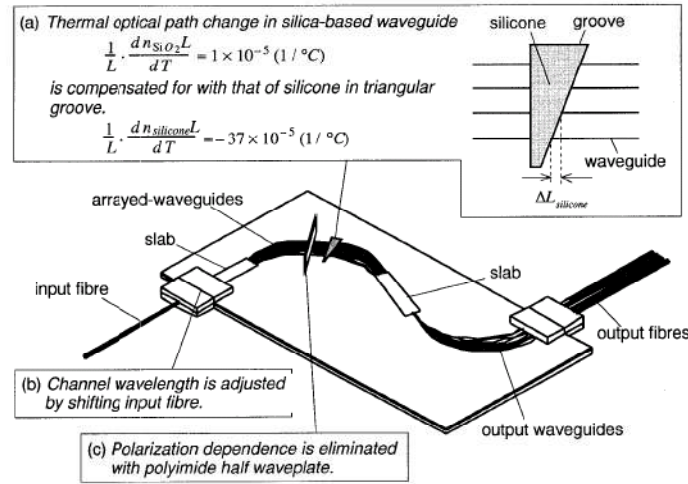
Figure 6. 1 Schematic configuration of athermal AWG by inserting a groove filled with silicone [97]

Figure 6. 1 shows the schematic configuration to achieve athermal silica-based AWGs [97]. A groove is inserted in the arrayed waveguides and filled with silicone to use the polymer's negative thermo-optic coefficient to compensate silica's positive thermo-optic coefficient. The groove is designed to satisfy the following equations,

$$\frac{d}{dT}(n_{SiO_2} \cdot \Delta L_{SiO_2}) + \frac{d}{dT}(n_{silicone} \cdot \Delta L_{silicone}) = 0 \qquad (6.4)$$

Where n_{SiO2} and $n_{silicone}$ are the effective index of the silica waveguides and silicone, ΔL_{SiO2} and $\Delta L_{silicone}$ are the path differences betwenen the arrayed

waveguides for silica and silicone. As shown in Figure 6. 1, a small length difference of $\Delta L_{silicone} = \Delta L_{SiO2} /37$ is needed to achieve an athermal AWG.

This method has a few excellent characteristics in exchange for a slight excess loss caused in the groove. This method was first proposed by NTT Company. Recently they demonstrated an athermal AWG module with low insertion loss [84].

6.1.2.2 Athermal silica-based AWG module by aligning cut slab waveguides

Furukawa Electric Company has successfully achieved athermal silica-based AWG module by the method [96] shown in Figure 6. 2. Each AWG circuit is cut at one of the slab waveguides into two pieces, one larger and one smaller, and these chips are connected by a compensating plate made of copper. As temperature fluctuates the copper plate expands and contracts, causing the small piece to slide. By adjusting the length of the copper compensating plate, athermal AWGs can be achieved.
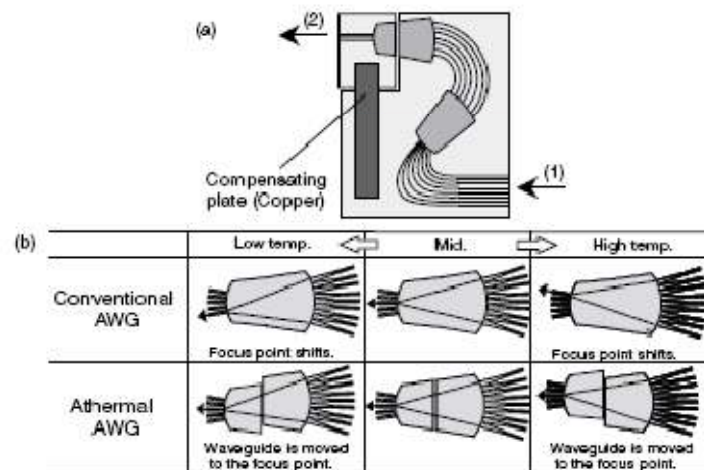
Figure 6. 2 Schematic configuration of athermal AWG by aligning cut slab waveguides [96]

6.1.2.3 Athermal silica-based AWG module with resin-filled trenches in slab region

This approach avoids extra phase errors when filling the trenches with resin in arrayed waveguide as mentioned before. The trenches are proposed to be in the slab waveguides and filled with silicone [98]. The advantages of this method are that it has

much tolerance for trench formation and low diffraction loss.
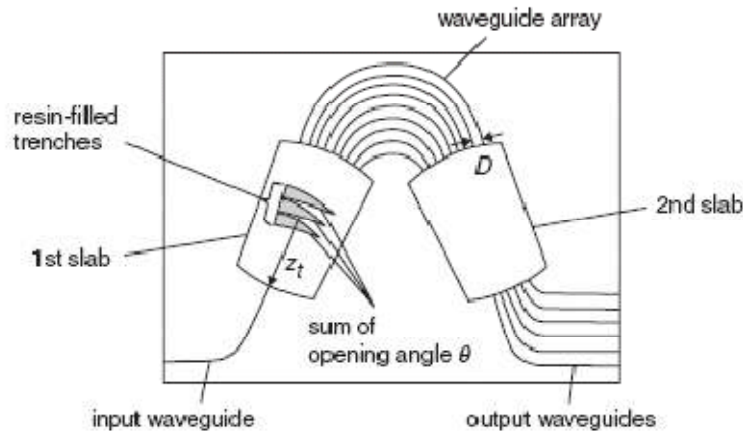
Figure 6. 3 Schematic configuration of athermal AWG with resin-filled trenches in slab region [98]

6.1.3 The possibility of achieving athermal silicon-based devices

Silica-based devices allow much flexibility for fabrication due to the relatively low index contrast compared to silicon and much larger waveguide dimensions. A lot of effort has been made to achieve athermal silica-based devices (as mentioned before). Only in recent years, the fabrication technology for silicon photonics wires has been well developed [99]. Low loss photonics wires and high performance AWGs are demonstrated [100-102]. The specific methods to achieve athermal silica-based AWGs mentioned in Section 6.12 cannot be applied to silicon AWGs due to the small size of the silicon circuits and the high index of silicon material.

Inspired by the successful use of hybrid SiO_2/Polymer waveguide structures to achieve athermal silica-based devices, recently a lot of attention has been drawn to applying this method to silicon-based devices [87-89]. The biggest obstacle for silicon waveguides to use this method is that silicon has a quite large thermal optical coefficient: the same order as polymer material (10^{-4}/°C), almost twenty times larger than silica, which requires almost half of the light to penetrate out of the silicon core into the polymer cladding to achieve athermal condition (of Eq.(6.3)).

In order to have more light penetrating into the polymer cladding, the dimension of the silicon waveguides is highly reduced either by narrowing the core width [87] or by thinning the core height [89], or by using a slot waveguide structure [88]. Narrowed waveguides and slot waveguides impose big challenges for fabrication. E-beam writing is employed in [87, 88] and results in large losses. Inaccurate control of the narrowed waveguide width or slot width seems

unsatisfactory for the athermal condition of silicon waveguides. E-beam writing itself is also less efficient for mass fabrication.

Winnie N. Ye etc. fabricated thinner silicon waveguide (700nm×100nm) by conventional lithography to avoid narrowing the waveguide width. However, the thinned layer is not thinned enough to achieve complete athermal condition: the wavelength shift is reduced down to 11.2pm/°C. For this thinned core structure, quite a large ring radius (100μm in [89]) has to be used to avoid extra bending loss. And the polymer they use for the cladding is not stable at high temperatures (with a Tg of 105°C).

In this chapter, we demonstrated athermal silicon devices by overlaying a polymer cladding on uniform narrowed silicon waveguides. The theoretical analysis and measurement results are described as follow.

6.2 Theoretical Analysis

As mentioned before, the resonant wavelength of ring resonators (or MZ interferometers, AWGs etc.) can be expressed as follow,

$$\frac{d\lambda_m}{dT} = \lambda_m \cdot (\frac{1}{n_{eff}} \cdot \frac{dn_{eff}}{dT} + \alpha_{sub}) \qquad (6.5)$$

In order to achieve the athermal condition, dn_{eff}/dT has to be negative as the thermal expansion coefficient is positive. The effective index of the waveguide core depends on a lot of parameters: the index of the waveguide core (n_{core}); the index of the waveguide cladding ($n_{cladding}$); the height of the waveguide (h); the width of the waveguide (w). Therefore, the dn_{eff}/dT can be expressed as a function of these parameters as follows,

$$\frac{dn_{eff}}{dT} = \frac{\partial n_{eff}}{\partial n_{core}} \cdot \frac{dn_{core}}{dT} + \frac{\partial n_{eff}}{\partial n_{cladding}} \cdot \frac{dn_{cladding}}{dT} + \frac{\partial n_{eff}}{\partial h} \cdot \frac{dh}{dT} + \frac{\partial n_{eff}}{\partial w} \cdot \frac{dw}{dT}$$

$$\approx \frac{\partial n_{eff}}{\partial n_{core}} \cdot \frac{dn_{core}}{dT} + \frac{\partial n_{eff}}{\partial n_{cladding}} \cdot \frac{dn_{cladding}}{dT} \qquad (6.6)$$

For a silicon waveguide, the variation of the waveguide width and height versus temperature are small. So the last two terms of Eq.(6.6), $\frac{\partial n_{eff}}{\partial h} \cdot \frac{dh}{dT}$ and $\frac{\partial n_{eff}}{\partial w} \cdot \frac{dw}{dT}$ can be neglected compared to $\frac{\partial n_{eff}}{\partial n_{core}} \cdot \frac{dn_{core}}{dT}$ and $\frac{\partial n_{eff}}{\partial n_{cladding}} \cdot \frac{dn_{cladding}}{dT}$.

As silicon has a large thermo-optic coefficient (1.8×10-4/°C), the same order of magnitude as polymer material, in order to counterbalance the two terms in Eq.(6.6),

more light has to penetrate into the polymer cladding to achieve a large ∂neff/∂ncladding value.

For the high index contrast waveguide, the dispersion effect has to be taken into account to calculate the temperature dependence of the resonant wavelength. This means that the effective index of the waveguide core also depends on the wavelength. The Eq.(6.5) can be modified as following,

$$\frac{d\lambda_m}{dT} = \frac{\lambda_m}{n_{eff}} \cdot (\frac{dn_{eff}}{dT} + \frac{\partial n_{eff}}{\partial \lambda_m} \cdot \frac{d\lambda_m}{dT}) + \alpha_{sub} \cdot \lambda_m \qquad (6.7)$$

The group index of the waveguide is expressed as,

$$n_{group} = n_{eff} - \lambda \cdot \frac{dn_{eff}}{d\lambda} \qquad (6.8)$$

Taking Eq.(6.8) into Eq.(6.7), the resonant wavelength temperature dependence is also related to the group index of the waveguide,

$$\frac{d\lambda_m}{dT} = \frac{\lambda_m}{n_g} \cdot (\frac{dn_{eff}}{dT} + \alpha_{sub} \cdot n_{eff}) \qquad (6.9)$$

Where n_g is the group index of the waveguide. An interesting thing is that Eq.(6.5) is almost the same as Eq.(6.9) except that n_{eff} is replaced by n_g. For silicon wires, the group index of the waveguide is almost twice the effective index of the waveguide. If the dispersion effect is not taken into account, the value of $d\lambda_m/dT$ will be almost twice the real value.

In this work, to achieve athermal silicon waveguides, the width of the silicon waveguide is highly reduced to allow more light coming out of the waveguide core. A standard SOI (silicon on insulator) structure with a height of 220nm is used (Figure 6. 4). Polymer PSQ-LH with thermo-optic coefficient of -2.4$\times$10^{-4}/$^\circ$C at 1550nm is used as the cladding material [53, 54]. This polymer has a low optic loss (<0.9dB/cm @1550nm) in the infrared window and a high thermal stability.

For designing the athermal waveguides, the value of $d\lambda_m/dT$ of different waveguide widths should be calculated. The value of dn_{eff}/dT and n_g (group index) are calculated by FIMMWAVE (©Photodesign). By using Eq.(6.9), the value of $d\lambda_m/dT$ for the TE mode of SOI straight waveguides with different widths is calculated (Figure 6. 5). The index and TO coefficient of silicon is set as 3.4757 (20°C) and 1.8$\times$10^{-4}/$^\circ$C. The index and silica and polymer PSQ-LH is set as 1.444 (20°C) and 1.515 (20°C). As shown in Figure 6. 5, the $d\lambda_m/dT$ of standard 500nm width SOI waveguides is near to 60pm/$^\circ$C; by narrowing the width of SOI waveguides, $d\lambda_m/dT$ is reduced down to zero and then becomes negative. From the theoretical calculation results, the ideal width for an athermal silicon waveguide is around 306nm (Figure 6. 5).
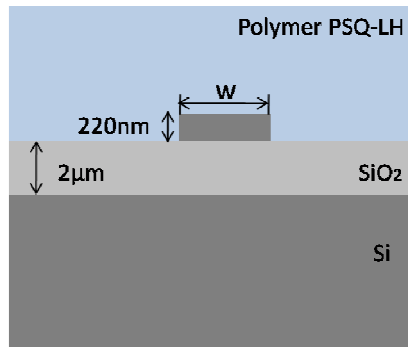
Figure 6. 4 SOI waveguide cross-section structure
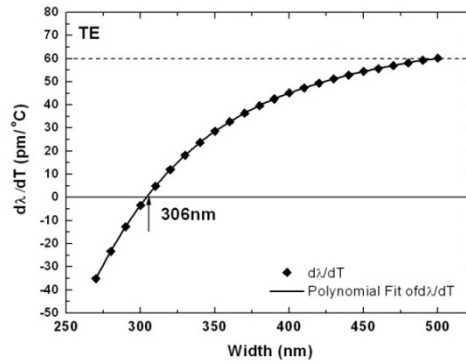
Figure 6. 5 Calculated TE mode wavelength temperature dependence of SOI waveguide at different widths (With a polymer cladding on top)

6.3 Design & Fabrication

The SOI wafer with a silicon thickness of 220nm and oxide layer of 2μm is used in this work (Figure 6. 4). As shown in Figure 6. 5, temperature dependence of the resonant wavelength is very sensitive to a reduction of waveguide core size. Therefore, high quality, high resolution fabrication technologies are required for these narrowing silicon waveguides. The narrow SOI waveguides in this work are fabricated by deep UV lithography with standard COMS (complementary metal-oxide-semiconductor) fabrication technology [5]. This technology offers both the required resolution and throughput for commercial application.

The fabrication process with deep UV lithography is similar to that of conventional optical projection lithography. The basic process flow is shown in Figure 6. 6. First, the photo-resist is coated on top of a 200mm-SOI wafer and then prebaked. On top of the resist, an antireflective (AR) coating is spun to eliminate reflection at the interface between air and photoresist. Then the wafer is sent to a

stepper, which illuminates the photoresist with the pattern on the mask. After lithography, the resist goes through a post-exposure bake and is then developed. After that, the patterns in the photoresist are etched into the underlying SOI by an ICP etching process. The SOI wafers we used were fabricated in CEA/LETI through ePIXfab (www.epixfab.eu), France.
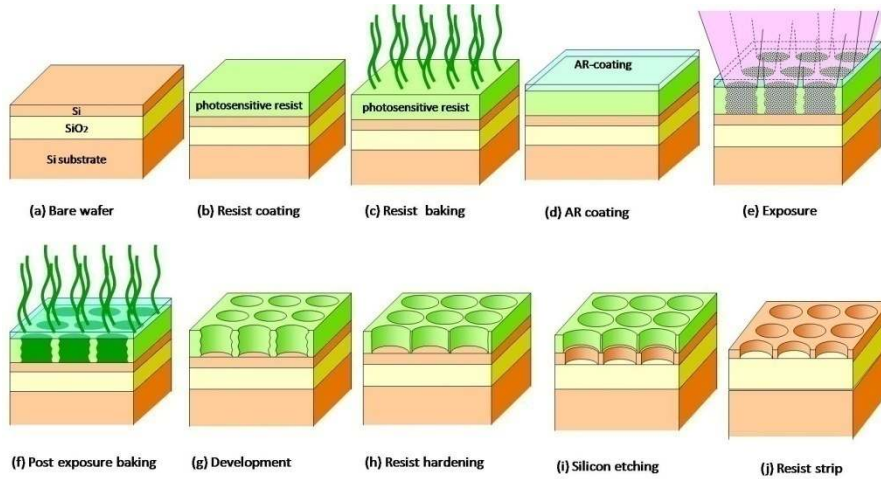
Figure 6. 6 Process flow for the fabrication of SOI nanophotonic structures

Simple racetrack ring resonators and MZ interferometers with different waveguide widths were designed and fabricated for the first run. Referring to the theoretical calculation results mentioned above, the ideal width for the athermal waveguides is around 306nm. So ring resonators and MZ interferometers with a narrow width of 300nm and 350nm were designed on the mask. Small variations of the waveguide width are obtained by varying the exposure dose across the wafer when doing deep UV lithography [99]. The SEM pictures of the fabricated ring resonators are shown in Figure 6. 7. The racetrack ring resonators are designed with different radius and a coupling length of 2μm, gap of 180nm. The SEM pictures of the fabricated MZ interferometers are shown in Figure 6. 8. The MZ interferometers are designed with a path length difference of 50μm.

(a)   (b)
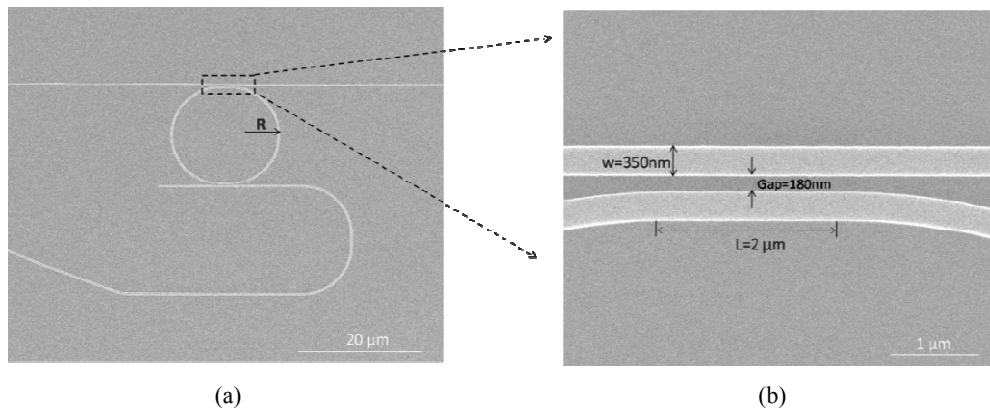
Figure 6. 7 SEM pictures of fabricated ring resonators with a width of 350nm
(a) the whole ring (b) the coupling region
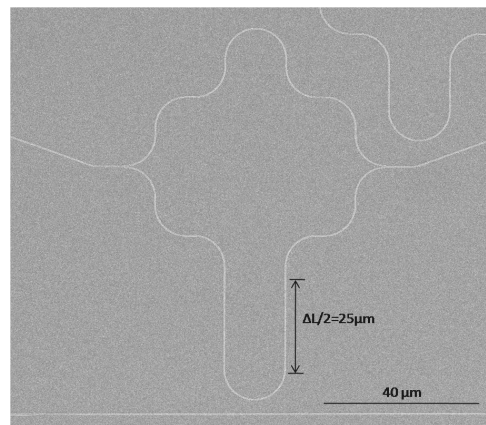
Figure 6. 8 The SEM pictures of the fabricated MZ interferometers with a path length
difference of 50μm

6.4 Measurement Results

6.4.1 Measurement setup
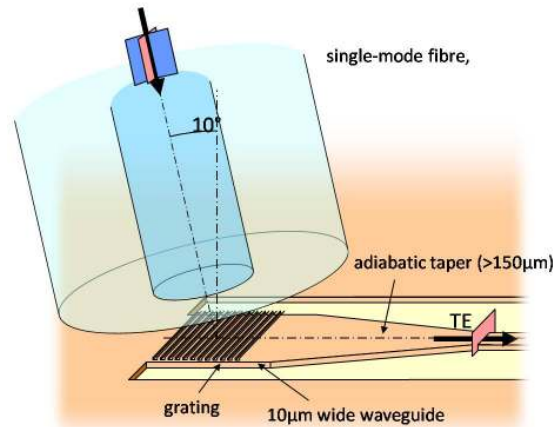
Figure 6. 9 Coupling light into and out of photonics circuits with fiber using grating couplers

In order to couple light in and out of the silicon photonics wires, shallowly etched grating couplers are fabricated on the edge of the waveguide by a separate step. As shown in Figure 6. 9, light is coupled to silicon wires from a single mode fiber into the grating coupler into silicon wires. This kind of grating has a polarization selectivity and therefore the transmission spectra measured below are all for TE mode polarization. A broadband infrared light source (SLED) and spectrum analyzer (Agilent 86140B) are used for the characterization of the transmission spectrum of the ring resonator. To measure the transmission spectrum at different temperatures, the sample is mounted on a heating system to accurately control the chip temperature.

6.4.2 Measurement results

The athermal SOI devices are expected to be achieved by narrowing down the waveguide width. For the first run, the waveguide width was designed to be 300nm, 350nm and 450nm. Small variation of the waveguide width is obtained by varying the exposure dose on different columns of the wafer[99]. Simple devices, like ring resonators, MZ interferometer with narrowed waveguide width are added into the mask for the first run. Athermal SOI ring resonators and MZs were successfully achieved at the first run. The ideal waveguide width to achieve athermal SOI devices was found to be 350nm (designed width on mask). For the second run, we added more complex interferometric devices, like AWGs. Unfortunately, the AWGs with narrowed waveguides perform badly. And for the second run the waveguides are less

etched due to insufficient exposure dose to achieve athermal SOI waveguides. The general description of the two runs is listed in Table 6. 1.

Table 6. 1 General description of the two runs

	First Run	**Second Run**
run name	LETI 02	LETI 03
devices	ring resonators, MZ interferometers	ring resonators, AWGs
waveguide parameters	designed waveguide width of 300nm, 350nm, 450nm	designed waveguide width of 350nm
measurement results	successfully achieved athermal ring resonators and MZ interferometers	not achieving athermal devices due to less etched waveguide, AWG with bad performance

6.4.2.1 Athermal SOI ring resonators and MZs
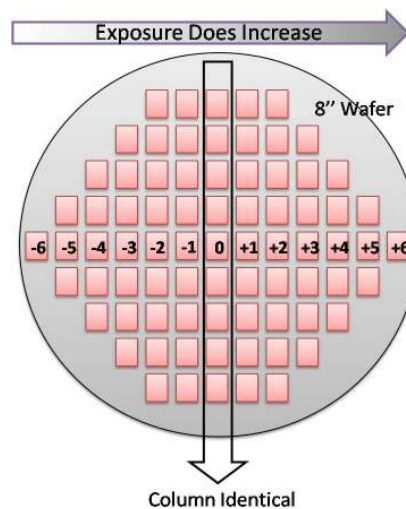
Figure 6. 10 Schematic picture for 8" Wafer after fabrication
(8" Wafer with rows of different exposure dose and identical columns)

According to the theoretical calculation results, the ideal width to achieve athermal SOI waveguides is around 306nm. Therefore the waveguide width of 300nm and 350nm was added into the mask layout for the first run. For an 8 inch wafer (as shown in Figure 6. 10), the exposure dose was increased gradually from left to right in each row. Each column is with the same exposure dose and which results in identical

waveguide dimension. Normally the center column (named C_0) is targeted for the designed width. The ones on the left side of the wafer are less exposed and have broader waveguides while the ones on the right side of the wafer are over exposed and have narrower waveguides. Even the central column has a small deviation from designed the dimensions; other columns can cover the target width.

The transmission spectrum of the ring resonators and MZ interferometers are measured for temperatures from 10°C to 50°C with an interval of 10°C. The resonance wavelengths are determined by Lorentz fitting of the transmission spectrum (for ring resonators). By linear fitting of one resonance wavelength at different temperatures, the wavelength temperature dependence dλ/dT is extracted. Figure 6. 11 and Figure 6. 12 shows the measured transmission spectrum of a ring resonator (Width=350nm, Gap=180nm, L=2μm, R=15μm) and MZ interferometers at different temperatures (central column, C_0: target for 350nm waveguide width). As shown in Figure 6. 11(b)(d), the wavelength temperature dependence of the 350nm-width ring resonator is reduced from 54.2±1.0pm/°C to -4.7±1.0pm/°C and for 350nm-width MZ interferometers, the wavelength temperature dependence is reduced from 55.8±1.7pm/°C to -2.4±1.7pm/°C after overlaying a polymer cladding (Figure 6. 12 (b)(d)). The ideal width for the athermal ring resonator is found to be around 350nm, a little different from the theoretically calculated value of 306nm.
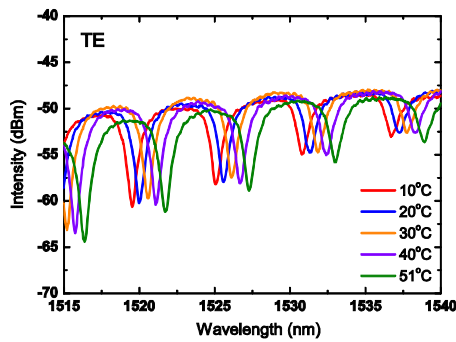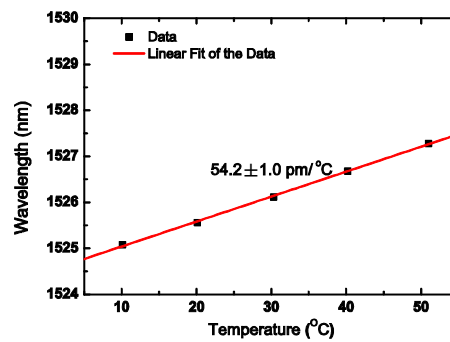
(a)   (b)
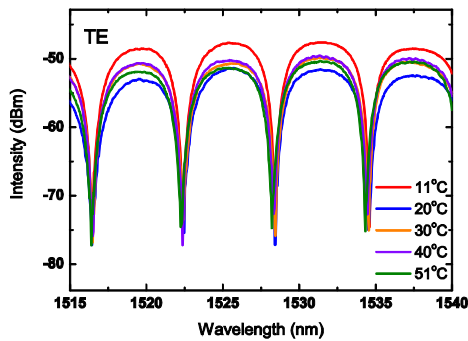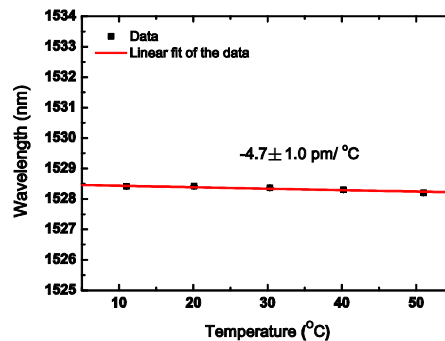
(c)   (d)

Figure 6. 11 (a) Transmission spectrum of a ring resonator with width of 350nm at different temperatures before overlaying a polymer cladding (b) Linear fit of the wavelength versus temperatures (c) Transmission spectrum of a ring resonator with width of 350nm at different temperatures after overlaying a polymer cladding (d) Linear fit of the wavelengths versus temperatures (Width=350nm, Gap=180nm, L=2μm, R=15μm)

(a)

(b)

(c)

(d)
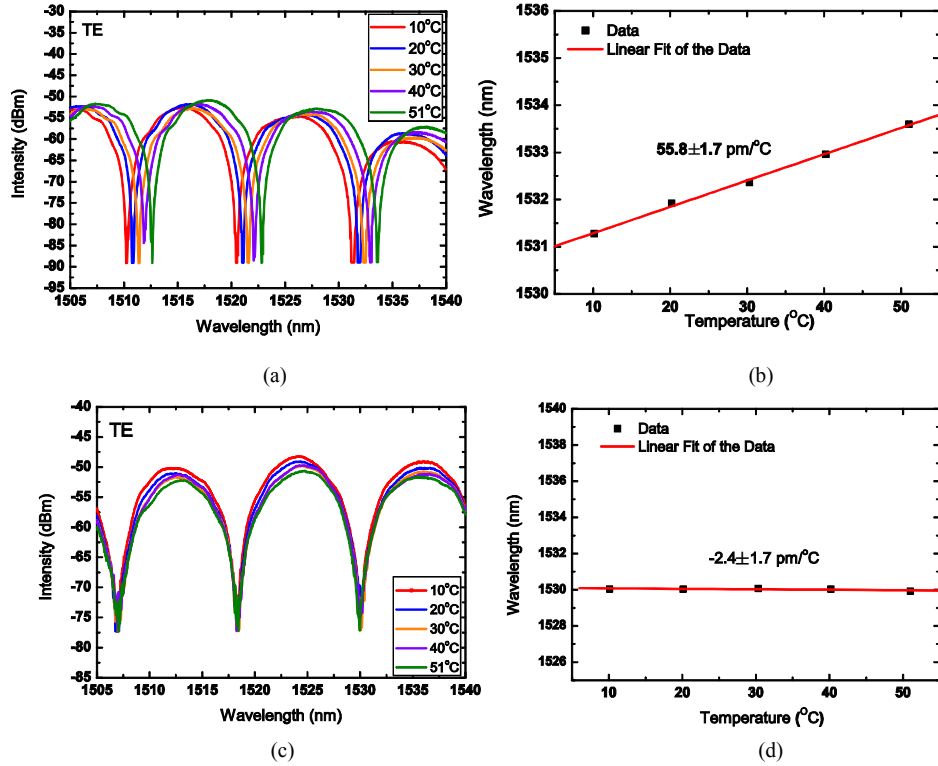
Figure 6. 12 (a) Transmission spectrum of a MZ interferometer with width of 350nm at different temperatures before overlaying a polymer cladding (b) Linear fit of the wavelength versus temperatures (c) Transmission spectrum of a MZ interferometer with width of 350nm at different temperatures after overlaying a polymer cladding (d) Linear fit of the wavelengths versus temperatures (Path length difference=50μm)

There are 13 columns on the 8'' wafer of LETI 02. The waveguide width from left to right of the entire wafer has a width variation of about ±10nm to the central column. The temperature dependence of other columns (C_-5, C_-3, C_+2, C_+5) is also measured. Table 6. 2 shows the measured results. The athermal condition is achieved from column -5 to column +5. This also means that our fabrication technology can well control the waveguide width with variation tolerance.

Table 6. 2 The temperature dependence SOI devices with a polymer cladding
(different columns on the wafer, LETI 02 run)

Column	dλ/dT (Ring Resonator)	dλ/dT (MZ Interferometer)
C -5	-1.1±1.7 pm/°C	0.03±2.0 pm/°C
C -3	-2.0±2.7 pm/°C	5.0±1.8 pm/°C
C 0	-4.7±1.0 pm/°C	-2.4±1.7 pm/°C
C +2	1.54±1.5 pm/°C	3.1±1.2 pm/°C
C +5	-1.2±1.8 pm/°C	1.6±0.5 pm/°C

It has to be pointed out that the value dλ/dT, which is calculated from the linear fitting of the data, is not an absolute value. The spectrum analyzer resolution (Agilent 86140B, minimum resolution of 0.06nm), temperature measurement range, the numbers of the data taking into account for linear fitting all have some influence on the value of dλ/dT, especially when the waveguide width is near the athermal condition and the dλ/dT slope is quite small. The data shown in Table 6. 2 also proves this point. Even taking into account the above uncertainties, the conclusion can still be drawn that the wavelength temperature dependence of a silicon ring resonator can be highly reduced down to less than 5.0±1.0pm/°C after deposition of a polymer cladding, almost 11 times less than normal silicon waveguides.

6.4.2.2 Performance of AWG inserted with narrowed waveguides

As we have successfully achieved athermal simple interferometeric devices, like ring resonators, MZ interferometers, more complicated devices, like AWGs were added into the mask layout of the second run. The resonance wavelength of the AWG depends on the length difference of the arrayed waveguides, so narrowed waveguides are inserted into the arrayed waveguides. The wafer of the second run is less exposed with broader waveguides compared to the previous run. The athermal condition is not fully achieved for this run. The measured temperature dependence of SOI ring resonators are shown in Table 6. 3. The dλ/dT is decreased to 30±3pm/°C from left columns to right columns. The temperature dependence of AWGs is consistent with that of ring resonators and experimental results also prove that. We measured the transmission spectrum of AWGs of different columns on the wafer. The performance of AWGs deteriorates as the waveguide width decreases (Figure 6. 13). The AWGs are designed to have 8 channels with spacing of 400GHz. The cross-talk of the AWGs is mainly caused by phase errors of the inserted narrow waveguides. As the waveguide becomes narrower, the AWG of right most column shows only 5dB extinction ratio. To present, it is difficult to achieve athermal AWGs with good performance.

Table 6. 3 The temperature dependence SOI ring resonators with a polymer cladding (Different columns on the wafer, LETI 03 run)

Column	dλ/dT (Ring Resonator)
C -7	76.2±6.0 pm/°C
C 0	38.5±1.6 pm/°C
C +3	36.7±3.0 pm/°C
C +6	30.0±3.0 pm/°C
C +9	30.0±3.0 pm/°C
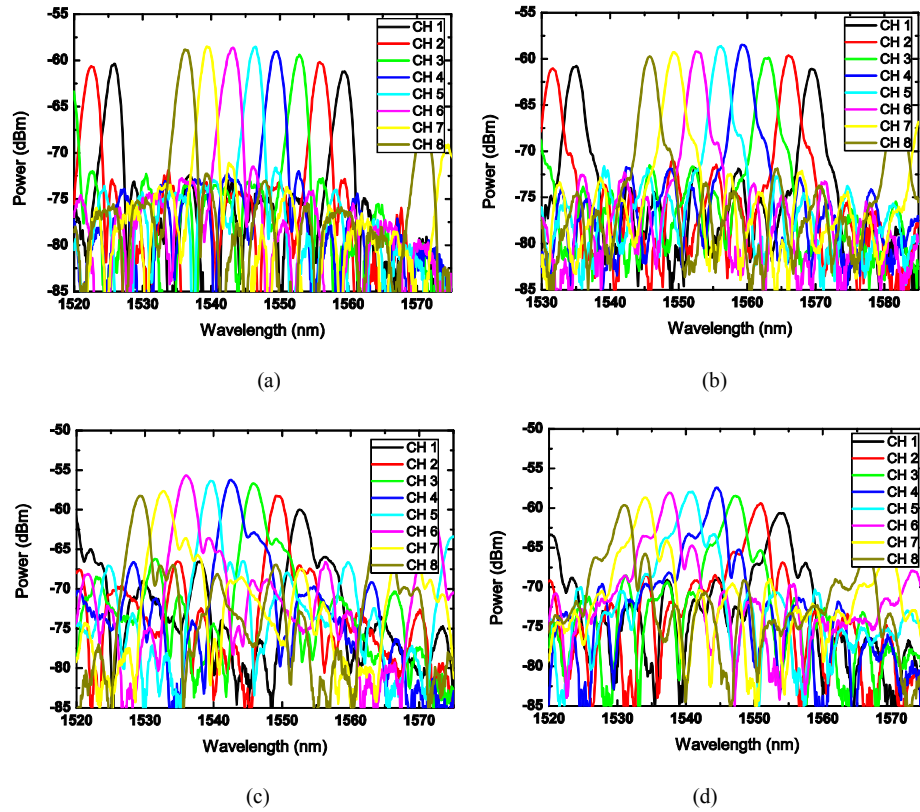
Figure 6. 13 Transmission spectrum of AWGs inserted with narrowed waveguides (Different columns on the wafer, LETI 03 run) (a) Column_-7 (b) Column_0 (c) Column_+6 (d) Column_+10

6.4.2.4 Loss estimation

Reducing the silicon waveguide width imposes a big challenge on fabrication technology. The extent to which the waveguide width can be reduced is compromised by the scattering loss caused by fabrication technology.

The total loss in the ring waveguides can be extracted by fitting of the transmission spectrum with a Lorenz-function. The total loss in the ring waveguides consists of bending loss, mode mismatch loss between bent waveguides and straight waveguides, coupling loss in the coupling region and scattering loss caused by sidewall roughness. Figure 6. 14 shows the transmission spectrum of the athermal SOI ring resonators before and after overlaying a polymer cladding. The total loss of the bending waveguides and the coupling coefficient are extracted by fitting the transmission spectrum. An interesting phenomenon is found. For the width of 350nm and a ring radius of 15μm, the fitted total loss of the bending waveguide is about 300dB/cm before overlaying a polymer cladding. After overlaying a polymer cladding, the fitted total loss is reduced to about 50dB/cm. The reduced loss of the bending waveguides is expected due to a reduction of the scattering loss for a decrease of the index contrast between the core and the cladding after overlaying a polymer cladding.

The coupling coefficient (the power percentage coupled to the ring) between the ring and the straight waveguides is increased from 50% to 75% after a polymer cladding (Figure 6. 14). Since our aim is to test the thermal behavior of the ring resonator, the coupling between the ring and the straight waveguide has not been optimized for the first run. The Q factor of the ring should decrease as the coupling power increases. Contrarily, the Q factor has significantly increased after overlaying a polymer cladding (Figure 6. 14), which also indicates a loss reduction after overlaying a polymer cladding.

(a)   (b)
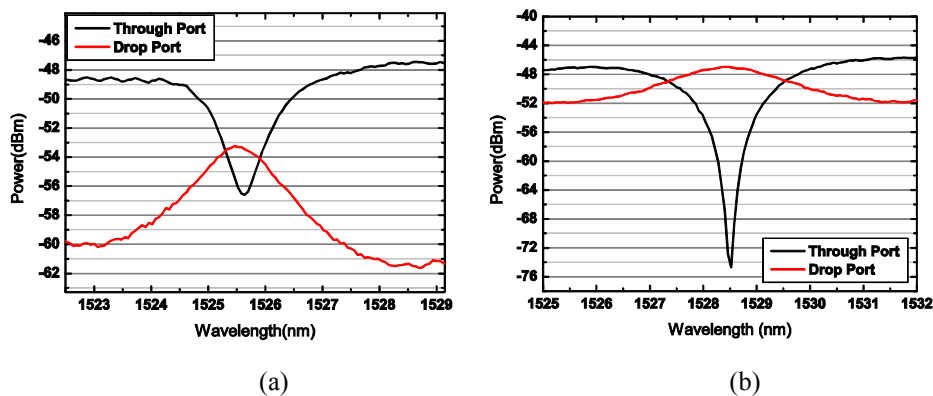
Figure 6. 14 Transmission spectrum of SOI ring resonator with width of 350nm at room temperature (a) Before overlaying a polymer cladding (b) After overlaying a polymer cladding (With a black line for the Through port and red line for the Drop port, Ring resonator parameters: Width=350nm, Gap=180nm, L=2μm, R=15μm)

6.5 Conclusion

The high temperature dependence of silicon material degrades the performance of silicon-based devices. External heaters or coolers have to be employed to stabilize the chip temperature, which takes extra space and reduces the power efficiency of the whole chip.

A simple method is used to suppress the temperature dependence of silicon-based devices. By overlaying a polymer PSQ-LH cladding on uniform narrowed silicon waveguides, athermal silicon ring resonators and Mach-Zehnder interferometers are successfully achieved. The wavelength temperature dependence of a silicon ring resonator is reduced to less than 5.0±1.0pm/°C, almost eleven times less than air-clad silicon waveguides. The ideal width to achieve athermal condition for the TE mode of 220nm-height SOI waveguides is found to be around 350nm.

Narrowed waveguides impose big challenges for fabrication. Standard deep UV lithography and dry etching are used for fabricating such silicon devices. The fitted total loss of the ring waveguides can be significantly reduced after overlaying a polymer cladding. More complicated devices, like AWGs are also tested in the second run. Unfortunately the AWGs perform badly with the inserted narrow waveguides.

Chapter 7 Conclusion and perspective

7.1 Conclusion

Fabrication of polymer based optical devices

As mentioned in the summary, this work consists of several parts. Our objective was to develop some kinds of polymers with high performance and apply them in the fabrication of low cost optical devices. In the preliminary stage, we finished the first run of the research, from the material synthesis to the device fabrication.

We have developed two main kinds of polymer materials: PPESK and PSQ-L. The polymer films have been prepared by spin-coating process. The optical and other properties of the polymer films have been tested. The properties of the polymer were adjusted and improved from the synthesis process. As the synthesis technique for polymer PSQ-L is mature and the properties of the material can satisfy the basic demands for optical applications, polymer PSQ-L was first chosen to fabricate polymer waveguides. Simple fabrication techniques were expected to reduce the cost of the device. Apart from conventional lithography and etching process, different imprint processes were tried to explore an appropriate way to fabricated PSQ-L waveguides. A simple soft-lithography process was found to be compatible with polymer PSQ-L. PSQ-L ring resonators were fabricated in this way. After fabrication, the ring resonators were characterized. A nice resonance spectrum was obtained, which also proves the compatibility of the fabrication technique with the materials.

During the PhD study, the synthesis of PPESK series polymer was not mature enough to put into applications.

At present, we have successfully fabricated PSQ-L based polymer waveguides. This is the basic work for further application of these polymer-based devices. However, there are still some problems for high volume fabrication of PSQ-L waveguides. Further optimization of the process is necessary in the future. Other applications of polymer-based devices are expected to be explored.

Athermal SOI devices

The large temperature dependence of silicon has always been a problem for silicon based devices. A simple method has been utilized to depress the temperature dependence of silicon based devices. The temperature dependence of silicon devices is significantly reduced by overlaying a polymer cladding on narrowed SOI waveguides. Polymer PSQ-LH with a large thermo-optic coefficient and low

absorption loss is used as a top-cladding. Athermal silicon ring resonators are experimentally demonstrated. The ideal width to achieve athermal condition for the TE mode of 220nm-height SOI waveguides is found to be around 350nm. After overlaying a polymer PSQ-L layer on the narrowed waveguides, the wavelength temperature dependence of the silicon ring resonator is reduced to less than 4.7 ± 1.0 pm/°C, almost eleven times less than that of normal silicon waveguides.

However, narrowed waveguides imposes big challenges on fabrication. At present, simple athermal SOI ring resonators and MZ interferometers are successfully achieved with tolerant performance. More complicated interferometric devices, like AWGs are difficult to achieve with good performance.

7.2 Perspective

Polymer circuits cannot be as compact as silicon circuits due to the low index contrast. However, the refractive index of polymer is similar to that of silica and the fabrication process is much easier and cheaper than for silica-based devices. Therefore it is a good alternative for silica material.

Since we have successfully achieved PSQ-L based fundamental devices, like microring resonators, application of this device will be previewed in this section. However, the polarization dependence and temperature dependence of polymer waveguides may cause some inconvenience in application of the polymer ring resonators. It is better to suppress the polarization dependence and temperature dependence of the waveguides before application. The low cost of the polymer-based circuits promise it to be a good candidate for bio-chemical sensing applications. Some specific applications also demand a specific cross-section structure of the waveguides and thus different fabrication processes.

Based on the previous work, several aspects of future work are proposed here as follow,

✧ Optimization of the imprint process

Different applications demand different cross-section design and thus different fabrication process. It is necessary to optimize the imprint process, especially to design new imprint processes or try new fabrication processes for polymer waveguides.

✧ Design of polarization independent waveguides

By designing the cross-section of the polymer waveguides, polarization independent polymer waveguides are expected to be achieved. The fabrication process should also be taken into account when designing the polarization independent waveguides.

✧ Athermal polymer waveguides

By using a polymer substrate, athermal polymer waveguides can be achieved. But it may be difficult for the polymer PSQ since it needs high temperature to be fully cure

(the substrate cannot resist such high temperature).

✧ **Sensing applications of polymer ring resonators**

It is quite promising for applying polymer-based devices in bio-sensing and other sensing applications due to the low cost of the devices. Theoretical simulation has to be done first to test the feasibility of those applications.

The aim of this PhD is to realize basic polymer devices like ring resonators. According to the experimental results (Chapter 5), we have successfully achieved PSQ-L ring resonators. Therefore we propose some aspects of future work. The future work is based on the improvement of the performance of the ring resonators and the application of polymer ring resonators.

Normally there are two modes (TE and TM mode) in the single mode polymer waveguide. A polarization selective element has to be employed in the measurement to separate two modes, which will cause extra cost to integrate a polarization control element on the polymer circuits. In this section, we first discuss the possibility of achieving polarization independent polymer waveguides by adjusting the waveguide structural parameters. Then we apply PSQ-L polymer ring resonators for biosensor applications, evaluate the performance of the PSQ-L ring resonators and discuss the potential of using it as biosensors.

7.2.1 Polarization independent PSQ-L waveguides

Normally there are two modes (TE and TM mode) in the single mode waveguide. Since TE and TM mode have different effective index, they will have different resonant wavelengths. The different effective index of TE mode and TM mode is caused by the asymmetrical index distribution of the waveguide cross-section in horizontal and vertical direction (Figure 7. 1 (a)). The polarization dependence can be completely eliminated by using channel buried waveguides with the same width and height (w=h in Figure 7. 1(a)).

However, to facilitate fabrication and some specific applications, ridge waveguides are often used (Figure 7. 1(b)(c)). The index distribution of the waveguide cross-section is not symmetric in horizontal and vertical direction. Little variation of the effective index of TE and TM mode can cause a difference in resonant wavelengths. According to the resonance condition of Eq.(3.19), the variation of the resonance wavelength can be expressed as Eq.(7.1). Taking the effective index of polymer waveguides as 1.5 at 1550nm, the variation of the effective index of 1×10^{-5} can cause a resonant wavelength shift of 10pm. That means if we want to suppress the resonant wavelength split of less than 10pm, the effective index variation of TE mode and TM mode should be less than 1×10^{-5}, a very critical demand for controlling the effective index variation of both modes.

$$\Delta\lambda_m = \frac{\Delta n_{eff}}{n_{eff}} \cdot \lambda_m \qquad (7.1)$$
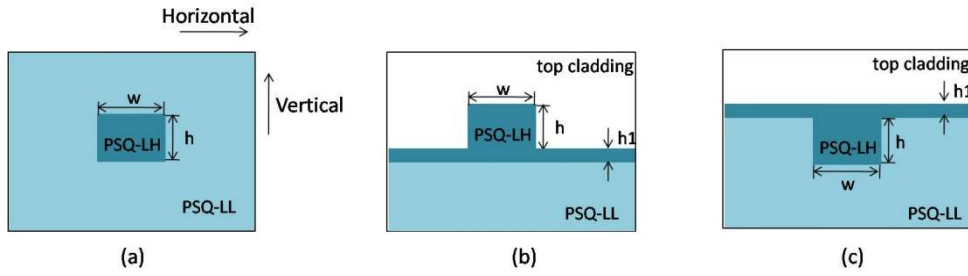
Figure 7. 1 Waveguides cross-section structure (a)channel waveguide (b)(c)ridge waveguide (the top cladding can be air or polymer)

By adjusting the dimensions of the cross-section of the ridge waveguide, the polarization dependence can also be eliminated. Taking the polymer waveguide with a cross-section as in Figure 7. 1(b) as an example, we calculated the effective index of TE mode and TM mode with different width (w) and height (h) and residual layer thickness (h1 in Figure 7. 1(b)). Figure 7. 2 shows that the effective index variation of both modes can be minimized by choosing suitable width and height of the waveguides.

However, as mentioned before, a small variation of the effective index of 10^{-5} can cause the resonance wavelength shift of 10pm. The accurate control of the width and height of the waveguides seems quite important. According to the calculation, the width and the height of the waveguide should be controlled with an accuracy of less than ±100nm. This is a big challenge for fabrication. On the other hand, it is also a big problem to accurately control the thickness of the residual layer.

The other option to eliminate the polarization dependence is by designing the waveguide structure with different loss coefficient for both modes. One mode will be attenuated during propagation; only the other mode will exist in the waveguide.

(a)　　　　　　　　　　　　　　(b)
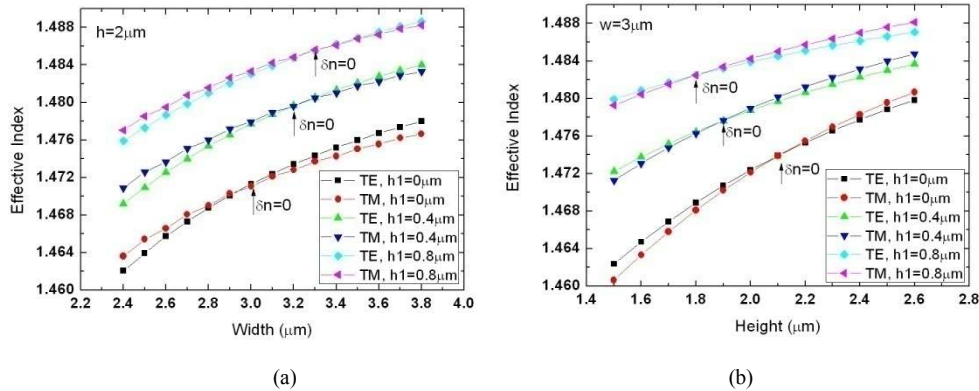
Figure 7. 2 Calculated effective index of polymer waveguides with different width and height (a)with a fixed height of 2μm (b) with a fixed width of 3μm

7.2.2 Bio-sensing based on PSQ-L resonators

Polymer microring resonators can be used for bio-chemical sensing applications. As the cost of the device is low, it is promising to achieve disposable bio-sensor chips. In this section, we first give an introduction of the sensing scheme. Then we will discuss the possibility of using polymer PSQ-L as biosensors. Design considerations will be proposed here.

7.2.2.1 Sensing scheme

For optical waveguide sensors, there are two sensing mechanisms that are commonly used: homogeneous sensing and surface sensing, as shown in Figure 7. 3. In homogeneous sensing, the device is surrounded with an analyte solution. The bulk index distribution in the analyte solution can be regarded as a top cladding for the waveguides. Therefore the variation of the concentration of the analyte solution can modify the effective index of the ring waveguides. However, in this mechanism, all the materials in the solution contribute to the waveguide effective index change. In order to solve this problem, the surface sensing is employed. In surface sensing, the optical device is pretreated to have receptors or binding sites on the sensor surfaces, which can selectively bind specific analytes. This method enables a specificity as well as label free detection.

There are two sensing schemes for the ring resonators to detect the amount of the analytes. One is to monitor the shift of the resonant wavelength (Figure 7. 4(a)). The other method is to monitor the variation of the intensity at a specific wavelength (Figure 7. 4(b)). The former one provides a wider detection range but requires a more sophisticated setup for the spectrum measurement. The latter scheme provides a higher sensitivity since a tiny shift of resonant wavelength can provide a larger detectable intensity variation. This sensing scheme also uses simple setup for detection since no spectrum analyzers are needed. However, this detection monitors the wavelength close to the resonant wavelength which leads to a small dynamic range.
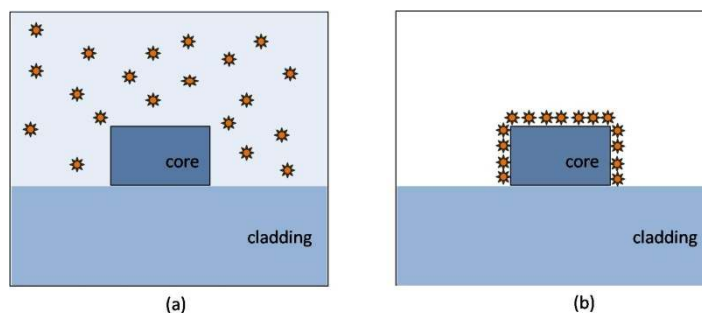
Figure 7. 3 Two sensing mechanisms (a) homogeneous sensing (b) surface sensing
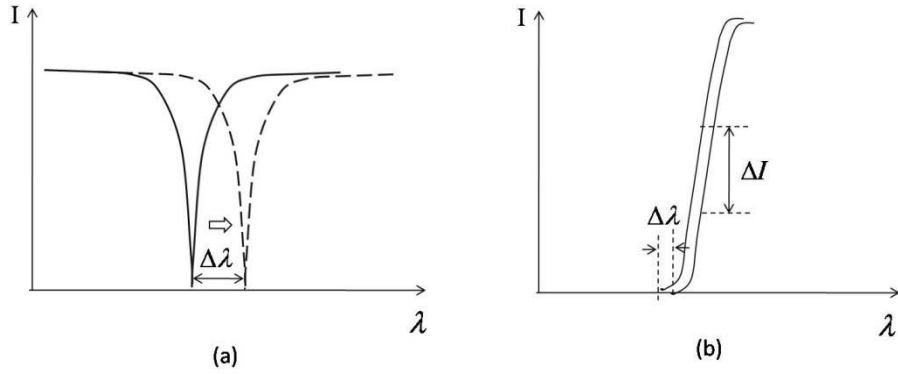
Figure 7. 4 two sensing schemes (a) resonant-wavelength shift (b) intensity variation

There are two important parameters to evaluate the sensing performance of the sensors. One is called sensitivity and the other is called detection limit. The following will take the homogeneous sensing for wavelength shift monitoring as an example to specify the two parameters.

For homogeneous sensing, the resonant wavelength shift is affected by the change of the cladding index (n_c). Therefore the sensitivity is defined as the ratio of resonance wavelength shift to the change of the cladding index as follow,

$$\Delta\lambda_m = \frac{\partial\lambda_m}{\partial n_c} \cdot \Delta n_c \equiv S \cdot \Delta n_c \tag{7.2}$$

According to the resonance condition of Eq.(3.19), the sensitivity can also be written as follow,

$$S \equiv \frac{\partial\lambda_m}{\partial n_c} = \frac{\partial\lambda_m}{\partial n_{eff}} \cdot \frac{\partial n_{eff}}{\partial n_c} = \frac{\lambda_m}{n_{eff}} \cdot \frac{\partial n_{eff}}{\partial n_c} \tag{7.3}$$

Therefore the sensitivity (S) is determined by the item of $\partial n_{eff}/\partial n_c$. In order to increase the sensitivity, a larger evanescent field at the waveguide boundary is desirable to probe the analytes. Some specific cross-section waveguide design, like using slot-waveguides [103], can provide a large sensitivity.

The other important parameter for biological and chemical sensors is detection limit. The detection limit is typically defined as the smallest detectable change of the waveguide parameters caused by analytes. For the homogeneous sensing of monitoring the resonance wavelength shift, the detection limit is proportional to the smallest detectable index change of top cladding (δn_c). According to Eq.(7.2), δn_c can be expressed as,

$$\delta n_c = \frac{\delta \lambda_m}{S} = \frac{\delta \lambda_m}{\dfrac{\lambda_m}{n_{eff}} \cdot \dfrac{\partial n_{eff}}{\partial n_c}} = \frac{\delta \lambda_m}{\lambda_m} \cdot n_{eff} \cdot \frac{\partial n_c}{\partial n_{eff}} \tag{7.4}$$

Assuming that the detection limit of the spectrum analyzer is small enough, the detection limit is determined by the bandwidth (FWHM) of the transmission spectrum and the sensitivity of the sensor. Eq.(7.4) can also be written as,

$$\delta n_c = \frac{\delta \lambda_m}{S} = \frac{\delta \lambda_m}{\lambda_m} \cdot n_{eff} \cdot \frac{\partial n_c}{\partial n_{eff}} \sim \frac{1}{Q \cdot S} \sim \frac{FWHM}{S} \tag{7.5}$$

In order to have a small detection limit, the sensor should have a large Q factor and high sensitivity.

7.2.2.2 Design considerations

In order to have more contact area for the evanescent field to the analytes, we choose the waveguide cross-section as Figure 7. 1(b). The aim of this design is to optimize the dimension of the ring resonator to achieve a high sensitivity and low detection limit. In addition, a high contrast ratio between ON and OFF resonance should be obtained to avoid the noise influence.

We take PSQ-LH ring resonators with a cross-section of Figure 7. 1(b) as an example and evaluate the potential possibility of using PSQ-L ring resonators as bio-sensors. We search for the optimal waveguide width (w) and bending radius (R) to obtain best sensing performance.

First we calculated the bending loss of the ridge waveguide with a top cladding (n_c=1.333@1550nm) with different radius (Figure 7. 5). According to the calculation, the waveguide width cannot be too narrow (below 2μm) and the residual layer should be reduced to avoid extra bending loss. Waveguides with a width of 2.5μm is good for biosensors with appropriate radius.

Next, we will calculate the sensitivity of the PSQ-L ring resonators. We first consider the influence of the waveguide width and residual layer thickness on the value of $\partial n_{eff}/\partial n_c$ (i.e. the Sensitivity). Figure 7. 6 shows the calculated value of $\partial n_{eff}/\partial n_c$ for different width and height. The value is calculated from straight waveguide and the bending waveguides show similar results. It is shown that reducing the waveguide width and height and residual layer thickness can increase the value of $\partial n_{eff}/\partial n_c$, and thus increase the sensitivity. But the waveguide width is also restricted by the bending loss and scattering loss of the waveguide.

Assuming the sensor works at 1550nm and the effective index of polymer core is 1.5, according to Eq.(7.3), the sensitivity is calculated to be 30nm~60nm/RIU for polymer PSQ-L ring resonators. This is a moderate value of the ring resonator biosensors [68, 104]. The other way is to reduce the polymer waveguide core index to have more light to penetrate out into the analyte cladding to increase the sensitivity.

The detection limit depends on the FWHM (Q-factor) and sensitivity of the ring. According to Eq.(3.26), increasing the radius of the ring can reduce the bandwidth.

However, increasing the radius of the ring also decreases the FSR of the ring. The radius of the ring cannot be too large, since we need a moderate FSR, i.e. detection range. We have experimentally achieved ring resonators with a Q-factor of $2{\sim}4{\times}10^4$, which is a high value comparable with other reported ring resonators. Therefore we believe we can achieve as good a detection limit (on the order of 10^{-4} for homogeneous sensing) as other polymer ring resonators. In order to have a higher Q-factor, we can reduce the loss factor and the coupling efficiency.

A high contrast ratio of ON and OFF resonance is designed to avoid noise disturbance. For a notch filter, the critical coupling condition is normally used for detection. For double waveguides coupled ring resonators, the drop port is normally used for detection. Because in this case in order to have a high Q-factor, the coupling efficiency is diminished. The contrast ratio of the through port is also reduced while the contrast ratio of the drop port is increased. Therefore the drop port is normally used for detection.

(a)   (b)
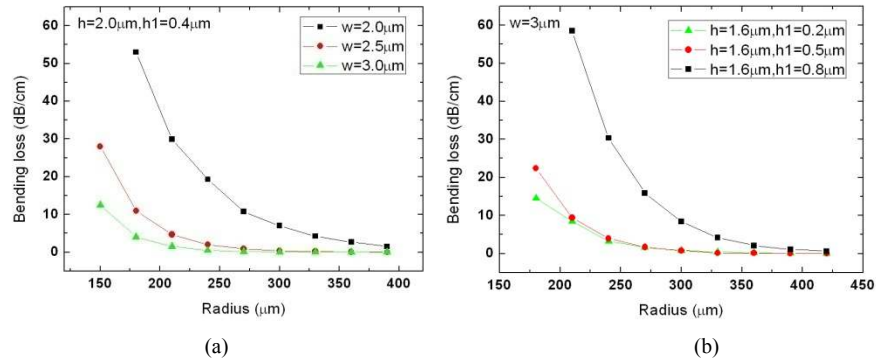
Figure 7. 5 Calculated bending loss of ridge polymer waveguides with different bending radius (a) Calculated bending loss of different width (b) Calculated bending loss of different residual layer thickness

(c)   (d)
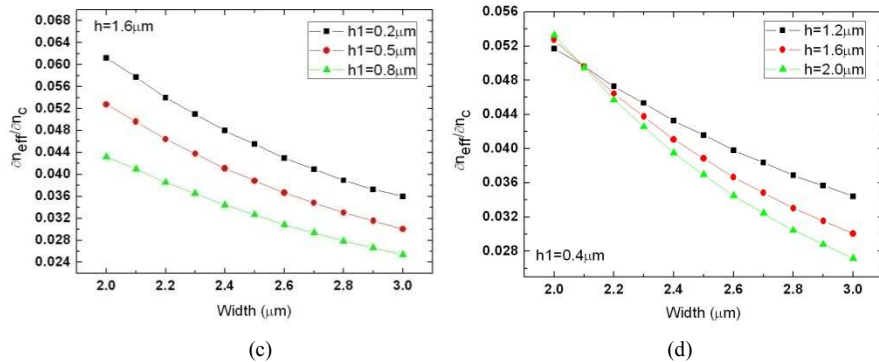
Figure 7. 6 Calculated value of $\partial n_{eff}/\partial n_c$ of polymer ridge waveguide with different waveguide width (a) Calculated value of $\partial n_{eff}/\partial n_c$ with different residual layer thickness (b) Calculated value of $\partial n_{eff}/\partial n_c$ with different waveguide height

Bibliography

[1]   L. Eldada, "Polymer microphotonics," *Nano-and Micro-Optics for Information Systems*, vol. 5225, pp. 49-60, 2003.

[2]   L. Eldada, "Organics in optoelectronics: advances and roadmap " *Optoelectronic Integrated Circuits VIII*, vol. 6124, pp. X1240-X1240, 2006.

[3]   C. Y. Chao, W. Fung, and L. J. Guo, "Polymer microring resonators for biochemical sensing applications," *IEEE Journal of Selected Topics in Quantum Electronics*, vol. 12, pp. 134-142, 2006.

[4]   A. T. Chen, H. S. Sun, A. Pyayt, L. R. Dalton, J. D. Luo, and A. K. Y. Jen, "Microring Resonators Made in Poled and Unpoled Chromophore-Containing Polymers for Optical Communication and Sensors," *IEEE Journal of Selected Topics in Quantum Electronics*, vol. 14, pp. 1281-1288, 2008.

[5]   B. Bortnik, Y. C. Hung, H. Tazawa, B. J. Seo, J. D. Luo, A. K. Y. Jen, W. H. Steier, and H. R. Fetterman, "Electrooptic polymer ring resonator modulation up to 165 GHz," *IEEE Journal of Selected Topics in Quantum Electronics*, vol. 13, pp. 104-110, 2007.

[6]   J. K. S. Poon, Y. Y. Huang, G. T. Paloczi, and A. Yariv, "Soft lithography replica molding of critically coupled polymer microring resonators," *IEEE Photonics Technology Letters*, vol. 16, pp. 2496-2498, 2004.

[7]   S. Herminghaus, D. Boese, D. Y. Yoon, and B. A. Smith, "Large Anisotropy in Optical-Properties of Thin Polyimide Films of Poly(P-Phenylene Biphenyltetracarboximide)," *Applied Physics Letters*, vol. 59, pp. 1043-1045, 1991.

[8]   W. B. Jackson, N. M. Amer, A. C. Boccara, and D. Fournier, "Photothermal Deflection Spectroscopy and Detection," *Applied Optics*, vol. 20, pp. 1333-1344, 1981.

[9]   H. Ma, A. K. Y. Jen, and L. R. Dalton, "Polymer-based optical waveguides: Materials, processing, and devices," *Advanced Materials*, vol. 14, pp. 1339-1365, 2002.

[10]   G. Van Steenberge, N. Hendrickx, E. Bosman, J. Van Erps, H. Thienpont, and P. Van Daele, "Laser ablation of parallel optical interconnect waveguides," *IEEE Photonics Technology Letters*, vol. 18, pp. 1106-1108, 2006.

[11]   Y. T. Chen, K. Naessens, R. Baets, Y. S. Liao, and A. A. Tseng, "Ablation of transparent materials using excimer lasers for photonic applications," *Optical Review*, vol. 12, pp. 427-441, 2005.

[12]   S. P. Wang, B. Borden, Y. Li, and P. Goel, "Laser direct writing of inorganic-organic hybrid polymeric channel waveguide for optical integrated circuits - art. no. 63890B," *Active and Passive Optical Components for Communications VI*, vol. 6389, pp. B3890-B3890, 2006.

[13]   A. A. Bettiol, S. V. Rao, T. C. Sum, J. A. van Kan, and F. Watt, "Fabrication of

optical waveguides using proton beam writing," *Journal of Crystal Growth*, vol. 288, pp. 209-212, 2006.

[14] V. Schmidt, L. Kuna, V. Satzinger, R. Houbertz, G. Jakopic, and G. Leising, "Application of two-photon 3D lithography for the fabrication of embedded ORMOCER (R) waveguides - art. no. 64760P," *Optoelectronic Integrated Circuits IX*, vol. 6476, pp. P4760-P4760, 2007.

[15] J. K. S. Poon, L. Zhu, G. A. DeRose, and A. Yariv, "Polymer microring coupled-resonator optical waveguides," *Journal of Lightwave Technology*, vol. 24, pp. 1843-1849, 2006.

[16] S. Y. Chou, P. R. Krauss, and P. J. Renstrom, "Imprint lithography with 25-nanometer resolution," *Science*, vol. 272, pp. 85-87, 1996.

[17] S. Y. Chou, P. R. Krauss, W. Zhang, L. J. Guo, and L. Zhuang, "Sub-10 nm imprint lithography and applications," *Journal of Vacuum Science & Technology B*, vol. 15, pp. 2897-2904, 1997.

[18] T. C. Bailey, S. C. Johnson, S. V. Sreenivasan, J. G. Ekerdt, C. G. Willson, and D. J. Resnick, "Step and flash imprint lithography: An efficient nanoscale printing technology," *Journal of Photopolymer Science and Technology*, vol. 15, pp. 481-486, 2002.

[19] L. J. Guo, "Recent progress in nanoimprint technology and its applications," *Journal of Physics D-Applied Physics*, vol. 37, pp. R123-R141, 2004.

[20] L. J. Guo, "Nanoimprint lithography: Methods and material requirements," *Advanced Materials*, vol. 19, pp. 495-513, 2007.

[21] C. Y. Chao and L. J. Guo, "Polymer microring resonators fabricated by nanoimprint technique," *Journal of Vacuum Science & Technology B*, vol. 20, pp. 2862-2866, 2002.

[22] S. W. Ahn, K. D. Lee, D. H. Kim, and S. S. Lee, "Polymeric wavelength filter based on a Bragg grating using nanoimprint technique," *IEEE Photonics Technology Letters*, vol. 17, pp. 2122-2124, 2005.

[23] X. Cheng, Y. T. Hong, J. Kanicki, and L. J. Guo, "High-resolution organic polymer light-emitting pixels fabricated by imprinting technique," *Journal of Vacuum Science & Technology B*, vol. 20, pp. 2877-2880, 2002.

[24] P. C. Kao, S. Y. Chu, T. Y. Chen, C. Y. Zhan, F. C. Hong, C. Y. Chang, L. C. Hsu, W. C. Liao, and M. H. Hon, "Fabrication of large-scaled organic light emitting devices on the flexible substrates using low-pressure imprinting lithography," *IEEE Transactions on Electron Devices*, vol. 52, pp. 1722-1726, 2005.

[25] L. J. Guo, X. Cheng, and C. F. Chou, "Fabrication of size-controllable nanofluidic channels by nanoimprinting and its application for DNA stretching," *Nano Letters*, vol. 4, pp. 69-73, 2004.

[26] J. D. Hoff, L. J. Cheng, E. Meyhofer, L. J. Guo, and A. J. Hunt, "Nanoscale protein patterning by imprint lithography," *Nano Letters*, vol. 4, pp. 853-857, 2004.

[27] N. Koo, M. Bender, U. Plachetka, A. Fuchs, T. Wahlbrink, J. Bolten, and H. Kurz, "Improved mold fabrication for the definition of high quality nanopatterns by soft UV-nanoimprint lithography using diluted PDMS material," *Microelectronic Engineering*, vol. 84, pp. 904-908, 2007.

[28]   E. Delamarche, H. Schmid, B. Michel, and H. Biebuyck, "Stability of molded polydimethylsiloxane microstructures," *Advanced Materials*, vol. 9, pp. 741-746, 1997.

[29]   Y. N. Xia and G. M. Whitesides, "Soft lithography," *Abstracts of Papers of the American Chemical Society*, vol. 214, pp. 348-PMSE, 1997.

[30]   E. S. Kang, W. S. Kim, D. J. Kim, and B. S. Bae, "Reducing the thermal dependence of silica-based arrayed-waveguide grating using inorganic-organic hybrid materials," *IEEE Photonics Technology Letters*, vol. 16, pp. 2625-2627, 2004.

[31]   G. T. Paloczi, Y. Huang, J. Scheuer, and A. Yariv, "Soft lithography molding of polymer integrated optical devices: Reduction of the background residue," *Journal of Vacuum Science & Technology B*, vol. 22, pp. 1764-1769, 2004.

[32]   Y. Y. Huang, G. T. Paloczi, A. Yariv, C. Zhang, and L. R. Dalton, "Fabrication and replication of polymer integrated optical devices using electron-beam lithography and soft lithography," *Journal of Physical Chemistry B*, vol. 108, pp. 8606-8613, 2004.

[33]   A. Flores, S. Song, S. Baig, and M. R. Wang, "Vacuum-assisted microfluidic technique for fabrication of guided wave devices," *IEEE Photonics Technology Letters*, vol. 20, pp. 1246-1248, 2008.

[34]   W. C. Chuang, C. T. Ho, and W. C. Chang, "Fabrication of polymer waveguides by a replication method," *Applied Optics*, vol. 45, pp. 8304-8307, 2006.

[35]   W. C. Chuang, C. K. Chao, and C. T. Ho, "Fabrication of high-resolution periodical structures on polymer waveguides using a replication process," *Optics Express*, vol. 15, pp. 8649-8659, 2007.

[36]   W. J. Lee, S. H. Hwang, J. W. Lim, and B. S. Rho, "Polymeric Waveguide Film With Embedded Mirror for Multilayer Optical Circuits," *IEEE Photonics Technology Letters*, vol. 21, pp. 12-14, 2009.

[37]   N. S. Lagali, J. F. P. van Nunen, D. Pant, and L. Eldada, "Ultra-low power and high dynamic range variable optical attenuator array," *Ecoc'01: 27th European Conference on Optical Communication, Vols 1-6*, pp. 430-431, 2001.

[38]   S. H. Nam, J. W. Kang, and J. J. Kim, "Tunable polymer waveguide Bragg filter fabricated by direct patterning of UV-curable polymer," *Optics Communications*, vol. 266, pp. 332-335, 2006.

[39]   Y. O. Noh, H. J. Lee, J. J. Ju, M. S. Kim, S. H. Oh, and M. C. Oh, "Continuously tunable compact lasers based on thermo-optic polymer waveguides with Bragg gratings," *Optics Express*, vol. 16, pp. 18194-18201, 2008.

[40]   A. Leinse, M. B. J. Diemeer, A. Rousseau, and A. Driessen, "A novel high-speed polymeric EO modulator based on a combination of a microring resonator and an MZI," *IEEE Photonics Technology Letters*, vol. 17, pp. 2074-2076, 2005.

[41]   H. Figi, M. Jazbinsek, C. Hunziker, M. Koechlin, and P. Gunter, "Electro-optic single-crystalline organic waveguides and nanowires grown from the melt," *Optics Express*, vol. 16, pp. 11310-11327, 2008.

[42]   H. Figi, M. Jazbinsek, C. Hunziker, M. Koechlin, and P. Gunter, "Electro-optic tuning and modulation of single-crystalline organic microring resonators," *Journal of the Optical Society of America B-Optical Physics*, vol. 26, pp. 1103-1110, 2009.

[43]   W. Z. Song, A. E. Vasdekis, Z. Y. Li, and D. Psaltis, "Low-order distributed feedback optofluidic dye laser with reduced threshold," *Applied Physics Letters*, vol. 94, 2009.

[44]   C. Adachi, M. A. Baldo, S. R. Forrest, and M. E. Thompson, "High-efficiency organic electrophosphorescent devices with tris(2-phenylpyridine)iridium doped into electron-transporting materials," *Applied Physics Letters*, vol. 77, pp. 904-906, 2000.

[45]   S. Ashkenazi, S. W. Huang, M. O'Donnell, C. Y. Chao, and L. J. Guo, "High-Frequency Ultrasound Transduction Using Polymer Microring Resonators," *2006 IEEE Ultrasonics Symposium, Vols 1-5, Proceedings*, pp. 1056-1059, 2006.

[46]   N. Pelletier, B. Beche, N. Tahani, J. Zyss, L. Camberlein, and E. Gaviot, "SU-8 waveguiding interferometric micro-sensor for gage pressure measurement," *Sensors and Actuators a-Physical*, vol. 135, pp. 179-184, 2007.

[47]   A. Airoudj, B. Beche, D. Debarnot, E. Gaviot, and F. Poncin-Epaillard, "Integrated SU-8 photonic gas sensors based on PANI polymer devices: Comparison between metrological parameters," *Optics Communications*, vol. 282, pp. 3839-3845, 2009.

[48]   T. Han, S. Madden, M. Zhang, R. Charters, and B. Luther-Davies, "Low loss high index contrast nanoimprinted polysiloxane waveguides," *Optics Express*, vol. 17, pp. 2623-2630, 2009.

[49]   A. Norris, J. DeGroot, T. Ogawa, T. Watanabe, T. Kowalczyk, A. Baugher, and R. Blum, "High reliability of silicone materials for use as polymer waveguides," *Linear and Nonlinear Optics of Organic Materials Iii*, vol. 5212, pp. 76-82, 2003.

[50]   L. W. Shacklette, R. Blomquist, J. M. Deng, P. M. Ferm, M. Maxfield, J. Mato, and H. Zou, "Ultra-low-loss acrylate polymers for planar light circuits," *Advanced Functional Materials*, vol. 13, pp. 453-462, 2003.

[51]   M. Usui, M. Hikita, T. Watanabe, M. Amano, S. Sugawara, S. Hayashida, and S. Imamura, "Low-loss passive polymer optical waveguides with high environmental stability," *Journal of Lightwave Technology*, vol. 14, pp. 2338-2343, 1996.

[52]   L. Eldada, "Advances in polymer optical interconnects," *2005 IEEE LEOS Annual Meeting Conference Proceedings (LEOS)*, pp. 360-361, 2005.

[53]   H. B. Zhang, J. Y. Wang, L. K. Li, Y. Song, M. S. Zhao, and X. G. Jian, "A study on liquid hybrid material for waveguides - Synthesis and property of PSQ-Ls for waveguides," *Journal of Macromolecular Science Part a-Pure and Applied Chemistry*, vol. 45, pp. 232-237, 2008.

[54]   H. B. Zhang, J. Y. Wang, L. K. Li, Y. Song, M. S. Zhao, and X. G. Jian, "Synthesis of liquid polysilisiquioxane resins and properties of cured films," *Thin Solid Films*, vol. 517, pp. 857-862, 2008.

[55]   R. Buestrich, F. Kahlenberg, M. Popall, P. Dannberg, R. Muller-Fiedler, and O. Rosch, "ORMOCER (R) s for optical interconnection technology," *Journal of Sol-Gel Science and Technology*, vol. 20, pp. 181-186, 2001.

[56]   T. Watanabe, N. Ooba, S. Hayashida, T. Kurihara, and S. Imamura, "Polymeric optical waveguide circuits formed using silicone resin," *Journal of Lightwave Technology*, vol. 16, pp. 1049-1055, 1998.

[57]   Y. Haruvy, I. Gilath, M. Maniewictz, and N. Eisenberg, "Sol-gel replication of microoptical elements and arrays," *Chemistry of Materials*, vol. 9, pp. 2604-2615, 1997.

[58]   C. C. Teng, "Precision-Measurements of the Optical Attenuation Profile Along the Propagation Path in Thin-Film Wave-Guides," *Applied Optics*, vol. 32, pp. 1051-1054, 1993.

[59]   N. Pugliano, N. Chiarotto, J. Fisher, N. Heiks, T. Ho, G. Khanarian, M. Moynihan, N. Pawlowski, J. Shelnut, D. Sherrer, B. Sicard, and H. B. Zheng, "Progress toward the development of manufacturable integrated optical data buses," *Photonics Packaging and Integration Iv*, vol. 5358, pp. 71-79, 2004.

[60]   Y. Gao, X. G. Jian, and J. Y. Wang, "Synthesis and characterization of poly (aryl ether ketone) containing phthalazinone and naphthalene moieties," *Chinese Chemical Letters*, vol. 11, pp. 777-778, 2000.

[61]   X. G. Jian, L. Z. Chen, X. Y. Guo, and W. X. Sun, "Synthesis and characterization of poly(ether amide)s containing phthalazinone moieties," *Chemical Research in Chinese Universities*, vol. 16, pp. 78-82, 2000.

[62]   Y. Song, J. Wang, G. Li, Q. Sun, X. Jian, J. Teng, and H. Zhang, "Synthesis, characterization and optical properties of fluorinated poly(aryl ether)s containing phthalazinone moieties," *Polymer*, vol. 49, pp. 4995-5001, 2008.

[63]   Y. Song, J. Y. Wang, G. H. Li, Q. M. Sun, X. G. Jian, J. Teng, and H. B. Zhang, "Synthesis, characterization and optical properties of cross-linkable poly (phthalazinone ether ketone sulfone)," *Polymer*, vol. 49, pp. 724-731, 2008.

[64]   S. T. Chu, B. E. Little, W. G. Pan, T. Kaneko, and Y. Kokubun, "Cascaded microring resonators for crosstalk reduction and spectrum cleanup in add-drop filters," *IEEE Photonics Technology Letters*, vol. 11, pp. 1423-1425, 1999.

[65]   E. J. Klein, D. H. Geuzebroek, H. Kelderman, G. Sengo, N. Baker, and A. Driessen, "Reconfigurable optical add-drop multiplexer using microring resonators," *IEEE Photonics Technology Letters*, vol. 17, pp. 2358-2360, 2005.

[66]   Q. F. Xu, S. Manipatruni, B. Schmidt, J. Shakya, and M. Lipson, "12.5 Gbit/s carrier-injection-based silicon micro-ring silicon modulators," *Optics Express*, vol. 15, pp. 430-436, 2007.

[67]   T. Chu, H. Yamada, S. Ishida, and Y. Arakawa, "Compact 1 x N thermo-optic switches based on silicon photonic wire waveguides," *Optics Express*, vol. 13, pp. 10109-10114, 2005.

[68]   K. De Vos, I. Bartolozzi, E. Schacht, P. Bienstman, and R. Baets, "Silicon-on-Insulator microring resonator for sensitive and label-free biosensing," *Optics Express*, vol. 15, pp. 7610-7615, 2007.

[69]   S. C. Hagness, D. Rafizadeh, S. T. Ho, and A. Taflove, "FDTD microcavity

simulations: Design and experimental realization of waveguide-coupled single-mode ring and whispering-gallery-mode disk resonators," *Journal of Lightwave Technology*, vol. 15, pp. 2154-2165, 1997.

[70]   B. E. Little, S. T. Chu, H. A. Haus, J. Foresi, and J. P. Laine, "Microring resonator channel dropping filters," *Journal of Lightwave Technology*, vol. 15, pp. 998-1005, 1997.

[71]   A. Yariv, "Coupled-Mode Theory for Guided-Wave Optics," *IEEE Journal of Quantum Electronics*, vol. QE 9, pp. 919-933, 1973.

[72]   J. K. S. Poon, J. Scheuer, S. Mookherjea, G. T. Paloczi, Y. Y. Huang, and A. Yariv, "Matrix analysis of microring coupled-resonator optical waveguides," *Optics Express*, vol. 12, pp. 90-103, 2004.

[73]   F. P. Payne and J. P. R. Lacey, "A Theoretical-Analysis of Scattering Loss from Planar Optical Wave-Guides," *Optical and Quantum Electronics*, vol. 26, pp. 977-986, 1994.

[74]   H. Schmitt, L. Frey, H. Ryssel, M. Rommel, and C. Lehrer, "UV nanoimprint materials: Surface energies, residual layers, and imprint quality," *Journal of Vacuum Science & Technology B*, vol. 25, pp. 785-790, 2007.

[75]   H. Lee, "Effect of imprinting pressure on residual layer thickness in UV nano-imprint lithography (vol 23, pg 1102, 2005)," *Journal of Vacuum Science & Technology B*, vol. 23, pp. 2176-2176, 2005.

[76]   D. X. Dai, B. Yang, L. Yang, Z. Sheng, and S. L. He, "Compact Microracetrack Resonator Devices Based on Small SU-8 Polymer Strip Waveguides," *IEEE Photonics Technology Letters*, vol. 21, pp. 254-256, 2009.

[77]   N. Yurt, K. Mune, R. Naito, T. Fukuoka, A. Mochizuki, K. Matsumoto, G. Meredith, N. Peyghambarian, and G. E. Jabbour, "Fabrication and characterization of low-loss optical waveguides using a novel photosensitive polyimide," *Journal of Lightwave Technology*, vol. 23, pp. 1291-1294, 2005.

[78]   J. J. Chiu and T. P. Perng, "The passive optical properties of a silicon nanoparticle-embedded benzocyclobutene polymer waveguide," *Nanotechnology*, vol. 19, 2008.

[79]   R. Regener and W. Sohler, "Loss in Low-Finesse Ti-Linbo3 Optical Wave-Guide Resonators," *Applied Physics B-Photophysics and Laser Chemistry*, vol. 36, pp. 143-147, 1985.

[80]   V. Van, P. P. Absil, J. V. Hryniewicz, and P. T. Ho, "Propagation loss in single-mode GaAs-AlGaAs microring resonators: Measurement and model," *Journal of Lightwave Technology*, vol. 19, pp. 1734-1739, 2001.

[81]   Y. Kokubun, S. Yoneda, and H. Tanaka, "Temperature-independent narrow-band optical filter by an athermal waveguide," *Ieice Transactions on Electronics*, vol. E80C, pp. 632-639, 1997.

[82]   S. Kamei, Y. Inoue, T. Mizuno, K. Iemura, T. Shibata, A. Kaneko, and H. Takahashi, "Extremely low-loss 1.5%-Delta 32-channel athermal arrayed-waveguide grating multi/demultiplexer," *Electronics Letters*, vol. 41, pp. 544-546, 2005.

[83]   S. Kamei, M. Oguma, M. Kohtoku, T. Shibata, and Y. Inoue, "Low-loss athermal silica-based lattice-form interleave filter with silicone-filled

grooves," *IEEE Photonics Technology Letters*, vol. 17, pp. 798-800, 2005.

[84] M. Itoh, S. Kamei, M. Ishii, T. Shibata, M. Tamura, and Y. Inoue, "Ultra-small 40-channel athermal arrayed-waveguide grating module with low-loss groove design," *Electronics Letters*, vol. 44, pp. 1271-U56, 2008.

[85] K. Maru and Y. Abe, "Low-loss, flat-passband and athermal arrayed-waveguide grating multi/demultiplexer," *Optics Express*, vol. 15, pp. 18351-18356, 2007.

[86] K. Maru, Y. Abe, and H. Uetsuka, "Demonstration of Compact and Low-Loss Athermal Arrayed-Waveguide Grating Module Based on 2.5%-Delta Silica-Based Waveguides," *Japanese Journal of Applied Physics*, vol. 47, pp. 7903-7908, 2008.

[87] J. M. Lee, D. J. Kim, H. Ahn, S. H. Park, and G. Kim, "Temperature dependence of silicon nanophotonic ring resonator with a polymeric overlayer," *Journal of Lightwave Technology*, vol. 25, pp. 2236-2243, 2007.

[88] J. M. Lee, D. J. Kim, G. H. Kim, O. K. Kwon, K. J. Kim, and G. Kim, "Controlling temperature dependence of silicon waveguide using slot structure," *Optics Express*, vol. 16, pp. 1645-1652, 2008.

[89] W. N. Ye, R. Sun, J. Michel, L. Eldada, D. Pant, and L. C. Kimerling, "Thermo-optical Compensation in High-index-contrast Waveguides," *2008 5th IEEE International Conference on Group Iv Photonics*, pp. 401-403, 2008.

[90] Y. Kokubun, N. Funato, and M. Takizawa, "Athermal Wave-Guides for Temperature-Independent Lightwave Devices," *IEEE Photonics Technology Letters*, vol. 5, pp. 1297-1300, 1993.

[91] K. Tsuzuki, H. Takeuchi, S. Oku, H. Tanobe, Y. Kadota, and M. Yamamoto, "Temperature insensitive InGaAsP/InP optical filter integrated with dual photodiodes," *Electronics Letters*, vol. 33, pp. 1948-1949, 1997.

[92] Y. Kokubun, S. Yoneda, and S. Matsuura, "Athermal narrow-band optical filter at 1.55 mu m wavelength by silica-based athermal waveguide," *Ieice Transactions on Electronics*, vol. E81C, pp. 1187-1194, 1998.

[93] H. Hirota, M. Itoh, M. Oguma, and Y. Hibino, "Athermal arrayed-waveguide grating multi/demultiplexers composed of TiO2-SiO2 waveguides on Si," *IEEE Photonics Technology Letters*, vol. 17, pp. 375-377, 2005.

[94] N. Keil, H. H. Yao, and C. Zawadzki, "Athermal polarisation-independent arrayed-waveguide grating (AWG) multiplexer using an all-polymer approach," *Applied Physics B-Lasers and Optics*, vol. 73, pp. 619-622, 2001.

[95] Y. Kokubun, S. Yoneda, and H. Tanaka, "Temperature-independent narrowband optical filter at 1.31 mu m wavelength by an athermal waveguide," *Electronics Letters*, vol. 32, pp. 1998-2000, 1996.

[96] J. Hasegawca and K. Nara, "Low-loss athermal AWG module with high reliability," *Electronics and Communications in Japan Part Ii-Electronics*, vol. 89, pp. 26-33, 2006.

[97] Y. Inoue, A. Kaneko, F. Hanawa, H. Takahashi, K. Hattori, and S. Sumida, "Athermal silica-based arrayed-waveguide grating (AWG) multiplexer," *Iooc-Ecoc 97 - 11th International Conference on Integrated Optics and Optical Fibre Communications / 23rd European Conference on Optical*

Communications, Vol 5, pp. 33-36, 1997.

[98]   K. Maru, K. Matsui, H. Ishikawa, Y. Abe, S. Kashimura, S. Himi, and H. Uetsuka, "Super-high-Delta athermal arrayed waveguide grating with resin-filled trenches in slab region," *Electronics Letters*, vol. 40, pp. 374-375, 2004.

[99]   W. Bogaerts, R. Baets, P. Dumon, V. Wiaux, S. Beckx, D. Taillaert, B. Luyssaert, J. Van Campenhout, P. Bienstman, and D. Van Thourhout, "Nanophotonic waveguides in silicon-on-insulator fabricated with CMOS technology," *Journal of Lightwave Technology*, vol. 23, pp. 401-412, 2005.

[100]   P. Dumon, W. Bogaerts, V. Wiaux, J. Wouters, S. Beckx, J. Van Campenhout, D. Taillaert, B. Luyssaert, P. Bienstman, D. Van Thourhout, and R. Baets, "Low-loss SOI photonic wires and ring resonators fabricated with deep UV lithography," *IEEE Photonics Technology Letters*, vol. 16, pp. 1328-1330, 2004.

[101]   W. Bogaerts, D. Taillaert, B. Luyssaert, P. Dumon, J. Van Campenhout, P. Bienstman, D. Van Thourhout, R. Baets, V. Wiaux, and S. Beckx, "Basic structures for photonic integrated circuits in silicon-on-insulator," *Optics Express*, vol. 12, pp. 1583-1591, 2004.

[102]   W. Bogaerts, V. Wiaux, D. Taillaert, S. Beckx, B. Luyssaert, P. Bienstman, and R. Baets, "Fabrication of photonic crystals in silicon-on-insulator using 248-nm deep UV lithography," *IEEE Journal of Selected Topics in Quantum Electronics*, vol. 8, pp. 928-934, 2002.

[103]   C. A. Barrios, "Optical Slot-Waveguide Based Biochemical Sensors," *Sensors*, vol. 9, pp. 4751-4765, 2009.

[104]   A. Yalcin, K. C. Popat, J. C. Aldridge, T. A. Desai, J. Hryniewicz, N. Chbouki, B. E. Little, O. King, V. Van, S. Chu, D. Gill, M. Anthes-Washburn, and M. S. Unlu, "Optical sensing of biomolecules using microring resonators," *IEEE Journal of Selected Topics in Quantum Electronics*, vol. 12, pp. 148-155, 2006.

Appendix A Working principle of prism coupler

A.1 The film refractive index measurement

We consider the case of a polymer film (or another film) deposited on the substrate; the index of the film, cover and substrate is set as n_f, n_c, n_s (Figure A. 1). The critical angle of the interface of the film and the cover and that of the interface of the film and the substrate can be expressed as,

$$\theta_{1c} = \sin^{-1}(n_c / n_f)$$
$$\theta_{2c} = \sin^{-1}(n_s / n_f)$$

(6)

Assuming that the refractive index of the substrate is higher than that of the cover ($n_s > n_c$), the critical angle for the interface of the film and the substrate is larger than that of the interface with the cover ($\theta_{2c} > \theta_{1c}$). If $n_f > n_s > n_c$, the light propagation in the film can be divided into three cases for different incidence angle θ,
1) $\theta < \theta_{1c}$, θ is smaller than both critical angles, the light will radiate out to the cover (Figure A. 2 (a));
2) $\theta_{1c} < \theta < \theta_{2c}$, θ is larger than the critical angle of film and cover interface but smaller than that of film and substrate interface. So there will be internal reflection between film and cover interface (Figure A. 2 (b));
3) $\theta > \theta_{2c}$, θ is larger than both critical angles. The light will be guided in the film (Figure A. 2 (c)).
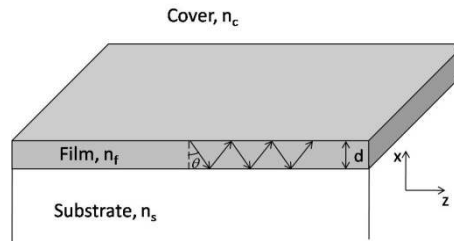
Figure A. 1 Structure of asymmetric planar waveguide

(a)   (b)   (c)
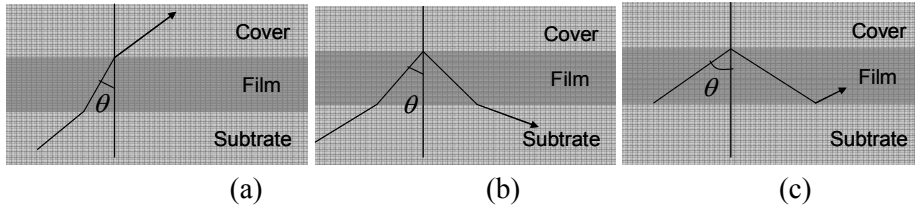
Figure A. 2 Light propagation in asymmetric slab waveguide
(a)Radiation mode (b) Substrate radiation mode (c) guided mode

According to the theory of wave optics, the standing wave in the film will exist when the phase in x direction satisfies the following condition,

$$2k_x d - \phi_c - \phi_s = 2k_0 n_f d \cos\theta - \phi_c - \phi_s = 2\pi \cdot m \qquad (7)$$

Where d is the thickness of the film, k_x is the propagation constant in the x direction (Figure A. 1), φ_c and φ_s are the phase shift after reflection at the interfaces, m is an integer. φ_c and φ_s can be theoretically calculated from Fresnel reflection.
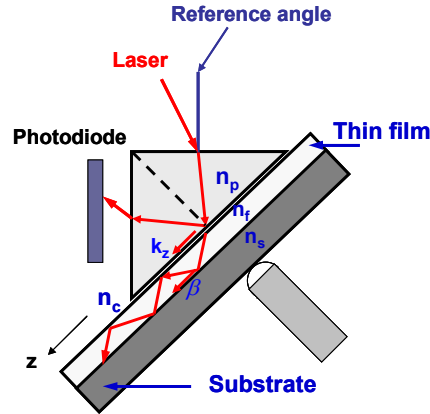
Figure A. 3 Set up of the prism coupler

Figure A. 3 shows the setup of the prism coupler. The light is coupled in and out of the film by a prism. By changing the incidence angle, the guided mode in the film will be stimulated. The detected light coupled out of the film will have a minimum intensity at the guided modes. Once the incident angles of the guided modes are known, we can calculate the propagation constants of the guided modes (propagation constant β in the propagation direction of the film). Back to Eq.(7), φ_c and φ_s can be theoretically calculated related to the index of the film and substrate. Only two parameters of film index (n_f) and film thickness (d) are unknown in the Eq.(7). So the film index (n_f) and film thickness (d) can be calculated by two equations. The measured film should be thick enough to support two modes in the film since there are two unknown parameters in Eq.(7). shows the measured light intensity coupled out from the polymer film by a prism coupler. For silicon substrate, as the index of silicon

is larger than polymer, the light will leak to the substrate, as in Figure A. 4 (b), so the detected intensity will decrease as the sweep angle increases. For silica substrate, the index of silica is smaller than polymer, so the light will have internal reflections in the film (Figure A. 4(c)).
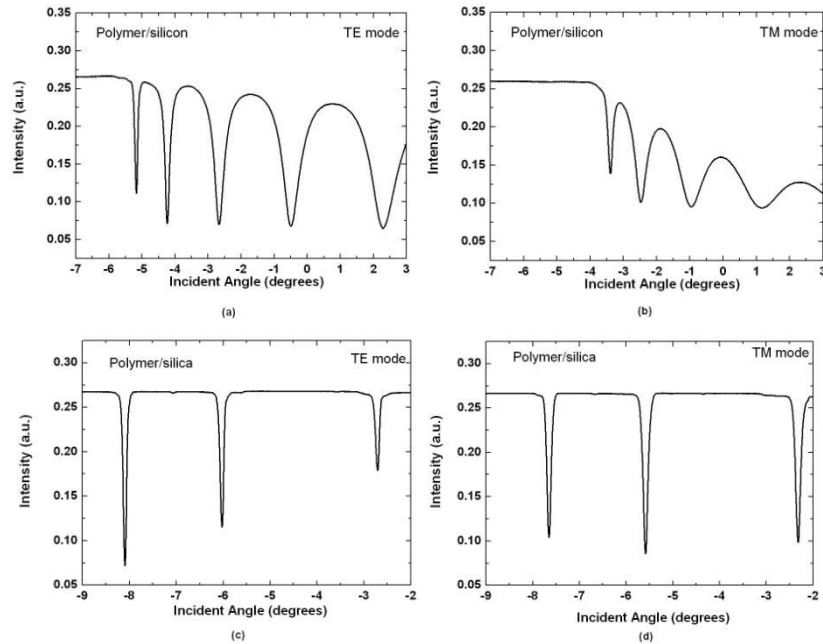
Figure A. 4 Polymer Film measured by prism coupler (SPA-4000)
(a) silicon substrate, TE mode (b)silicon substrate, TM mode
(c) silica substrate, TE mode (d) silicon substrate, TM mode

A.2 The film loss measurement
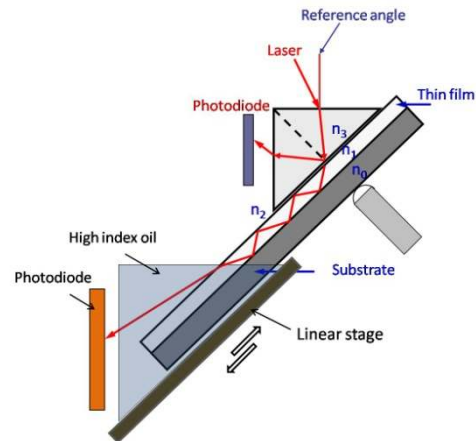
Figure A. 5 Loss measurement of polymer film by prism coupler

The optical loss of polymer films is measured by immersion oil method. In this method, light is coupled into the slab waveguide by prism coupling (Figure A. 5). The film should be deposited on a lower index cladding or substrate to form internal reflection of light in the film waveguide. The film waveguide is immerged in the high-index oil. After propagating a certain distance, the light is out coupled from the waveguide to the high-index liquid. The out-coupled power is measured as a function of film immerging distance. Thus the loss of the waveguide can be extracted from the measured intensity as a function of the immersion distance of the film.

Appendix B Contact lithography mask layout for polymer waveguides

The mask layout for the polymer waveguides are shown in Figure B. 1. We have straight waveguides, racetrack ring resonators, notch filters and racetrack ring resonators with MMI coupling regions. Figure B. 2 shows a single ring on the mask. Figure B. 3 shows the layout of the region RTMRs1. The regions of Straight waveguides, RTMRs1 (regular racetrack ring resonators with different gap dimension), RTMRs2 (regular racetrack ring resonators with different coupling length dimension) and RTMRNFs (notch filters) are mostly used for the fabrication of polymer waveguides.

(a) (b)
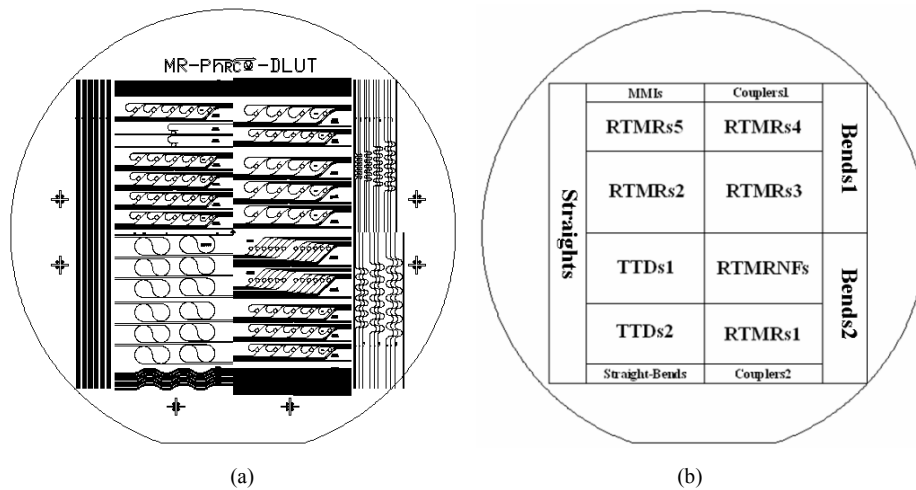
Figure B. 1 Layout of the contact mask for polymer waveguides

(a)   (b)
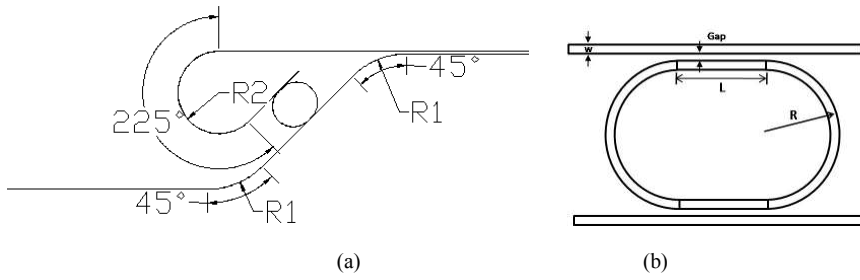
Figure B. 2 Structure of the ring resonators in the mask layout
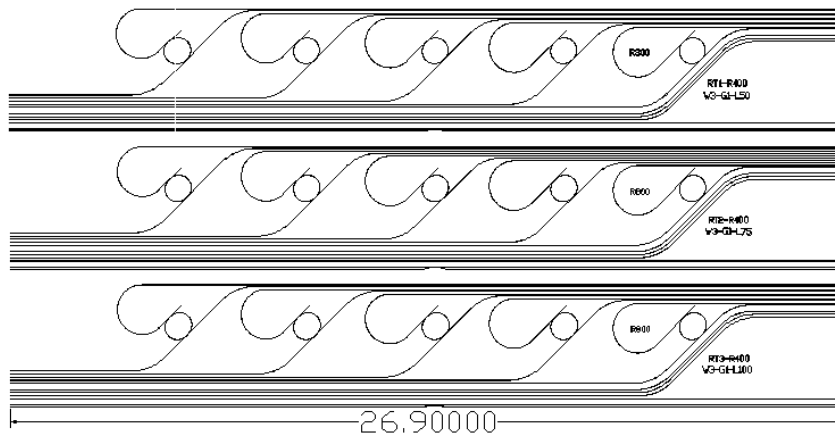
Figure B. 3 Layout of region 'RTMRs1'

Table B.1 Parameters of different regions on the mask

Region	Variable Parameters	Other Parrameters
RTMRs1	Racetrack ring resonator: Coupling length L=50μm, 75μm, 100μm	w=3μm, Gap=1μm, R=400μm R1=1500μm, R2=800μm.
RTMRs2	Racetrack ring resonator: Gap=1.2μm, 1.4μm, 1.6μm, 1.8μm	w=3μm, R=400μm, R1=1500μm, R2=800μm.
RTMRs3	Racetrack ring resonator: Radius= 403.7μm, 409.3μm, 414.9μm	w=4μm, Gap=1μm, L= 132μm, R1=3000μm, R2=1200μm
RTMRs4	Racetrack ring resonator: Offset= 0.15μm, L= 50μm, others are the same as region RTMRs1 Offset=0.35μm, R= 414.9μm, others are the same as region RTMRs3	

RTMRs5	Racetrack ring resonator: w=3μm, R=400μm, Gap=1.4μm, L=150μm Ring resonators (with MMI coupling region): Gap:4μm, L_MMI:244.5μm, R=400μm, R1=1500μm, R2=900μm	
RTMRNFs	Notch filters: Gap, R= 1.00μm, 400μm 1.15μm, 402.2μm 1.30μm, 404.4μm 1.45μm, 406.6μm	w=3μm, L=50μm, R1=1500μm

Appendix C Mask layout for athermal SOI devices

C.1 LETI 02
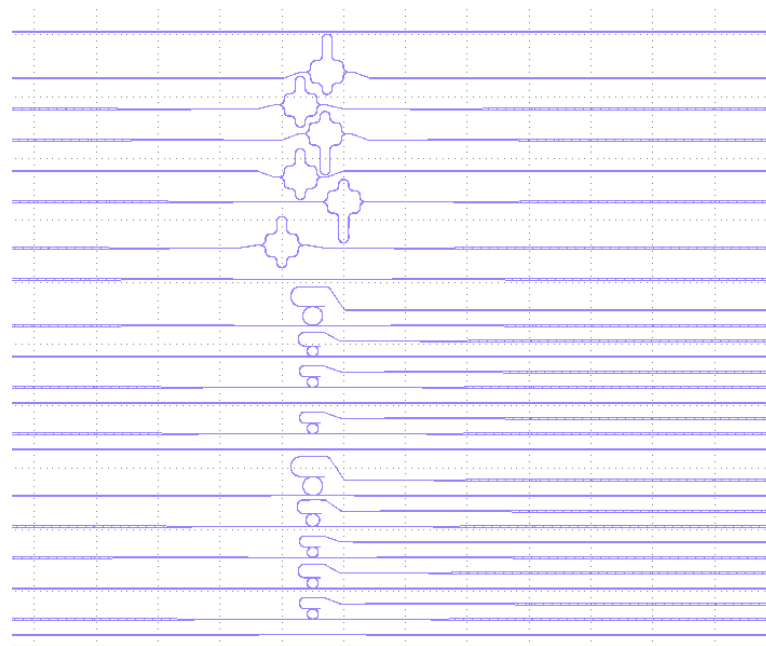
Figure C. 1 Mask layout of LETI 02 for athermal SOI devices

Table C.1 Parameters of ring resonators and MZs on LETI 02 mask

	waveguide width	other parameters
MZs	300nm	length difference between two arms: ΔL=20μm, 60μm
	350nm	ΔL=20μm, 50μm
	450nm	ΔL=20μm, 60μm
Ring resonators	300nm	R=8,10,15μm, Gap=180nm, L=2μm
	350nm	R=8,10,15μm, Gap=180nm, L=2μm
	450nm	R=8,10,15μm, Gap=180nm, L=2μm

C.2 LETI 03

(a)

(b)
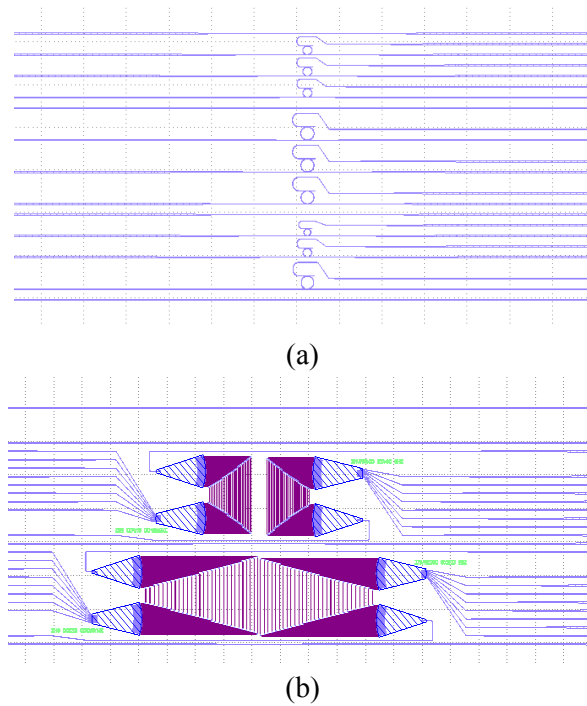
Figure C. 2 Mask layout of LETI 02 for athermal SOI devices (a) ring resonators (b) AWGs

Table C.2 Parameters of ring resonators and AWGs on LETI 03 mask

	Parameters
Ring resonators	w=350nm, R=10μm, Gap=180nm, L=0.6μm, 1μm, 1.4μm L=2μm
	w=350nm, R=15μm, Gap=180nm, L=0.6μm, 1μm, 1.4μm L=2μm
	w=350nm, L=0μm, Gap=180nm, R=8,10,15μm
AWGs	w=450nm with inserted narrow width of 350nm, channel spacing 400GHz, 200GHz

Appendix D Publications

International Journals
1. **J. Teng**, P. Dumon, W. Bogaerts, H. B. Zhang, X. G. Jian, X. Y. Han, M. S. Zhao, G. Morthier, and R. Baets, "Athermal Silicon-on-insulator ring resonators by overlaying a polymer cladding on narrowed waveguides," *Optics Express*, vol. 17, pp. 14627-14633, 2009.
2. **J. Teng**, S. Scheerlinck, H. B. Zhang, X. G. Jian, G. Morthier, R. Beats, X. Y. Han, and M. S. Zhao, "A PSQ-L Polymer Microring Resonator Fabricated by a Simple UV-Based Soft-Lithography Process," *IEEE Photonics Technology Letters*, vol. 21, pp. 1323-1325, 2009.
3. **J. Teng**, Y. Song, X. G. Jian, and M. S. Zhao, "Optical properties of polymer poly (phthalazinone
   ether sulfone ketone) film waveguide," *Chinese Optics Letters*, vol. 6, pp. 74-75, 2008.
4. Y. Song, J. Wang, G. Li, Q. Sun, X. Jian, **J. Teng**, and H. Zhang, "Synthesis, characterization and optical properties of fluorinated poly(aryl ether)s containing phthalazinone moieties," *Polymer*, vol. 49, pp. 4995-5001, 2008.
5. Y. Song, J. Y. Wang, G. H. Li, Q. M. Sun, X. G. Jian, **J. Teng**, and H. B. Zhang, "Synthesis, characterization and optical properties of cross-linkable poly (phthalazinone ether ketone sulfone)," *Polymer*, vol. 49, pp. 724-731, 2008
6. Y. Song, G. H. Li, J. Y. Wang, Q. M. Sun, X. G. Jian, **J. Teng**, and H. B. Zhang, "Fluorinated poly(phthalazinone ether)s with tunable refractive index: synthesis, characterization and optical properties," *Polymer Journal*, vol. 40, pp. 92-93, 2008
7. L. K. Li, J. Teng, Y. Song, H.B. Zhang, X. Y. Han, J. Y. Wang, "Film Preparation and Optical Properties of Novel Polymer PPESK", 光学学报, 2007, 27(12): 2189～2193 (in chinese)
   李林科，**滕婕**，宋媛，张洪波，韩秀友，王锦艳，塞锡高，赵明山，"新型杂萘联苯型聚芳醚砜硐聚合物光子材料成膜和光学特性"，光学学报, 2007, 27(12): 2189-2193.

International Cofenrences
1. **J. Teng**, P. Dumon, W. Bogaerts, H. Zhang, X. Jian, M. Zhao, G. Morthier, R. Baets, *"Athermal SOI ring resonators by overlaying a polymer cladding on narrowed waveguides"*, 6th IEEE International Conference on Group IV Photonics, United States, Speech, p.ThB2 (2009).
2. **J. Teng**, S. Scheerlinck, G. Morthier, R. Baets, *"A PSQ-L Polymer Microring Resonator Fabricated by a Simple UV-Based Soft-Lithography Process"*, Conference on Lasers and Electro-Optics-European Quantum Electronics Conference (CLEO Europe- EQEC 2009), Germany, Poster, (2009).
3. **J. Teng**, S. Scheerlinck, G. Morthier, R. Baets, *"Fabrication of all-polymer microring resonator by using a novel polymer PSQ-L"*, Proceedings Annual Symposium of the IEEE/LEOS Benelux Chapter, 2008, Netherlands, Poster, p.179-182 (2008).

4. **J. Teng**, "*Fabrication of polymer-based devices using nanoimprint technology*", ePIXnetSpring School '08, Technology for Photonics Integration, Italy, p.44 -poster nr. 12 (2008).